



**HAL**  
open science

# Therapeutic oxygen delivery by perfluorocarbon-based colloids

Marie Pierre Krafft, Jean G Riess

► **To cite this version:**

Marie Pierre Krafft, Jean G Riess. Therapeutic oxygen delivery by perfluorocarbon-based colloids. *Advances in Colloid and Interface Science*, 2021, 294, pp.102407. 10.1016/j.cis.2021.102407 . hal-03873075

**HAL Id: hal-03873075**

**<https://hal.science/hal-03873075v1>**

Submitted on 26 Nov 2022

**HAL** is a multi-disciplinary open access archive for the deposit and dissemination of scientific research documents, whether they are published or not. The documents may come from teaching and research institutions in France or abroad, or from public or private research centers.

L'archive ouverte pluridisciplinaire **HAL**, est destinée au dépôt et à la diffusion de documents scientifiques de niveau recherche, publiés ou non, émanant des établissements d'enseignement et de recherche français ou étrangers, des laboratoires publics ou privés.



## Therapeutic oxygen delivery by perfluorocarbon-based colloids

Marie Pierre Krafft <sup>a,\*</sup>, Jean G. Riess <sup>b</sup>

<sup>a</sup> University of Strasbourg, Institut Charles Sadron (CNRS), 23 rue du Loess, 67034 Strasbourg, France

<sup>b</sup> Harangoutte Institute, 68160 Ste Croix-aux-Mines, France



### ARTICLE INFO

18 March 2021

Available online 01 May 2021

#### Keywords:

Fluorocarbon nanoemulsion  
Microbubble  
Phase-shift emulsion  
Stimuli-responsive colloid  
Ultrasound activation  
Blood substitute  
Hypoxia

### ABSTRACT

After the protocol-related indecisive clinical trial of *Oxygent*, a perfluorooctylbromide/phospholipid nanoemulsion, in cardiac surgery, that often unduly assigned the observed untoward effects to the product, the development of perfluorocarbon (PFC)-based O<sub>2</sub> nanoemulsions (“blood substitutes”) has come to a low. Yet, significant further demonstrations of PFC O<sub>2</sub>-delivery efficacy have continuously been reported, such as relief of hypoxia after myocardial infarction or stroke; protection of vital organs during surgery; potentiation of O<sub>2</sub>-dependent cancer therapies, including radio-, photodynamic-, chemo- and immunotherapies; regeneration of damaged nerve, bone or cartilage; preservation of organ grafts destined for transplantation; and control of gas supply in tissue engineering and biotechnological productions. PFC colloids capable of augmenting O<sub>2</sub> delivery include primarily injectable PFC nanoemulsions, microbubbles and phase-shift nanoemulsions. Careful selection of PFC and other colloid components is critical. The basics of O<sub>2</sub> delivery by PFC nanoemulsions will be briefly reminded. Improved knowledge of O<sub>2</sub> delivery mechanisms has been acquired. Advanced, size-adjustable O<sub>2</sub>-delivering nanoemulsions have been designed that have extended room-temperature shelf-stability. Alternate O<sub>2</sub> delivery options are being investigated that rely on injectable PFC-stabilized microbubbles or phase-shift PFC nanoemulsions. The latter combine prolonged circulation in the vasculature, capacity for penetrating tumor tissues, and acute responsiveness to ultrasound and other external stimuli. Progress in microbubble and phase-shift emulsion engineering, control of phase-shift activation (vaporization), understanding and control of bubble/ultrasound/tissue interactions is discussed. Control of the phase-shift event and of microbubble size require utmost attention. Further PFC-based colloidal systems, including polymeric micelles, PFC-loaded organic or inorganic nanoparticles and scaffolds, have been devised that also carry substantial amounts of O<sub>2</sub>. Local, on-demand O<sub>2</sub> delivery can be triggered by external stimuli, including focused ultrasound irradiation or tumor microenvironment. PFC colloid functionalization and targeting can help adjust their properties for specific indications, augment their efficacy, improve safety profiles, and expand the range of their indications. Many new medical and biotechnological applications involving fluorinated colloids are being assessed, including in the clinic. Further uses of PFC-based colloidal nanotherapeutics will be briefly mentioned that concern contrast diagnostic imaging, including molecular imaging and immune cell tracking; controlled delivery of therapeutic energy, as for noninvasive surgical ablation and sonothrombolysis; and delivery of drugs and genes, including across the blood-brain barrier. Even when the fluorinated colloids investigated are designed for other purposes than O<sub>2</sub> supply, they will inevitably also carry and deliver a certain amount of O<sub>2</sub>, and may thus be considered for O<sub>2</sub> delivery or co-delivery applications. Conversely, O<sub>2</sub>-carrying PFC nanoemulsions possess by nature a unique aptitude for <sup>19</sup>F MR imaging, and hence, cell tracking, while PFC-stabilized microbubbles are ideal resonators for ultrasound contrast imaging and can undergo precise manipulation and on-demand destruction by ultrasound waves, thereby opening multiple theranostic opportunities.

© 2021 Published by Elsevier B.V.

### Contents

1. Introduction . . . . .	2
2. An inconclusive clinical trial. . . . .	3
3. The perfluorocarbon colloids at work . . . . .	4

\* Corresponding author.

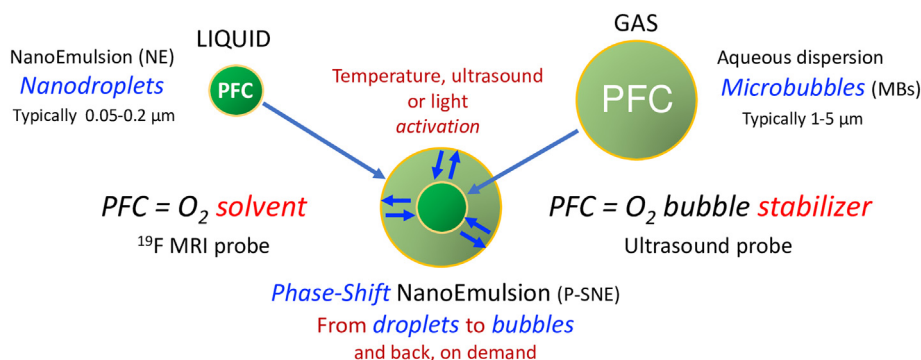
E-mail address: [krafft@unistra.fr](mailto:krafft@unistra.fr) (M.P. Krafft).

3.1.	The key components—their selection is a critical step . . . . .	4
3.1.1.	Selecting the perfluorocarbon . . . . .	4
3.1.2.	Emulsifiers and other shell components . . . . .	7
3.2.	Nanoemulsions of gas-dissolving perfluorocarbons . . . . .	8
3.3.	Perfluorocarbon-stabilized injectable micro- and nanobubbles that respond to ultrasound . . . . .	9
3.4.	Perfluorocarbon nanoemulsions that phase-change into microbubbles . . . . .	12
3.5.	Further medically-oriented, PFC-based oxygen-carrying colloids . . . . .	13
3.5.1.	Reverse and multiple emulsions . . . . .	13
3.5.2.	PFC-loaded nanoparticles and matrices . . . . .	14
3.5.3.	Interconnected and nested colloids . . . . .	14
3.5.4.	Polymer micelles and nanoparticles with perfluoroalkylated or arylated components . . . . .	16
3.6.	Functionalization and targeting of perfluorocarbon colloids . . . . .	17
4.	Oxygen delivery by PFC nanoemulsions . . . . .	18
4.1.	Basics of oxygen transport and delivery by perfluorocarbon nanoemulsions . . . . .	18
4.2.	Development status of O <sub>2</sub> -carrying PFC nanoemulsion products . . . . .	18
4.3.	Further demonstration of oxygen delivery efficacy by PFC nanoemulsions . . . . .	19
4.3.1.	Protecting and salvaging tissues from hypoxia . . . . .	19
4.3.2.	Enabling oxygen-dependent cancer therapies . . . . .	20
4.3.3.	Regenerating bones, nerves, and engineering tissues . . . . .	21
4.3.4.	Preserving isolated organs and tissues . . . . .	22
5.	The O <sub>2</sub> microbubble delivery option—a change in paradigm . . . . .	22
5.1.	Injectable PFC-stabilized micro- and nanobubbles . . . . .	22
5.2.	Microbubbles generated through acoustic nanoemulsion droplet vaporization . . . . .	23
6.	O <sub>2</sub> delivery by further PFC-based colloids . . . . .	23
7.	Perfluorocarbon colloids can also deliver other gases, contrast, energy, drugs, genes, and have a clear vocation for theranostics . . . . .	25
7.1.	Delivery, or removal, of therapeutic gases other than oxygen . . . . .	25
7.2.	<sup>19</sup> F MRI, ultrasound and multimodal imaging for diagnosis of disease, guidance for procedure, assessment of treatment outcome . . . . .	26
7.3.	Controlled delivery and channeling of therapeutic energy . . . . .	27
7.4.	Delivery of drugs, genes, tracers, nanoparticles, cells . . . . .	28
7.5.	Pulmonary, ophthalmic and other applications . . . . .	28
7.6.	A vocation for theranostics . . . . .	29
8.	Prospects . . . . .	29
	Declaration of Competing Interest . . . . .	31
	Acknowledgments . . . . .	31
	References . . . . .	31

## 1. Introduction

Once the flagship of medically-dedicated perfluorocarbon (PFC) research, and catching most of the limelight, oxygen-carrying PFC nanoemulsions, the so-called “blood substitutes”, have so far not met expectations. No satisfactory injectable O<sub>2</sub>-delivering product has yet reached the marketplace. By contrast, another primary endeavor in medically-oriented PFC research, that is, the development of contrast-enhancing agents for diagnostic imaging, has been more successful. Several products have been licensed for use as contrast agents for ultrasound (US) imaging, as well as for ophthalmology and for in vivo cell tracking. The search for O<sub>2</sub>-delivering therapeutics

has, however, not been forsaken. Further colloidal PFC products, including nanoemulsions (NEs), microbubbles (MBs) and phase-shift nanoemulsions (P-SNEs) (Scheme 1), are undergoing clinical investigations for O<sub>2</sub> delivery, in particular for O<sub>2</sub>-dependent cancer radiotherapy, chemotherapy and photodynamic therapy. Concurrently, further PFC-based products are undergoing clinical trials for molecular imaging diagnosis of liver, breast, ovarian, prostate and colon cancers; guidance for surgical procedures; enhancement of immunotherapy; ablation of uterine fibroids; treatment of allergic asthma; treatment of smoke inhalation injury; delivery of drugs to the brain, as for management of brain tumors and neurodegenerative diseases, and assessment of treatment efficacy.



**Scheme 1.** Injectable PFC colloids most investigated in medicine: nanoemulsion (NE) droplets, phase-shift emulsion (P-SNE) droplets, and microbubbles (MBs). While for emulsions, the liquid PFC operates as an O<sub>2</sub> solvent, in MBs the primary role of the PFC gas is to stabilize the MB, which represents a drastic shift in paradigm and provides an alternative option for O<sub>2</sub> delivery: the direct administration, instead of O<sub>2</sub>-loaded PFC nanodroplets, of PFC-stabilized O<sub>2</sub> MBs. P-SNEs, when activated by heat, ultrasound, laser light or other forms of energy, turn into PFC-stabilized MBs. Re-condensation into NE droplets can be achieved by pressurizing and/or cooling.

Starting with a critical assessment of a problematic Phase III trial of *Oxygent* (Alliance Pharmaceutical Corp., San Diego, CA), an O<sub>2</sub>-carrying PFC NE product, in cardiac surgery, this short review will present PFC-based colloids that are, or may be, used for O<sub>2</sub> delivery. It will insist on the critical question of PFC selection and NE design and fabrication, highlight recent advances in the field and progress in our understanding of PFC behavior at fluid interfaces. After a brief reminder of the basics of PFC NE-based O<sub>2</sub> transport and delivery, it will expose further demonstration of their capacity to deliver O<sub>2</sub> to tissues in various circumstances. We will then discuss alternative O<sub>2</sub>-delivery options that rely on the administration of PFC-stabilized injectable MBs or on MBs generated *in vivo* by vaporization of P-SNEs, as well as on other colloids and scaffolds that involve PFCs or other highly fluorinated components. We will also allude to other emerging PFC-based procedures and indications that are being investigated for diagnostic, therapeutic and theranostic purposes, embracing contrast imaging, cell tracking, controlled delivery of energy and of therapeutics, including across the blood-brain barrier. Even when developed for other purposes, these products possess a definite O<sub>2</sub> carrying capacity and the knowledge acquired in their investigation could benefit to O<sub>2</sub> carrier development. Finally, the Prospects section will highlight some critical issues, desirable developments, and offer some opinions about the development of PFC-based O<sub>2</sub> delivery products. The paper's organization is further detailed in the Table of Content.

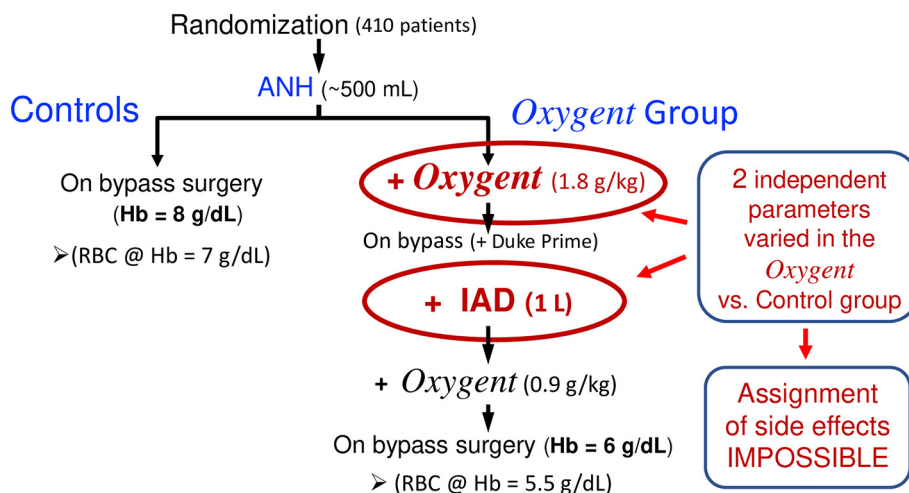
Citations are leaning towards recent reviews from which numerous earlier papers can be retrieved. The italicized prefix *F*- conventionally signifies perfluoro. *F*-colloids will refer to colloids comprising highly fluorinated components. Recourse to acronyms will be minimized. Commercial PFC-based product names are in *italics*.

## 2. An inconclusive clinical trial

PFC-based oxygen carriers have suffered a serious drawback when Alliance Pharmaceutical Corp. closed its operations subsequent to a failed clinical study. The development of the most advanced PFC nanoemulsion of that time, *Oxygent* AF0144, a phospholipid-shelled 60% w/v *F*-octylbromide (C<sub>8</sub>F<sub>17</sub>Br **3**) emulsion comprising a small fraction of *F*-decylbromide (C<sub>10</sub>F<sub>21</sub>Br **4**, 2%) for stabilization against Ostwald ripening [1,2], was interrupted in 2001 when a Phase III study in coronary artery bypass graft surgery patients showed a higher incidence of adverse neurologic and bleeding events in the test group versus control patients [3].

A previous Phase III clinical study in general surgery had established that *Oxygent* effectually reversed physiological transfusion triggers and diminished the need for transfusion of allogeneic red blood cells (RBCs) [4,5]. The *Oxygent*-treated patients remained stable and were adequately oxygenated at substantially lower hemoglobin (Hb) levels than the control patients; no major safety issues were reported. In cardiac surgery, an earlier Phase II study had indicated that *Oxygent*-treated patients could tolerate a greater amount of preoperative autologous blood harvesting and that the procedure tended to reduce or avoid allogeneic blood transfusion [5,6].

The failure of the subsequent cardiac surgery Phase III study was essentially due to a flawed clinical protocol that, by design, could not be conclusive. Indecisiveness was indeed inscribed in the protocol design (Scheme 2) because two independent parameters that affected the test patients and control patients differently were varied simultaneously [3,7]. Both patient groups first underwent autologous normovolemic hemodilution (ANH), but the *Oxygent* patients i) then received a first dose of the test material, while the controls did not, and ii) also underwent a *rapid additional* one-liter blood withdrawal (or intraoperative autologous donation, IAD), which the control group did not incur, thus creating a double imbalance between the two groups. Consequently, this protocol design made it impossible to allocate any observed higher incidence of untoward effects to the test material or to the additional large and rapid blood harvesting procedure solely incurred by the *Oxygent* patient group. Although the overall rates of adverse events were within expectations or lower than those reported in the literature, they were higher in the *Oxygent*-treated patients than in the control patients, leading to voluntary suspension of the trial [3]. These results should draw attention on the protocol that may have involved too rapid and too aggressive autologous blood harvesting, resulting in hypotension and hypoxia in critical organs, including the brain. At the time of the studies, PFC-augmented ANH was considered as rather safe [6,8]. However, the efficacy of mild ANH has been questioned [9], whilst deep ANH exposes the patient to low Hb levels that may not be well tolerated by some patients [10]. Hemodilution during cardiopulmonary bypass was since reported to cause neurologic injury in rats [11]. An independent direct association was also found between degree of hemodilution during cardiopulmonary bypass surgery and increased risk of perioperative stroke [12]. Greater decline in cognitive function was observed with elderly patients, for whom extreme hemodilution is thus not advisable [13]. The severe hemodilution



**Scheme 2.** Schematic representation of the study protocol (intraoperative phase) of a Phase III clinical trial of *Oxygent* in coronary artery bypass graft surgery patients. Both *Oxygent* and Control patients first underwent acute normovolemic hemodilution (ANH). Then, in contrast with the control patients, the test patients received both a dose of *Oxygent*, and underwent an additional blood withdrawal (intraoperative autologous donation, IAD), which reduced their hemoglobin (Hb) level to only 6 g/dL. Two independent variables (circled and squared area) were thus changed simultaneously in the control vs. test group, therefore forbidding assignment of any untoward effect to either product or protocol. Hence, no causal link can be drawn between the observed bleeding and neurologic effects and PFC emulsion. Adapted from [7].



**Table 1**  
PFC properties useful for diagnostics and therapeutics.

o Thermal stability and chemical inertness	o High bioacceptance
o High gas solubilities and transport capacity	o No metabolism, pulmonary excretion
o Extreme hydrophobicity, and hence, low water solubility, associated with strong lipophobicity	o Heat transfer capacities, cooling agents
o High propensity for self-segregation	o Functional fluids for mechanical and acoustic pressure transmission
o High volatility/low Bp relative to MW	o Can have a positive spreading coefficient
o High density and compressibility	o Magnetic susceptibility close to tissues'
o Low surface tension	o <sup>19</sup> F MRI, most sensitive nucleus after <sup>1</sup> H
o Low dielectric constant and refractive index	o Absence of <sup>1</sup> H
o Low viscosity	o Radiopaque, e.g. if brominated

Outstanding properties and combinations of properties provide a unique toolbox for delivery of O<sub>2</sub>, energy, contrast, drugs, genes and other therapeutics.

used in the *Oxygent* trial may likely have constituted an independent risk of adverse neurologic outcome [14].

Subsequent analysis of all available clinical data concluded that excessive and too rapid hemodilution, rather than *Oxygent* administration, was the likely cause of, or primary contributor to the observed imbalance in adverse effects [3,15]. In other words, the clinical testing protocol, rather than the O<sub>2</sub> carrier, is probably responsible for these effects. It is noteworthy that the rate of untoward effects was also associated with a lower familiarity of surgical teams with the ANH procedure and with an inadequate management of blood pressure during rapid blood harvesting. The clinical data signpost the combined ANH and excessive and rapid IAD as an inappropriate procedure. The procedure was subsequently discouraged for patients with coronary or pulmonary disease [10]. No evidence was found that linked the imbalance in side effects to the emulsion. No perturbation of hemostasis, viscosity or tendency for coagulation was induced by the colloidal product that could be relevant to bleeding and neurologic events [7]. Altogether, this means that the too often repeated statement that the neurologic side effects seen during that trial were due to the product is, as of now, unfounded. Although the regulatory institutions (FDA and EMEA) did not object to resuming the *Oxygent* trials, the Company's financial situation did not allow it.

This setback did not preclude research and development of PFC-assisted diagnostic, therapeutic and theranostic procedures and nanomedicines from taking momentum in multiple areas. An effective, safe oxygen delivery system is still needed, including as a bridge to blood transfusion in case of emergency, trauma or shock; for treatment of ischemia related to myocardial infarction and stroke; for perioperative organ protection; potentiation of O<sub>2</sub>-dependent cancer therapies (e.g. radio-, chemo-, immunotherapies); regeneration of damaged tissues; preservation of isolated organs; and beyond. Many more PFC-related opportunities have emerged that do not aim primarily at O<sub>2</sub> delivery but could also serve for O<sub>2</sub>-delivery or co-delivery applications.

### 3. The perfluorocarbon colloids at work

Intravascular administration of PFCs requires their dispersion as injectable aqueous formulations. The colloids used in nanomedicines for O<sub>2</sub> delivery (Sections 3–6) and other purposes (Section 7) consist primarily of NEs, MBs, and P-SNEs (Scheme 1). The latter involve liquid NE droplets that can be converted in vivo into gas MBs upon activation (vaporization) by heat, sound or light. Further colloids intended for biomedical use that can carry and deliver O<sub>2</sub> include reverse water-in-PFC emulsions, multiple emulsions, highly fluorinated polymeric micelles, and various types of PFC-loaded nanoparticles (NPs) and scaffolds (Section 6).

#### 3.1. The key components—their selection is a critical step

Selection of suitable PFCs and other colloid components, of their chemical structure, molecular weight (MW), purity, physical and biological characteristics, is a critical step in any investigation or development endeavor involving PFC colloids and depends decisively

on their intended use (Tables 1–3). PFC selection largely determines colloid stability, effectiveness, safety, practical developability, regulatory approval, and commercial success. Product consistency, current good manufacturing practices (cGMP) and quality control need to comply with regulations and will condition the acceptability of the drug product. Thorough pharmacokinetics (adsorption, distribution, metabolism and excretion) and pharmacodynamics (mechanism of action, biochemical and physiological dose-responses to drug, beneficial and adverse) studies are mandatory. Neglecting these rungs may nurture difficulties further along, from experimental data reproducibility and interpretation to sub-optimal patient care. As a result, clinical translation may be compromised and regulatory hurdles anticipated.

#### 3.1.1. Selecting the perfluorocarbon

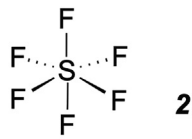
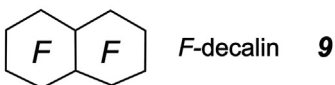
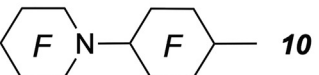
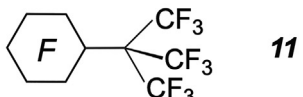
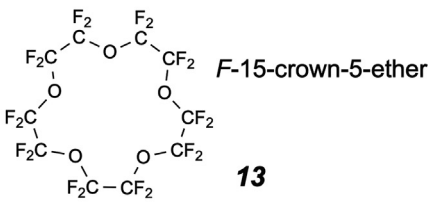
Perfluorocarbons form a vast family of man-made molecules that offer unique combinations of physical, chemical and biological properties, including high gas-dissolving capacity, volatility, density, compressibility and heat-transfer capacity; extreme hydrophobicity, distinctively coupled with marked lipophobicity; low surface tension, magnetic susceptibilities that can match those of tissues; high <sup>19</sup>F nuclei concentration and absence of protons (Table 1). These features are associated with excellent thermal, chemical and biological inertness, including absence of metabolization [2,16–20]. The chemistry of PFCs is much simpler than that of hemoglobin and can be precisely controlled, especially for linear PFCs [1,21]. The PFCs used for medical purposes should be clearly distinguished from *F*-alkylated surfactants (next sub-section).

Our basic understanding of PFC behavior at interfaces and in dispersed self-assemblies has progressed significantly [2,7,22–25]. PFCs were found, quite unexpectedly, to exercise co-surfactant activity in phospholipid films [26–28]. PFCs are partly soluble in phospholipid monolayers, especially when light or lipophilic, and can modify their properties [29–31]. The amount of *F*-hexane present in phospholipid monolayers has been quantified by neutron reflectometry [32]. A trans-membrane fluorine/fluorine recognition interaction has been discovered that has implications for drug loading and delivery [23,33–35]. More basically, it has been recognized that a PFC present within a colloid can no longer be viewed as forming an entirely separate inert phase, but needs now to be considered as an active component that can exercise its influence well beyond and even across interfacial boundaries (Fig. 1). The notion that, PFCs being inert, any interactions with cells and tissues are solely with the colloid's shell, is no longer valid.

The earliest commercial PFC NE-based injectable O<sub>2</sub>-carrying product, *Fluosol* (based on a mixture of *F*-decalin **9** and *F*-tripropylamine **6**; Green Cross Corp., Japan) was approved by the FDA in 1989 for reducing tissue ischemia in high-risk transluminal coronary balloon angioplasty, but could not achieve commercial success, largely because, prior to use, it required a complicated and cumbersome, multi-step thawing and reconstitution procedure involving three separate packages, one of which, the stem emulsion, had to be shipped and stored in the frozen state.

The criteria for PFC selection for NE products have since been periodically reassessed and refined [1,2,36]. Relevant properties can indeed

**Table 2**  
Perfluorochemicals and fluorosurfactants frequently used in medical fluorinated colloid design.

$F$ - $n$ -alkanes $C_nF_{2n+2}$ <b>1</b>	$n = 3$ : $F$ -propane $n = 4$ : $F$ -butane $n = 5$ : $F$ -pentane $n = 6$ : $F$ -hexane $n = 8$ : $F$ -octane		<b>2</b> Sulfur hexafluoride
$C_8F_{17}Br$	$F$ -octylbromide	<b>3</b>	
$C_{10}F_{21}Br$	$F$ -decylbromide	<b>4</b>	
$ClC_8F_{16}Cl$	$F$ - $\alpha,\omega$ -dichlorooctane	<b>5</b>	
$N(C_3F_7)_3$	$F$ -tripropylamine	<b>6</b>	
$N(C_4F_9)_3$	$F$ -tributylamine	<b>7</b>	
$C_4F_9CH = CHC_4F_9$	<b>8</b>		
$R[CF_2CF_2O]_nR'$	$F$ -poly(ethylether)	<b>12</b>	
$C_nF_{2n+1}C_mH_{2m+1}$ $F$ -(alkyl)alkane ( $F_nH_m$ diblock)	<b>14</b>		
$C_nF_{2n+1}(CH_2)_mOP(O)[N \text{ (cyclohexane ring) } O]_2$	$F$ -(alkyl)alkyl dimorpholinophosphate	<b>15</b>	
$C_7F_{15}C(O)NH(CH_2)_3N(O)(CH_3)_2$	$F$ -alkylated nitric oxide	<b>16</b>	
$F-(CF_2CF_2)_{3-8}-[CH_2CH_2O]_y-H$	(Zonyl FSO)	<b>17</b>	
$F-[CF(CF_3)CF_2O]_n-CF(CF_3)COOH$	(Krytox 157FS)	<b>18</b>	
$C_3F_7O-[CF(CF_3)CF_2O]_n-CF(CF_3)C(O)NH-[CH_2CH_2O]_m-CH_2CH_2NHC(O)CF(CF_3)-[OCF_2CF(CF_3)]_n-OC_3F_7$	<b>19</b>		
$C_3F_7O-[CF(CF_3)CF_2O]_n-CF(CF_3)C(O)N \begin{cases} CH[CH_2OCH_2CH(OH)CH_2OH]_2 \\ CH[CH_2OCH_2CH(OH)CH_2OH]_2 \end{cases}$	<b>20</b>		
$C_8F_{17}-CH_2-CH_2-CH_2-NH-CO-NH-[CH_2CH_2]_9-CO-NH-CH_2-CH_2-[O-CH_2-CH_2]_n-O$	<b>21</b>		
			
			
			
			

differ substantially among PFCs, including within a homologous series, as they are often highly sensitive to MW. For any in vivo use, PFCs should be pure and well defined in terms of molecular composition, which depends greatly on synthetic procedure. When used parenterally, their organ retention half-life should be limited to a few days. Industrial production feasibility in better than 99% purity on a large scale at a reasonable cost is needed. The PFC must also be amenable to production of stable, highly reproducible small-sized narrowly dispersed heat-sterilizable and easily scalable NEs. Frozen storage or need for any reconstitution procedure in the operating theater is hardly acceptable.

The tetrafluoroethene telomerization route can achieve the required degree of purity for linear PFCs and also benefits from easy scalability. Linear PFCs have a non-negligible advantage over cyclic ones of comparable MW in term of  $O_2$  solubility (e.g. 50 vol% for  $F$ -octylbromide **3** vs. 40 vol% for  $F$ -decalin **9** at 25 °C) [1]. Notably,  $CO_2$  solubility is always much larger than  $O_2$  solubility. The organ retention half-life of PFCs, a critical selection parameter, is primarily correlated, and increases exponentially with their MW (e.g., for the same dose,  $F$ -decalin **9**, MW 462: ~7 days;  $F$ -tripropylamine **6**, MW 521: ~65 days;  $F$ -tributylamine **7**, MW 671: over 2 years). Organ retention can be effectually lessened by

**Table 3**  
Selected physical properties of frequently used perfluorochemicals in medical colloids.

Compound	<i>F</i> -pentane	<i>F</i> -hexane	<i>F</i> -octane	<i>F</i> -octylbromide	<i>F</i> -decalin (cis + trans)	<i>F</i> -tripropylamine	<i>F</i> -tributylamine	<i>F</i> -15-crown-5-ether
Formula	C <sub>5</sub> F <sub>12</sub>	C <sub>6</sub> F <sub>14</sub>	C <sub>8</sub> F <sub>18</sub>	C <sub>8</sub> F <sub>17</sub> Br	C <sub>10</sub> F <sub>18</sub>	N(C <sub>3</sub> F <sub>7</sub> ) <sub>3</sub>	N(C <sub>4</sub> F <sub>9</sub> ) <sub>3</sub>	(CF <sub>2</sub> CF <sub>2</sub> O) <sub>5</sub>
MW (g mol <sup>-1</sup> )	288	338	438	499	462	521	671	580
Molar volume (cm <sup>3</sup> mol <sup>-1</sup> )	177	201	253	261	238	285	381	–
Boiling point (°C)	28–30	58–60	99–106	143	140–143	131	178	145
Density (g cm <sup>3</sup> , 25 °C)	1.59	1.68	1.73	1.92	1.94	1.74	1.88	1.78
Saturated vapor pressure (10 <sup>3</sup> Pa, 25 °C)	85 <sup>a</sup>	27–29 <sup>a</sup>	5 <sup>a</sup>	1.4 <sup>b</sup>	1.9 <sup>b</sup>	1.4	0.2	–
Water solubility (mol L <sup>-1</sup> )	4.0 10 <sup>-6</sup> <sup>a</sup>	2.7 10 <sup>-7</sup> <sup>a</sup> (25 °C)	3.8 10 <sup>-9</sup> <sup>a</sup> (25 °C)	5 × 10 <sup>-9</sup> <sup>b</sup>	10 × 10 <sup>-9</sup> <sup>b</sup>	2.8 × 10 <sup>-10</sup> <sup>a</sup>	–	–
O <sub>2</sub> solub. (vol%, 25 °C)	54 (est.)	70.0	52.1 <sup>c</sup>	52.7 <sup>c</sup>	40.3 <sup>c</sup>	45.3 (37 °C) <sup>d</sup>	33.2–38 <sup>d</sup>	–
CO <sub>2</sub> solub. (vol%, 25 °C)	–	156	–	210 <sup>c</sup>	142 <sup>c</sup>	166 (37 °C) <sup>d</sup>	127–152 <sup>d</sup>	–
CST <sub>hex</sub> (°C) <sup>e</sup>	–	5	20	–20	22	32	60	–
Organ T <sub>1/2</sub> (days) <sup>e,f</sup>	1.8–2.5 min <sup>g</sup>	~8 h (est.)	~3 (est.)	~4	6–7	65	900	–

<sup>a</sup> [39].

<sup>b</sup> [1].

<sup>c</sup> [40].

<sup>d</sup> [41].

<sup>e</sup> Estimated using [38].

<sup>f</sup> [36].

<sup>g</sup> [42].

conferring some lipophilic character to the PFC (as reflected by a reduction of its critical solution temperature in hexane or increased solubility in olive oil). This was achieved by introducing a polarizable bromine atom as in *F*-octylbromide (MW 499), thus reducing its organ half-life to 3–4 days in humans (for a 2.7 g/kg dose). Similar lipophilic character is obtained with *F*-octyl ethane, C<sub>8</sub>F<sub>17</sub>C<sub>2</sub>H<sub>5</sub> **14** ( $n = 8, m = 16$ ) or by introducing two chlorine atoms, as in *F*- $\alpha,\omega$ -dichlorooctane **5**. The PFCs most frequently used for medical purposes are collected in Table 2 and some of their physical characteristics provided in Tables 3 and 4. Eventually, only a very small number of PFCs were found eligible for intravascular O<sub>2</sub> delivery [1,2,37,38].

*F*-octylbromide (PFOB, perflubron, **3**) stands out among PFCs for medical uses. It provides a good compromise in terms of excretion rate, O<sub>2</sub> and CO<sub>2</sub> solubilities, capacity for forming stable NEs and cost-effective high-purity industrial feasibility. The very low equilibrium interfacial tension with water that can be reached in the presence of egg phospholipids, near 1 mN m<sup>-1</sup> [47], heightens phospholipid-based NE stability. Additionally, its radiopaque bromine atom provides contrast for diagnostic radiography, and its positive spreading coefficient (2.7 mN m<sup>-1</sup>) is advantageous in pulmonary applications.

The perfluorochemicals selected for preparing MBs and P-SNEs are generally the short volatile *F*-alkanes (C<sub>*n*</sub>F<sub>2*n*+2</sub>,  $n = 3$  to 6, **1**), several

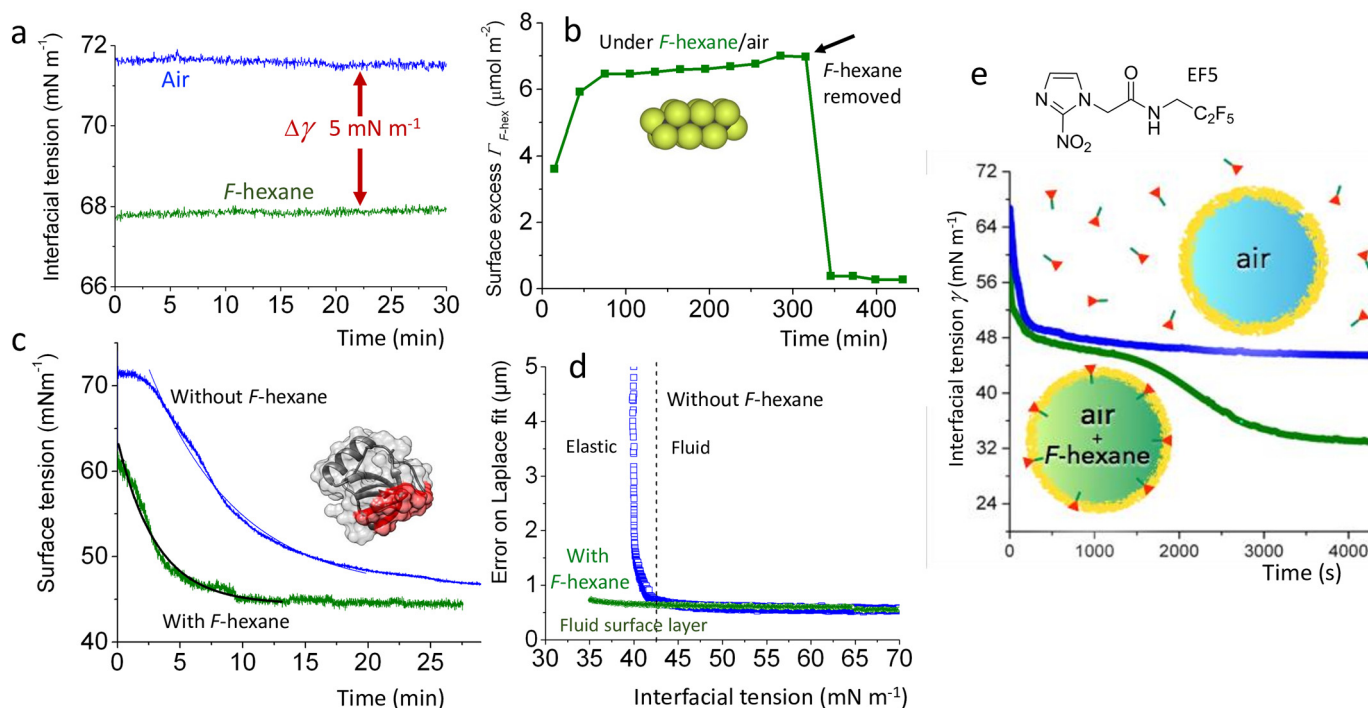


**Fig. 1.** Exposure to a PFC gas can impact colloid shell structure and properties, as demonstrated on interfacial film studies. a) *F*-hexane is surface active, reduces air/water interfacial tension (bubble shape analysis tensiometry); b) its surface excess is  $\sim 6 \mu\text{mol m}^{-2}$ , as measured by neutron reflectometry; c) it accelerates the diffusion of film-forming protein hydrophobin HFB II at the air/water interface; d) it can erase the fluid/elastic phase transition, thereby fluidizing the interfacial protein film; e) *F*-hexane can also help recognize, recruit and immobilize hydrophilic species, here a hypoxia biomarker (EF5), across an interfacial phospholipid monolayer. Adapted from a) [27], b) [32,35], c-d) [33] and e) [23].

**Table 4**  
Selected physical properties of frequently perfluorochemicals in their gas phase.

Compound	Sulfur hexafluoride	F-propane	F-butane	F-pentane	F-hexane
Formula	SF <sub>6</sub>	C <sub>3</sub> F <sub>8</sub>	C <sub>4</sub> F <sub>10</sub>	C <sub>5</sub> F <sub>12</sub>	C <sub>6</sub> F <sub>14</sub>
MW (g mol <sup>-1</sup> )	146	188	238	288	338
Molar volume (cm <sup>3</sup> mol <sup>-1</sup> )	64	145	153	177	201
Boiling point (°C, 1 atm)	-68 (subl.)	-36 to -39	-1.7	28-30	58-60
Density (g cm <sup>-3</sup> )	1.37 <sup>a</sup>	1.35 <sup>b</sup>	1.52	1.59	1.69 <sup>c</sup>
Saturated vapor pressure (10 <sup>3</sup> Pa, 25 °C)	2.24 × 10 <sup>3</sup> (20 °C) <sup>a</sup>	0.98 × 10 <sup>3</sup> (29 °C) <sup>b</sup>	2.6 × 10 <sup>2d</sup>	85 <sup>d</sup>	27-29 <sup>d</sup>
Saturated vapor concentration (25 °C, mol m <sup>-3</sup> )	-	535 (30 °C) <sup>b</sup>	105.6 <sup>d</sup>	34.14 <sup>d</sup>	11.66 <sup>d</sup>
Water solubility <sup>e</sup> (mol m <sup>-3</sup> )	-	-	0.021 <sup>d</sup>	4.0 × 10 <sup>-3 d</sup>	2.7 × 10 <sup>-4 d</sup>
Ostwald coefficient <sup>e</sup> (C <sub>water</sub> /C <sub>gas</sub> )	5.4 × 10 <sup>-3</sup>	5.2 × 10 <sup>-4</sup>	2.02 × 10 <sup>-4</sup>	1.17 × 10 <sup>-4</sup>	2.3 × 10 <sup>-5</sup>
Diffusivity coefficient in water <sup>e</sup> (m <sup>2</sup> s <sup>-1</sup> ) <sup>*</sup>	1.2 × 10 <sup>-9</sup>	7.45 × 10 <sup>-10</sup>	6.9 × 10 <sup>-10</sup>	6.3 × 10 <sup>-10</sup>	5.8 × 10 <sup>-10</sup>
Permeability through a shell (m s <sup>-1</sup> ) <sup>e**</sup>	8.7 × 10 <sup>-6</sup>	1.2 × 10 <sup>-6</sup>	2.57 × 10 <sup>-7</sup>	9.04 × 10 <sup>-8</sup>	4.44 × 10 <sup>-8</sup>

<sup>a</sup> [43].<sup>b</sup> [44].<sup>c</sup> [45].<sup>d</sup> [39].<sup>e</sup> [46].<sup>\*</sup> Diffusivity of air in water: 2.05 × 10<sup>-9</sup> m<sup>2</sup> s<sup>-1</sup>.<sup>\*\*</sup> Permeability of air through the shell: 2.857 × 10<sup>-5</sup> m s<sup>-1</sup>.

of which are gaseous at room or body temperature, or sulfur hexafluoride, SF<sub>6</sub> **2**, which has a comparably dense fluorine covering and properties similar to those of C<sub>2</sub>F<sub>6</sub> and C<sub>3</sub>F<sub>8</sub>. F-pentane is commonly used because its boiling point (29 °C) is close to body temperature. Partially hydrogenated PFCs (e.g. 2H,3H-decafluoropentane) have been proposed to help adjust the boiling point [48]. PFC mixtures, e.g. F-butane with F-pentane, should be used precociously since the lighter PFC will tend to diffuse out of a nanodroplet or microbubble faster than the heavier one, causing composition and properties to vary over time.

The rather heavy F-15-crown-5-ether **13** and F-poly(ethylethers) (R(CF<sub>2</sub>CF<sub>2</sub>O)<sub>n</sub>R' **12** (n ~ 10), with their numerous magnetically equivalent fluorine nuclei, are often selected when <sup>19</sup>F MRI is a primary objective and the injected doses are small. Bis(F-butyl)ethene **8**, which is easily produced in pure form, has an organ retention half-life comparable to that of F-decalin and a superior O<sub>2</sub> solubility [1], may also provide a valuable candidate for O<sub>2</sub> delivery. Various functional F-alkylated or F-arylated components that are being used in micelles and nanoparticles generally intended for drug delivery, also display O<sub>2</sub>-transport abilities (Sections 3.5.4 and 6).

### 3.1.2. Emulsifiers and other shell components

The most commonly used emulsifiers and shell components of medical F-colloids are pharmaceutical grade phospholipids. Many injectable NEs rely on egg yolk phospholipids, a natural mixture of phospholipids that has a long history of use in lipid emulsions for parenteral nutrition. Complementation of phospholipids with molecular fluorocarbon-hydrocarbon diblock amphiphiles (C<sub>n</sub>F<sub>2n+1</sub>C<sub>m</sub>H<sub>2m+1</sub>, FnHm **14**) provides outstanding NE stability [49,50]. Other frequently used shell constituents include proteins such as albumin (generally

heat-denaturalized), red blood cell or macrophage envelope fragments or components [51-55], and polysaccharides such as chitosan [56], dextran [57] or hyaluronic acid [58]. Synthetic polymers include poly(oxyethylene)-poly(oxypropylene)-poly(oxyethylene) triblock copolymers (poloxamers, such as *Pluronic*s) and poly(lactic-co-glycolic acid) (PLGA), which is biodegradable and FDA-approved, and silica. The latter usually provide more rigid shells or capsules. Multiple superposed coatings are also utilized [59,60]. The capacity to emulsify PFCs, stabilize PFC colloids, and other properties have been investigated for a large panoply of molecular and polymeric surfactants [17,61]. A study of the safety of poly(n-butyl cyanoacrylate)-encapsulated F-decalin uncovered several side effects and the accumulation of polymeric material in various organs [62]. Product formulation may also include electrolytes, oncotic agents and other active components. In any case, PFC formulations need to be compatible with any fluid that may be administered concurrently during treatment [63-66].

MBs, which are generally dispensed in much smaller doses than O<sub>2</sub>-carrying NEs, are commonly shelled with synthetic mixtures of phospholipids such as dipalmitoyl- and distearoylphosphatidylcholine (DPPC and DSPC), often supplemented with poly(ethylene glycol)-fitted (PEGylated) phospholipids (e.g. DSPC-PEG2000) that provide added stability and a hydrophilic coating that helps evade phagocytosis. Addition of dipalmitoylphosphatidylethanolamine (DPPE), egg phosphatidylserine, or phosphatidic acids confers negative charges to the shell. An additional emulsifier (e.g. lipopolymers such as DSPE-PEG2000) appears indispensable for MB formation [67]. An amount of ~5% of DSPE-PEG2000 was deemed optimal for DPPC MB abundance, stability and mechanical properties [68]. Span 60 (sorbitan monostearate) was also used to stabilize O<sub>2</sub> MBs [69], as well as Tween 80 (poly(oxyethylene) sorbitan monooleate) [70]. The shell

**Table 5**  
Properties and issues of PFC nanoemulsions related to PFC versus colloid shell and versus colloidal form.

Related to the PFC	Related to the shell	Related to the colloidal form
<ul style="list-style-type: none"> <li>o Linear O<sub>2</sub> vs. pO<sub>2</sub> dissolution – no bonding no saturation</li> <li>o passive delivery, instant availability</li> <li>o high extraction ratio</li> <li>o O<sub>2</sub> solubility preserved at lower temp.</li> <li>o CO<sub>2</sub> dissolution and removal ensured</li> <li>o No NO scavenging and vasoconstriction</li> <li>o Emulsion stability increases with MW</li> <li>o Organ retention increases with MW, decreases with lipophilic character</li> <li>o Diagnostic imaging (multiple <sup>19</sup>F, no <sup>1</sup>H)</li> <li>o Can dissolve highly fluorinated agents</li> </ul>	<ul style="list-style-type: none"> <li>o Contributes to stability</li> <li>o Can affect droplet size</li> <li>o Can affect rheology, mechanical prop.</li> <li>o Reduces diffusion of dissolved gases</li> <li>o Affects PFC's vaporization rate</li> <li>o Can affect in vivo recognition, intravascular persistence</li> <li>o organ distribution</li> <li>o side effects</li> <li>o Can be functionalized</li> <li>o Can be targeted to disease</li> <li>o Can host therapeutics for delivery</li> <li>o Can serve for binding other colloids</li> </ul>	<ul style="list-style-type: none"> <li>o Small sizes vs. RBC (0.1-0.3 vs. 7 μm) no extravasation, blood pool agent</li> <li>o Normally restricted to blood pool</li> <li>o Many particles - facilitates O<sub>2</sub> diffusion</li> <li>o Viscosity similar to water, plasma</li> <li>o Mechanical resistance (pumps, filters)</li> <li>o Foreign particles - RES clearance, short intravascular persistence, may activate macrophages (flu-like symptoms)</li> <li>o High yield additive production process</li> <li>o Easy large-scale manufacturing</li> <li>o Terminal heat sterilization possible</li> </ul>



formulation of P-SNEs that serve as precursors of MBs is often similar to that of MBs.

Fluorosurfactants (*F*-surfactants), which associate a highly fluorophilic and lipo- and hydrophobic *F*-alkyl tail with a hydrophilic polar head, develop the ultimate in terms of surface activity, fostering numerous industrial applications, as well as valuable “fluorous” synthesis and separation technologies [16,18,71,72]. *F*-surfactants hold a distinctive place when it comes to PFC colloid preparation [17,19,73–75]. Both molecular and polymeric *F*-surfactants (Table 2) allow production of stable NEs, MBs, reverse water-in-PFC emulsions, multiple emulsions or high internal phase ratio gel-emulsions. While use of *F*-surfactants is no longer needed for stable NE production, they are often used for preparing P-SNEs from volatile PFCs [76–78], and have so far been systematically used for reverse PFC emulsion preparation. *F*-surfactants are also relevant to colloid preparation through microfluidic procedures. Highly effective, single-molecule *F*-surfactants (e.g. **15**, **16**) have been derived from polar heads such as phosphatidyl groups, sugars, proteins and more [17,79]. Such *F*-surfactants have an outstanding propensity to segregate, self-assemble into compartmentalized colloids [80]. Polymeric *F*-surfactants fulfill numerous industrial purposes [71]. Those most frequently used for medical *F*-colloid preparation comprise a *F*-alkyl chain grafted on a hydrophilic PEG chain (e.g. *Zonyl* FSO **17**, now replaced by the *Capstone* series, e.g. *Capstone* FS-63, that features an environmentally more acceptable shorter *F*-hexyl hydrophobic chain) or a poly(*F*-propylene oxide) chain with a terminal carboxylic function (e.g. *Krytox* 157 FS **18**, Chemours, Wilmington, DE). Amphiphilic triblock PEGylated fluorinated amphiphiles **19** were used to stabilize phospholipid-shelled *F*-butane MBs [75]. *F*-surfactants **20** with poly(*F*-propylene oxide) chains and dendritic glycerol polar head groups were shown to minimize inter-droplet exchange of small encapsulated molecules [81]. *F*-surfactant **21**, with a *F*-octyl chain, a hydrocarbon spacer and a PEG chain was synthesized to stabilize cationic *F*-butane/lipid MBs [82]. Stable but large-sized Pickering-type (i.e. surface NP-stabilized) NEs of *F*-pentane, *F*-hexane, *F*-octylbromide were obtained with (*F*-octyl)ethyl grafted silica NPs [83]. When comparable in effectiveness, short molecular *F*-surfactants should likely be preferred over the less well defined, polydisperse polymeric ones. The use of long chain functional *F*-alkylated substances, which are eventually degraded into persistent *F*-alkyl acids, is now strictly regulated due to environmental concerns [84]. However, exemptions should be obtainable for medical uses when no satisfactory alternative is available, mainly because such uses only involve very small tonnages and deliver a very high benefit/risk ratio.

### 3.2. Nanoemulsions of gas-dissolving perfluorocarbons

Nanoemulsion design, formulation, stability and property control, and understanding of in vivo behavior have progressed. The core PFC, surrounding shell, and colloidal form play different roles in the colloid's overall behavior that need to be clearly differentiated (Table 5). NE droplet size and size distribution are here central parameters. Average droplet size in the currently investigated concentrated (20–60% w/v) injectable NEs is in the 0.1–0.3  $\mu\text{m}$  range, well below the  $\sim 7 \mu\text{m}$  of RBCs. Intravascular persistence, and hence  $\text{O}_2$ -carrying duration, augments when droplet size is reduced (Fig. 2). Concurrently, side effects such as the flu-like symptoms related to particle clearance from the circulation by the reticuloendothelial system diminish when droplet size diminishes [85]. A tail of large particles in the droplet size histogram should therefore be avoided [1,2].

Particle size increase over time in PFC NEs is primarily due to molecular diffusion (Ostwald ripening). The latter can easily be counteracted by adding a higher MW PFC, which, however, does not go without a sharp, soon unacceptable increase in organ dwelling time. Resolution of this catch-22 situation can again be achieved by selection of a somewhat lipophilic higher MW PFC additive. Addition of 2 w/vol% of *F*-decylbromide (organ half-life around 23 days) in a 58 w/vol%

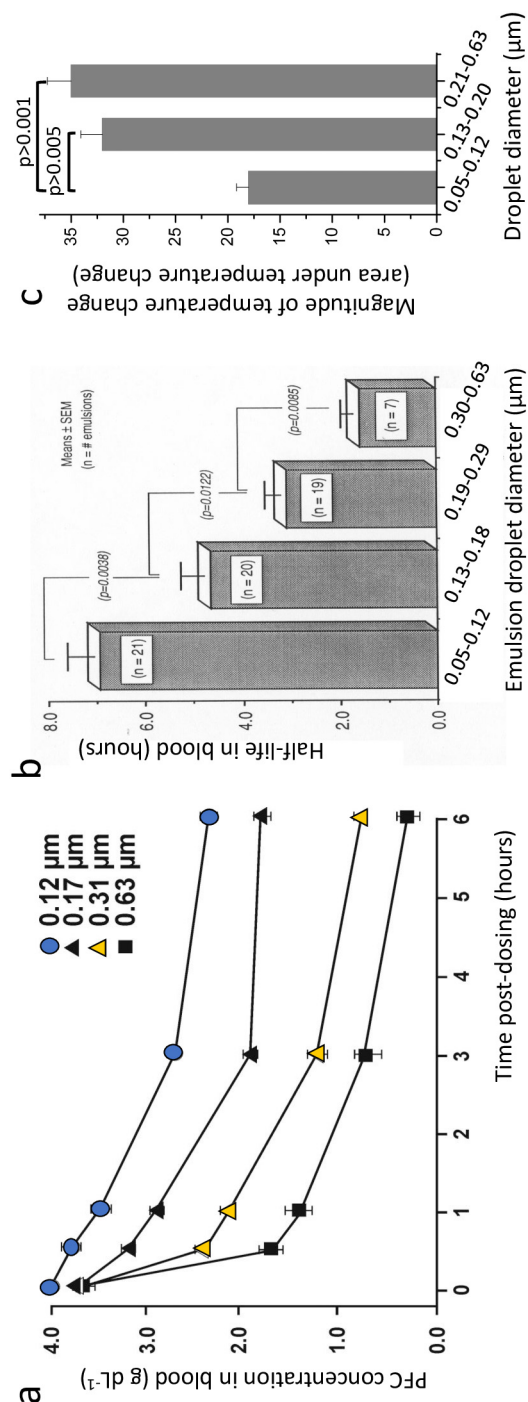


Fig. 2. Effects in rats of mean nanoemulsion droplet size on a) intravascular persistence over time; b) blood half-life; c) febrile response to NE administration (the area under the change in temperature over time curve integrates both intensity and duration). Adapted from [85].



emulsion of *F*-octylbromide solved the problem in the case of *Oxygent* [38,86].

A different approach consists in increasing the cohesion of the PFC/phospholipid interface by complementing the phospholipid emulsifier with an equimolar amount of a semi-fluorinated alkane (*F<sub>n</sub>H<sub>m</sub>*) diblock that can be envisioned as providing “molecular dowels” at the interface [22,49,50]. This approach produced NEs that withstand standard heat sterilization and forced coalescence through shaking, and proved stable for over two years at room temperature (Fig. 3). Precise control of NE droplet size could be achieved over an extended range, typically from 0.012 to 16 μm post-sterilization. Further stabilization schemes use more rigid polymeric droplet shells or capsules, which have their own advantages and limitations.

Diverse technologies can be implemented for PFC NE production. The most effective in terms of droplet size control, reproducibility and throughput rely on high-pressure, high-shear homogenizers commonly used in industry. Impinging jet devices (microfluidization) also produce quality PFC NE batches. Uniform commercial-scale terminal heat sterilization can be achieved in a rotating autoclave at 121 °C in standard conditions when the NE is stable enough to withstand these conditions. Sterilization of metastable colloidal formulations requires, however, specific knowhow, multiparameter optimization and thorough validation. Lab-scale samples are most often prepared by tip sonication, which is easy to implement but yields widespread droplet size distributions, has poor reproducibility and defies lab-to-lab comparisons. Small-capacity high-shear emulsifiers (e.g. *Emulsiflex*, Avestin, Ottawa, Canada) are available that secure much better droplet size control and reproducibility, and should be preferred for lab-size NE production.

### 3.3. Perfluorocarbon-stabilized injectable micro- and nanobubbles that respond to ultrasound

We will see (Section 5) that O<sub>2</sub> MBs can offer an alternate approach to parenteral NE-mediated O<sub>2</sub> administration. MB design, preparation and characterization have been discussed in numerous articles [67,87–108].

Naked MBs are extremely short-lived (Fig. 4). Gaseous PFCs (or SF<sub>6</sub>) were chosen as the core of MB contrast agents for US imaging because of their much lower solubility in water as compared to O<sub>2</sub> or N<sub>2</sub> (e.g. 4.0 10<sup>-6</sup> mol L<sup>-1</sup> for *F*-pentane vs. 1.2 10<sup>-3</sup> mol L<sup>-1</sup> for O<sub>2</sub>), thus extending the MBs circulatory half-life sufficiently to enable practical diagnostic examination.

When MBs containing only a PFC gas are introduced in the circulation they will absorb gases present in the blood and swell until a diffusion equilibrium is reached and the partial pressure of air in the MB equals the ambient concentration and the partial pressure of the PFC equals the joint Laplace and arterial blood pressures (Fig. 4b). To prevent in vivo swelling, MBs can be designed in which the partial pressure of the PFC exactly counterbalances the Laplace and blood pressures (Fig. 4c) thereby ensuring safe, sustained circulation [39,87,110]. This osmotic stabilization principle was applied to the development of *Imagent*, a product that was provided as spray-dried microspheres made of water-soluble hydroxyethylstarch, DMPC and a poloxamer under an atmosphere of *F*-hexane and N<sub>2</sub> in such proportions (~1/5) that the MBs formed after dissolution of the microspheres would stabilize around 3 μm in vivo and could not grow. The same principle was used to produce DSPC/DSPE-PEG2000-shelled injectable O<sub>2</sub> MBs osmotically stabilized by 5% of *F*-butane [111]. In some cases MBs of SF<sub>6</sub> or *F*-

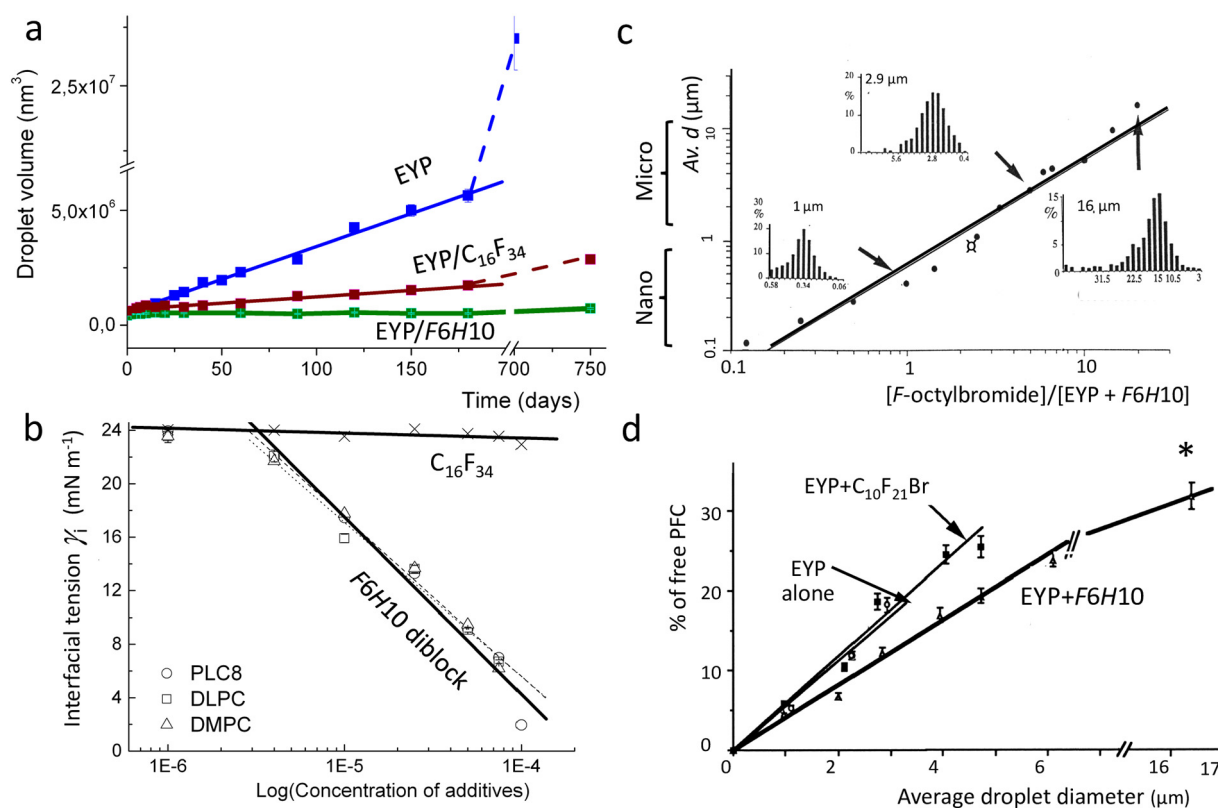


**Fig. 3.** *F*-octylbromide nanoemulsion stabilization by (*F*-alkyl)alkyl diblocks (C<sub>*n*</sub>F<sub>2*n*+1</sub>C<sub>*m*</sub>H<sub>2*m*+1</sub>, *F<sub>n</sub>H<sub>m</sub>*). a) Addition of *F6H10* diblock to egg yolk phospholipids (EYP) in equimolar amounts provides nanoemulsions that are stable for several years at room temperature (green); this stabilization approach is different and significantly more effective than the heavy PFC (C<sub>16</sub>F<sub>34</sub>, bordeaux) approach, and with EYP alone (blue); note the linear volume increase over time, characteristic of Ostwald ripening; b) *F*-octylbromide/water interfacial tension variation over concentration of added *F6H10* diblock for various phospholipids, as compared to addition of the heavy PFC C<sub>16</sub>F<sub>34</sub>; c) exquisite droplet size control is achievable over a large range of sizes (*F6H10*/EYP molar ratio is always 1); d) resistance to NE droplet coalescence through shaking is also remarkably superior with *F6H10* addition as compared to those achieved with EYP alone or with C<sub>10</sub>F<sub>21</sub>Br adjunction. Adapted from [22,50]. (For interpretation of the references to colour in this figure legend, the reader is referred to the web version of this article.)

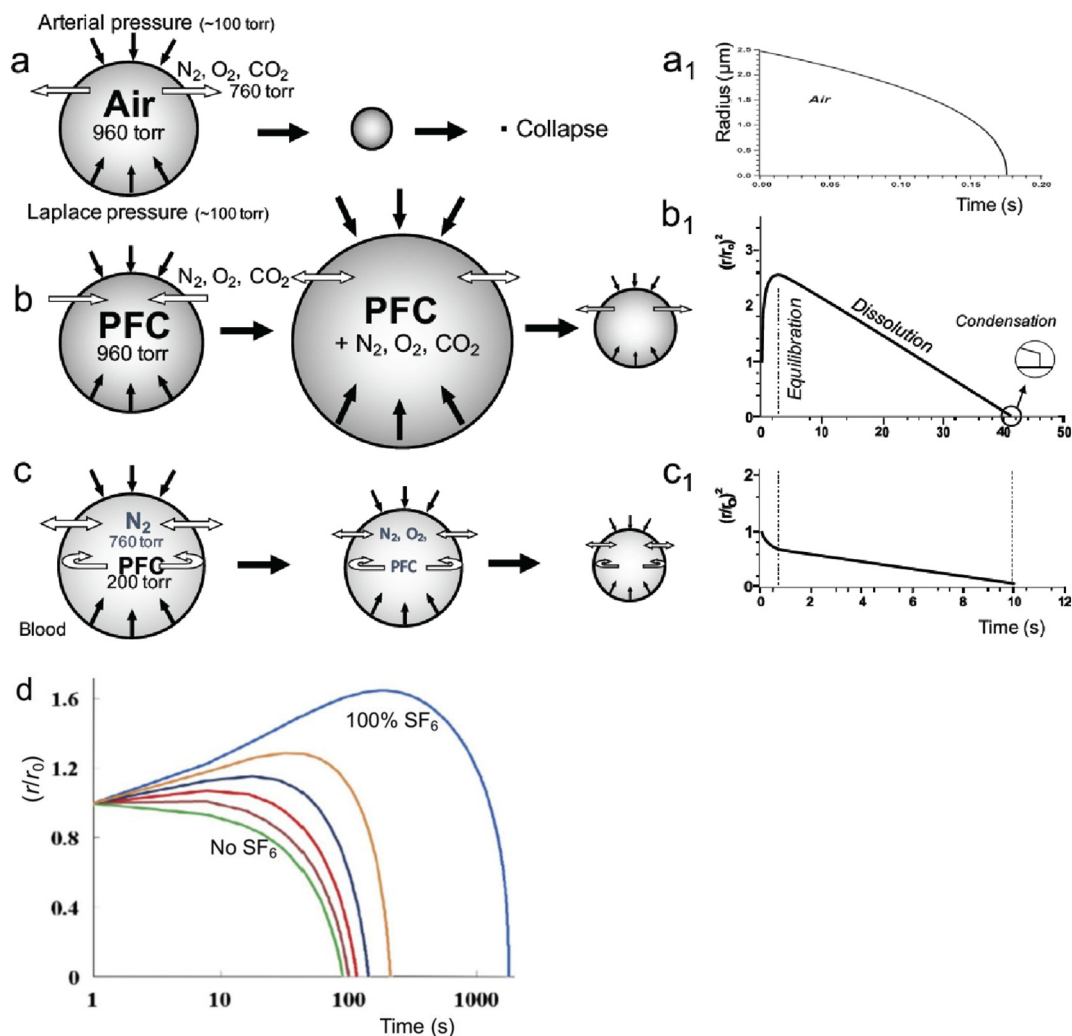


**Fig. 4.** In vivo fate in water of microbubbles of a) air; b) a PFC gas, and c) nitrogen osmotically stabilized by a PFC gas; b<sub>1</sub>-c<sub>1</sub>) calculated size change  $(r/r_0)^2$  of the MBs over time. d) Calculated variation of relative radius,  $r/r_0$ , as a function of partial pressure of SF<sub>6</sub> during dissolution of a MB coated with distearylphosphatidylcholine in air-saturated water (surface tension  $24.7 \text{ mN m}^{-1}$ , shell resistance to gas transfer  $3100 \text{ s m}^{-1}$ , shell elasticity  $8 \text{ mN m}^{-1}$ ); SF<sub>6</sub> fractions are 0 (green), 0.2 (brown), 0.4 (red), 0.6 (black), 0.8 (yellow) and 1 (blue). a-c) Adapted from [39,87]; d) from [109]. (For interpretation of the references to colour in this figure legend, the reader is referred to the web version of this article.)

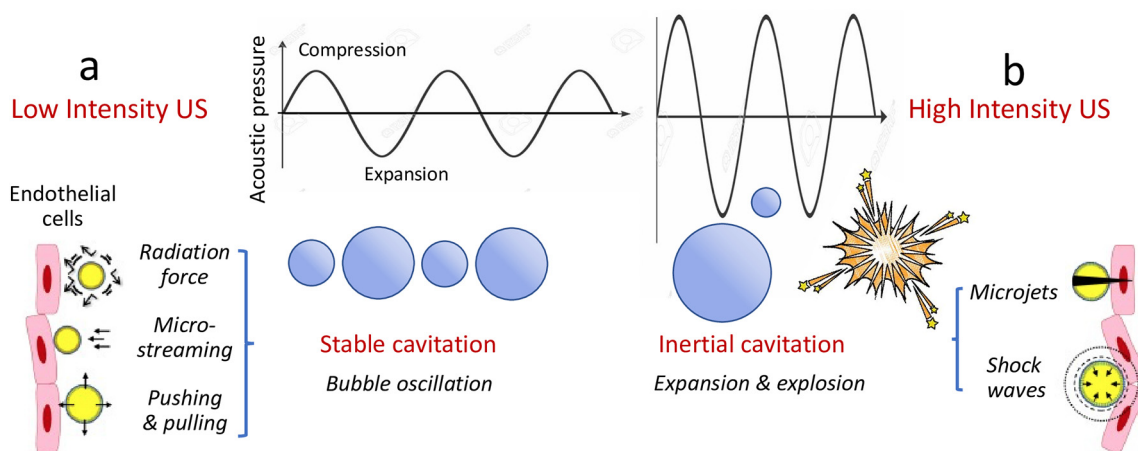
butane were formed that were subsequently sparged with O<sub>2</sub> [112,113]. Bubble dynamics in complex aqueous environments has since been modeled considering shell properties and their variations during dissolution and mass transfers between MBs [67,109,114,115], as exemplified for phospholipid shelled SF<sub>6</sub> MBs in Fig. 4d.

The shell of the MB, whether soft and resilient (e.g. phospholipids) or more rigid (polymers), also contributes greatly to MB stability and influences shell viscoelasticity, and hence, response to ultrasound. Phospholipids provide soft shells, ideal for sound reflection. Other shells involve albumin, dextran or hyaluronic acid. Acoustically active lipospheres were prepared for drug and gene delivery that are MBs, the gas core of which is surrounded by a layer of viscous hydrophobic liquid oil destined to contain a cargo and is enclosed in a phospholipid film [116]. MBs can be manipulated by US waves and emit energy in various forms, allowing various imaging modes, as well as control over O<sub>2</sub> release, thermal and mechanical energy delivery for surgical procedures, and delivery of therapeutics (Scheme 3) [117].

MBs can be obtained by sonication, extrusion, mechanical vibration/amalgamation, and other procedures [67,106,107]. Essentially all these techniques yield highly polydisperse MB populations. Subsequent population size narrowing can be achieved by flotation [93], differential centrifugation [118], pore filtration, acoustic sorting, which relies on the

size-related response to US [119], or microfluidics techniques such as pinched flow fractionation [120]. Direct preparation of narrowly sized MB populations can be attained with microfluidic procedures, including T-junction, and axisymmetric and asymmetric flow focusing [121,122], but the throughput of these techniques, although it has considerably improved [107,123], remains difficult to consider for industrial development.

All the commercial MB products approved for contrast US imaging rely on perfluorochemicals for stability. They include *SonoVue/Lumason* (Bracco Imaging, Milan, Italy), a SF<sub>6</sub>/phospholipids formulation that is now approved in 36 countries for assessment of cardiac regional wall motion, characterization of focal liver and breast lesions, evaluation of cerebral arteries, carotid and peripheral arteries, and assessment of vesico-ureteral reflux in children; *Optison* (F-propane/albumin; GE Healthcare, Princeton, NJ); *Definity/Lumivity* (F-propane/phospholipids; Lantheus, North Billerica, MA), and *Sonazoid* (F-butane/phospholipids; GE Healthcare, Amersham, UK), which is notably used in Japan for liver mass characterization. An osmotically stabilized MB product, *Imagent* (F-hexane/phospholipid; Alliance Pharm. Co.) was approved by the FDA but never marketed, a collateral victim of Alliance's debacle. These agents, which were all developed some 20 years ago, typically display an average MB size of 1–3  $\mu\text{m}$  in number, with over 99% of them below



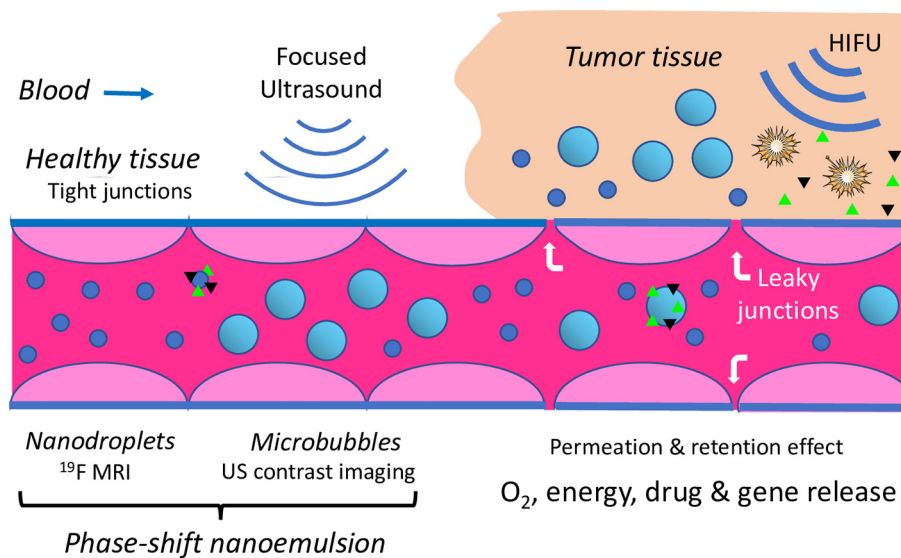
**Scheme 3.** Microbubbles in an ultrasound wave field. MBs can be manipulated by US waves, undergo a) stable or b) inertial cavitation on-demand, and emit energy in various forms, allowing different imaging modes, as well as control over O<sub>2</sub> release, thermal and mechanical energy delivery for surgical procedures, and delivery of therapeutics. Adapted in part from [117].

10  $\mu\text{m}$ , and concentrations of  $\sim 10^8$ – $10^{10}$  MB per mL [124]. Their main limitations, besides their being confined in the vascular space, include broad size distributions, short vascular half-life, usually below 5 min, absence of specificity and limited functionality. In a polydisperse MB sample, only a fraction of the bubbles is effective at a given US frequency.

A first molecular imaging agent, the vascular endothelial growth factor receptor 2 (VEGFR2)-targeted *F*-butane MB agent *BR55* (Bracco, Geneva Switzerland) has been FDA-approved in 2016 for liver mass characterization and for voiding cystourethrography in children. VEGFR2 is a key regulator of the formation of blood vessels in cancer (neangiogenesis). Further clinical studies involve detection and monitoring of treatment of prostate [125], breast and ovarian [126], colon [127] or kidney [128] cancers. More targeted MB products are available for research, such as *Visistar* (Targeson, San Diego), a VEGFR2 or vascular cell adhesion molecule 1 (VCAM-1) or integrin-targeted *F*-butane MB, and *Vevo MicroMarker*<sup>TM</sup> (VisualSonics, Toronto), a *F*-butane MB that can be streptavidin-pre-targeted, as well as various *F*-propane/lipid MBs, e.g. *USphere Labeler* (Trust Bio-sonics, Zhubei, Hsinchu, Taiwan).

These MBs have all the capacity to absorb O<sub>2</sub> dissolved in blood and carry it to the tissues. Facile manipulation by sound waves, a distinctive attribute of MBs, can produce stable or inertial cavitation, eventually leading to focused, on-demand destruction and release of content. O<sub>2</sub> release from MBs can thus be activated by exposure to US (Schemes 3 and 4) [111–113]. The characteristics of MBs oscillating in an US wave field, in particular the knowledge about MB size, gas composition, MB shell structure and rheology, stabilization mechanisms, carrier capacity, response to US wave form, frequencies, intensities and pulse sequences, development of new MB-based imaging techniques have been thoroughly discussed [90,108,129–135]. Understanding of MB interactions with cells, especially endothelial cells, and tissues has progressed considerably [87,107,108,115,136]. Specific MB tailoring for MB-assisted US therapies and the difficulties that may be encountered in clinical translation have also been considered [137].

Among the currently tackled challenges, one can cite the development of nanometer-sized bubbles (NBs), in spite of the increasing Laplace pressure that should drive them towards dissolution [60,138–140]. Advantages resulting from the sub-micrometer size



**Scheme 4.** Phase-shift nanoemulsions in vivo. P-SNEs can be turned locally into MBs under US irradiation. They can extravasate through leaky capillaries and accumulate into tumor tissue, where they can be phase-shifted into MBs. High-intensity focused US (HIFU) can then cause inertial cavitation and eventual MB disruption for focused local delivery of O<sub>2</sub>, energy and drugs (black and green triangles).

include longer half-life, easier extravasation to tumor tissue through EPR effect, and facilitated cellular uptake. NBs can be separated from MBs by centrifugation or filtration. *Pluronics* and PEGylated lipids were found effective to reduce bubble size [103,141]. Iron oxide NP-containing NBs have been prepared [142], in particular O<sub>2</sub>-loaded superparamagnetic NBs to enhance tumor oxygenation during hyperthermia [143]. Further investigation of this topic is warranted both on a theoretical basis and through experimental NB characterization. A Special Issue on “Nanodroplets and Nanobubbles” is presently being published [144].

### 3.4. Perfluorocarbon nanoemulsions that phase-change into microbubbles

Phase-shift NEs that can reversibly switch from liquid NE droplets to gaseous MBs (Scheme 1) when activated by heat, sound or light after having been positioned in target tissues currently draw considerable attention [102,130,145–160]. P-SNEs benefit from the small initial size and relatively long intravascular circulation half-life (up to a few days) of NE droplets, allowing extravasation and retention in tumor tissue (the still debated EPR effect) [161,162], and, after vaporization, acquire the responsiveness of MBs to US (resonance, inertial cavitation and destruction) needed for on-demand, site-selected delivery of O<sub>2</sub> and other therapeutics (Table 6, Scheme 4). A specific research topic is the use of P-SNEs for crossing the blood-brain barrier (BBB) [163,164].

As far as we know, all the P-SNEs investigated for medical uses rely on a phase-changing PFC core. The P-SNE shell is similar to those used for MBs, but for a more frequent use of fluorosurfactants. It can be soft and resilient, as with phospholipids, or harder as with polymers or silica. *F*-pentane P-SNEs stabilized with a dextran/poly(vinylpyrrolidone) [165] or chitosan shell [56] have been reported, as well as polydopamine-shelled *F*-hexane P-SNEs [166]. Shift from the liquid to the gas state produces a marked increase in size (typically 5-fold or more) and a huge rise of acoustic impedance, and hence, in echogenicity. Soft (e.g. lipid)- and hard (e.g. polymer)-shelled NEs can require markedly different US intensities for phase-shift, inertial cavitation and drug release [167,168]. While liquid PFC droplets have an obvious aptitude for <sup>19</sup>F MRI, their gaseous MB form is ideally suited for US imaging and manipulation by US waves. P-SNEs, upon vaporization, thus switch from <sup>19</sup>F-MRI to US contrast agents, and vice versa upon condensation. Rapid repeated phase shifts (vaporization and recondensation) led to blinking nanodevices [169,170].

P-SNE preparation usually relies on sonication, extrusion, high shear homogenization, microfluidics, as well as on condensation of microbubbles [151,156,171]. Size distributions can be adjusted as for MBs. Reversal from MB to NE can be achieved by cooling or compression, meaning that P-SNEs can be obtained from commercially available MBs that were approved for use as contrast agents [160,172–179].

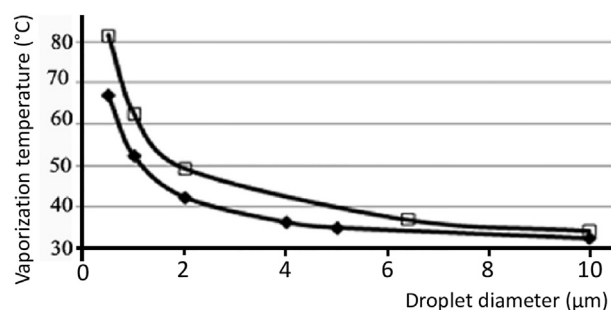


Fig. 5. Calculated effect of droplet size on *F*-pentane vaporization temperature for surface tensions of 30 and 50 mN m<sup>-1</sup> (black diamonds and open squares, respectively). Adapted from [146].

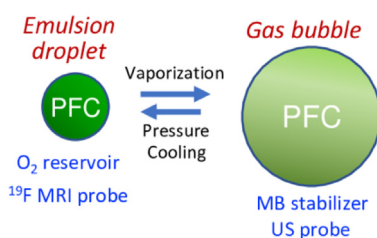
However, the much-investigated US-induced acoustic droplet vaporization (ADV) of the core PFC is a complex, multiparameter process that requires MB nucleation, depends on multiple MB, sound wave and physiologic parameters, can involve different mechanisms, and is difficult to control. [180–184] The persistence of superheated nanodroplets that remain in the liquid state at temperatures and pressures above the saturation curve cannot be explained by thermodynamics alone [151]. This suppression of nanodroplet thermal vaporization was first ascribed to Laplace pressure, which shifts the equilibrium saturation curve (Antoine's equation) to higher temperatures and lower pressures [185]. Suppressed vaporization was later assigned to the energy barrier that opposes nucleation of a vapor seed of critical size [186]. The homogenous nucleation theory accurately predicts the elevated pressures needed to condense MBs. The vaporization pressure increases as droplet size is reduced and also depends on nanodroplet shell and fluorocarbon [151,187,188]. A super-harmonic focusing effect was reported that combines two phenomena: a highly non-linear distortion of the acoustic wave and its focusing by the droplet; the larger the droplet, the stronger the focusing, which locally increases peak negative pressure and initiates vaporization [189].

Simply due to Laplace pressure the vaporization temperature of *F*-pentane NEs is expected to increase significantly when droplet size diminishes below ~4 μm (Fig. 5), causing 1 μm-size naked droplets to vaporize at over 60 °C only, versus 29 °C for bulk *F*-pentane, thus remaining in a superheated liquid state at body temperature [146]. Phase change can also be induced by ultrasound, laser light or use of small diameter injection needles [146]. Indocyanine green-loaded *F*-pentane/albumin MBs rapidly re-condensed into NE droplets when laser light activation was interrupted [150]. Even lipid-coated *F*-propane and *F*-butane NEs did not vaporize spontaneously at body temperature [190]. *F*-propane (boiling point minus 36.7 °C) droplets (condensed *Definity*) did not return spontaneously to MBs after

Table 6

Pros (left) and cons (right) of phase-shift PFC nanoemulsions.

- Small *sub-micron* size
- Long intravascular *half-life*
- Can *accumulate* in tumors (permeation & retention effect)
- *Multiple activation* modes (heat, sound, light, microwave..)
- Can be reversed
- Convert to MBs at *US- or laser-light focus*
- Ease *sonoporation* & *BBB crossing*
- Can release O<sub>2</sub>, drug cargo *on-demand*
- Low *response to US becomes high*



- Vaporization (phase shift) is a *complex, multiparameter* event
- *Requires nucleation*
- *Vaporization energy threshold needs to be minimized*
- Inertial cavitation requires considerable attention
- *Control and reproducibility* of in vivo MB size is mandatory
- *Transfer* of PFC from NDs to MBs must be minimized to avoid inflation
- Above points are safety issues



intravenous injections in pigs, but required application of acoustic power to induce vaporization [175]. On the other hand, even heavy, high boiling point PFCs such as *F*-15-crown-5-ether and *F*-octylbromide can generate MBs under US activation due to mechanisms that involve recruitment of dissolved gases, including O<sub>2</sub>, from the surroundings [146,191].

The importance of a thorough command of the phase-shift event, including equilibrium with the environment, and proper control of acoustic cavitation, cannot be emphasized enough [78,135,155,160,192]. PFCs with a relatively higher MW (e.g. *F*-hexane rather than *F*-pentane) demonstrate advantages when repeated therapeutic activation is pursued, providing higher contrast, increased drug payload and higher in vivo stability, especially for theranostics applications [193,194]. A serious safety issue with P-SNEs concerns indeed the accurate control of vaporization and the size of the resulting MBs. Prolonged myocardial opacification with a *F*-pentane emulsion was, for example, related to the formation of very large (30–50 μm in diameter) MBs, with a negative impact on hemodynamic parameters [195]. A similar *F*-pentane emulsion when used as an O<sub>2</sub> therapeutic also showed a transient increase in mean pulmonary artery pressure [196]. Size increase results not only from PFC expansion through phase change, but also involves inward osmotic recruitment of gases dissolved in the surrounding aqueous medium, as well as transfer of PFC from co-existing, not yet vaporized PFC nanodroplets. In the case of *F*-butane/phospholipid MBs such transfer from droplet to bubble was shown to cause a MB volume

inflation by several orders of magnitude, with a risk of vessel occlusion (Fig. 6) [160]. Resolution of this issue was, however, deemed possible through suitable P-SNE design, including use of less volatile PFCs and of a polymeric heat-denatured albumin shell.

No phase-shift PFC emulsion is on the market yet. An early *F*-pentane (2% w/v)/*F*-surfactant- and *Pluronic*-based P-SNE, *Echogen* (Sonos, Bothel, WA), was approved for use as a contrast agent in Europe in 1998, but was never marketed, likely because of inadequate control of phase shift in vivo. A buffered version of *Echogen*, *NVX-108* (NuvOx Pharma, Tucson AZ) is presently being investigated, including for O<sub>2</sub> delivery during treatment of cancer and stroke [197]. The *F*-surfactant utilized is a purified *Zonyl-FSO*-type fluoropolymer [198].

### 3.5. Further medically-oriented, PFC-based oxygen-carrying colloids

Further PFC-based colloids and constructs investigated for O<sub>2</sub> delivery and other biomedical purposes include reverse and multiple emulsions and gel-emulsions, porous PFC-loaded NPs and scaffolds, nested and connected colloids, in particular liposomes, and polymeric micelles that comprise *F*-alkylated or *F*-arylated moieties.

#### 3.5.1. Reverse and multiple emulsions

Reverse, water-in-PFC nanoemulsions (Scheme 5a) are mainly aimed at delivering water-soluble drugs, in particular through the pulmonary route, as with metered-dose inhalers [17,20,199–205].

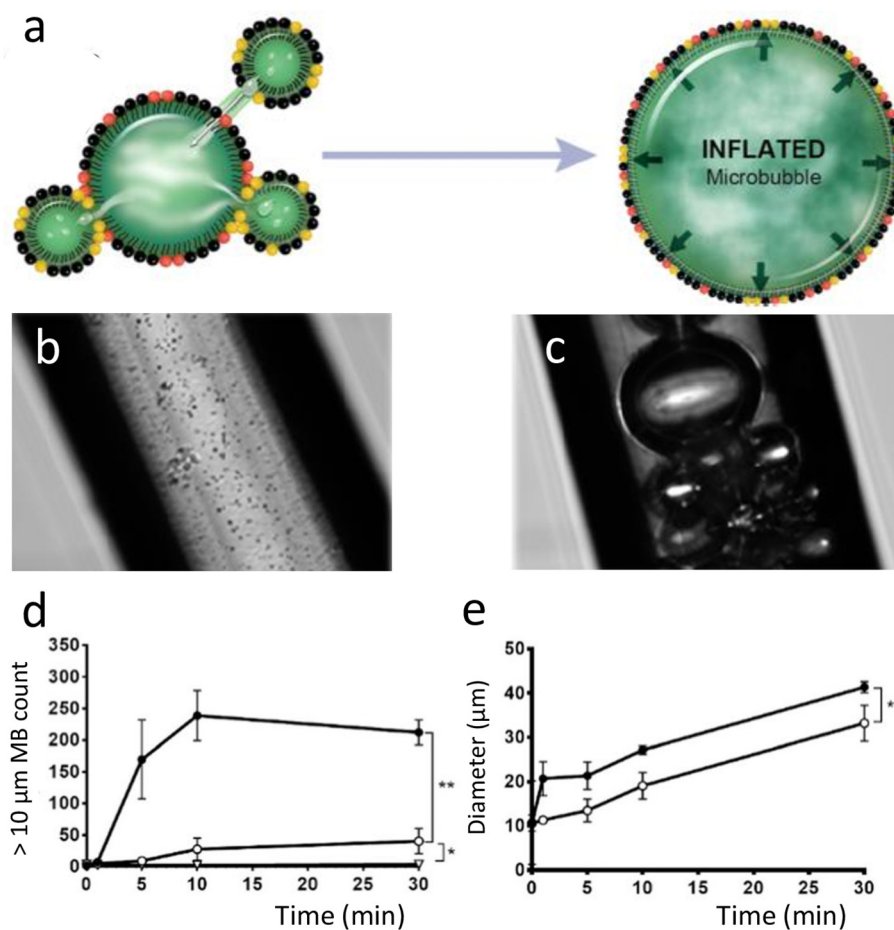
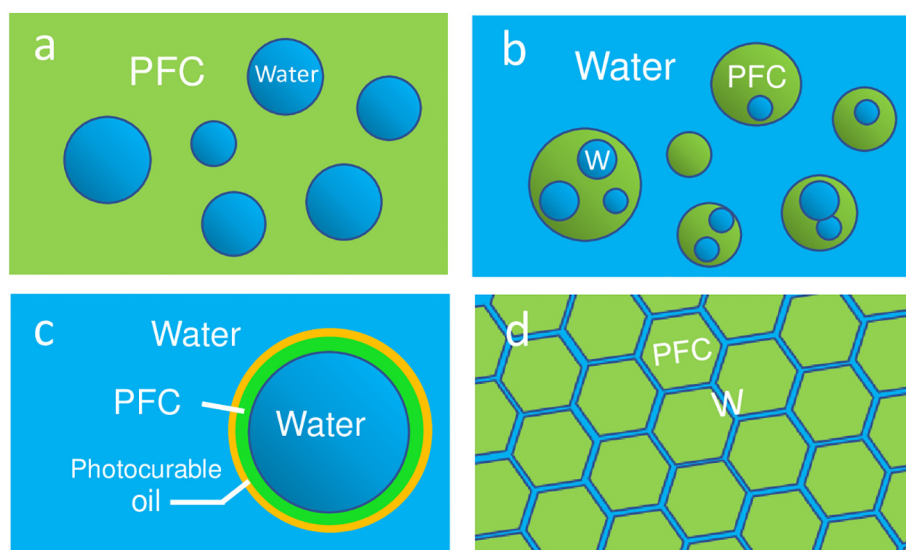


**Fig. 6.** a) Transfer of *F*-butane from co-existing not yet vaporized soft-shell lipid-coated NE droplets to MBs can cause a considerable increase in MB size (by up to 6 orders of magnitude), with a risk of vessel occlusion; b-c) bright-field micrographs of MBs before and after infusion of PFC nanodroplets (the inner tubing diameter is 200 μm); d) the same phenomenon as with *F*-butane (black circles) was observed with *F*-pentane (open circles), but to a lesser extent, and is no longer significant with *F*-hexane (open triangles); e) average size of inflated MBs over time after addition of *F*-butane (black circles) or *F*-pentane (open circles) emulsion nanodroplets to a MB suspension. Adapted from [160].





**Scheme 5.** Examples of further soft-shell PFC colloids. a) Reverse water-in-PFC emulsion; b) water-in-PFC-in-water double emulsion; c) triple water-in-PFC-in-oil-in-water emulsion droplet; d) high internal phase ratio (up to 99%) PFC-in-water gel emulsion. Adapted from [17,217,218].

A non-ionic, molecular *F*-alkyldimorpholinophosphate **15** (Table 2) produced, for example, stable, heat-sterilizable reverse emulsions of water-in-*F*-octylbromide in which a variety of drugs could be loaded [199,206]. Thermodynamically stable, transparent emulsions (called “microemulsions” [207]) were also obtained (average diameter 12 nm) [203]. Reverse emulsions can as well serve in microfluidics techniques for a range of applications, including single-molecule polymerase chain reactions (PCR), proteome analysis, clinical diagnosis on human physiological fluids, protein crystallization, and titration of anticoagulants [208–210]. They have also been used to encapsulate prokaryotic and eukaryotic cells [211].

Emulsions used in microfluidics usually involve a polymeric fluorosurfactant (Table 2) such as the poly(*F*-propylether)-PEG triblock copolymer **19** [75,211]. The PFCs used as continuous phase in the latter studies include a mix of tertiary *F*-alkylamines. Reverse water-in-PFC emulsions have also been produced using *F*-alkylated silica NPs in microfluidics channels, yielding NP-stabilized (Pickering-type) emulsions that effectively alleviated undesirable inter-drop exchange of contents [212]. Dendronized fluorosurfactant with mono- or polyglycerol polar head groups (e.g. **20**) can also minimize interdroplet transfer of small molecules [81].

Water-in-PFC-in-water double emulsions (Scheme 5b), chiefly destined for delivery of fragile hydrophilic drugs [17,171,213–215], again relied on a *F*-surfactant for the water-in-PFC emulsification step. For example, water-in-*F*-pentane NEs were prepared with Krytox [215] and water-in-*F*-hexane NEs with Krytox-derived *F*-surfactant **19** [171], which were re-emulsified in water using phospholipids or Pluronic F-68, respectively. A water-in-*F*-hexane-in-water phase-shift double emulsion was embedded in an acoustically responsive fibrin matrix for controlled drug release [216]. A poly(ethylene imine)-coated water-in-*F*-octylbromide-in-water double emulsion was loaded with indocyanine green and doxorubicin, and targeted to HER2-overexpressing cancer cells for photo- and chemotherapeutic treatments [214].

Triple emulsions, in which a thin layer of a heavy PFC separates the inner aqueous or organic encapsulant phase from an external photocurable oily shell within the continuous aqueous phase (Scheme 5c), have been prepared using microfluidics [217]. Highly stable, heat-sterilizable high internal phase ratio gel-emulsions (up to 99% of diverse PFCs) with a polyaphron structure (Scheme 5d), obtained with neutral molecular amine oxide *F*-surfactant **16**, could find topical uses [218].

### 3.5.2. PFC-loaded nanoparticles and matrices

PFCs have been loaded, along with various drugs, within diverse mesoporous nanomaterials [219], such as Prussian blue (ferric hexacyanoferrate) nanocubes [220], surface-modified hollow molybdenum sulfide NPs [221], porous paramagnetic Fe<sub>3</sub>O<sub>4</sub> NPs [222,223], hollow Bi<sub>2</sub>Se<sub>3</sub> NPs [224], gold nanoshells [225], silica NPs [19,226–228]. *F*-hexane-loaded fullerene NPs also helped generate reactive oxygen species [229]. *F*-15-crown-5-ether-loaded, poly(vinyl alcohol)-stabilized PLGA NPs with an atypical multicore structure, that is, ~100 nm NPs consisting of agglomerated smaller PLGA-coated *F*-15-crown-5-ether droplets, have been reported [24].

Rather complex “nanomotors” consisting of gold nanowires coated with *F*-octylbromide NE droplets cloaked with RBC membranes were built that could be propelled under US activation into hypoxic macrophages to provide intracellular O<sub>2</sub> delivery (Fig. 7) [55]. In the same vein, focused US-triggered phase-shift of *F*-nonane/*F*-surfactant droplets was used to fire silica or polymer “nanobullets” from “microcannons” fabricated through electrodeposition techniques [230,231].

PFCs have also been incorporated in implantable hydrogel scaffolds to deliver O<sub>2</sub> and bioactive agents for tissue engineering. For example, an O<sub>2</sub>-carrying *F*-tributylamine-loaded fibrin hydrogel scaffold accelerated sciatic nerve regeneration and functional recovery in rats [232]. Further hydrogels that embedded PFC MBs or P-SNEs and provided acoustically responsive scaffolds for delivery of regenerative growth factors and drugs, can potentially transport O<sub>2</sub> as well [48,216,233–237].

### 3.5.3. Interconnected and nested colloids

Further PFC-based colloids that will inevitably transport some O<sub>2</sub> although they were not designed for this purpose include “acoustic clusters” that associate negatively charged *F*-butane MBs (*Sonazoid*) and positively charged, phase-shiftable *F*-methylcyclopentane/phospholipid/stearylamine microdroplets intended for US-mediated chemotherapeutic drug delivery [238,239]. Controlled aggregation of *F*-butane MBs was also obtained through avidin/biotin linkage [240].

PFC NE droplets have been associated with liposomes in order to combine their respective assets, i.e. increase the loading capacity of the NE for hydrophilic drugs and confer sensitivity to US to the liposomes (Fig. 8). Biotinylated cationic liposomes complexed with mRNA (lipoplexes) were thus attached on the surface of avidinylated *F*-butane/lipid MBs for mRNA delivery [241]. Paclitaxel-loaded liposomes have been tethered covalently to the periphery of SF<sub>6</sub> NBs, or through biotin/avidin linkage to *F*-propane MBs, for combined US imaging and

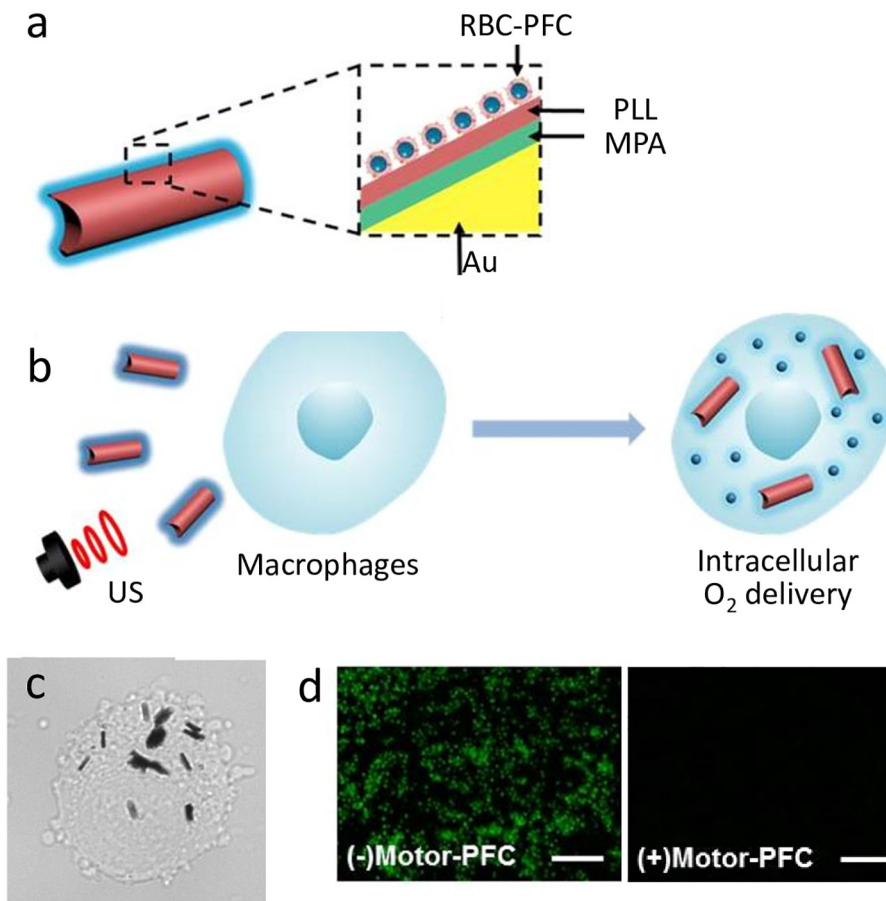


**Fig. 7.** A sophisticated “nanomotor”-based O<sub>2</sub> delivery system. a) A gold nanorod coated with mercaptopropionic acid (MPA), then poly-L-lysine (PLL), then with RBC fragments-shelled *F*-octylbromide droplets; b) these devices were propelled by US into hypoxic macrophages for acoustically-assisted O<sub>2</sub> delivery; c) they were internalized in macrophages under US exposure (optical microscopy), and d) they alleviated hypoxic stress as indicated by the suppression of the green fluorescence of a hypoxia marker. Adapted from [55].

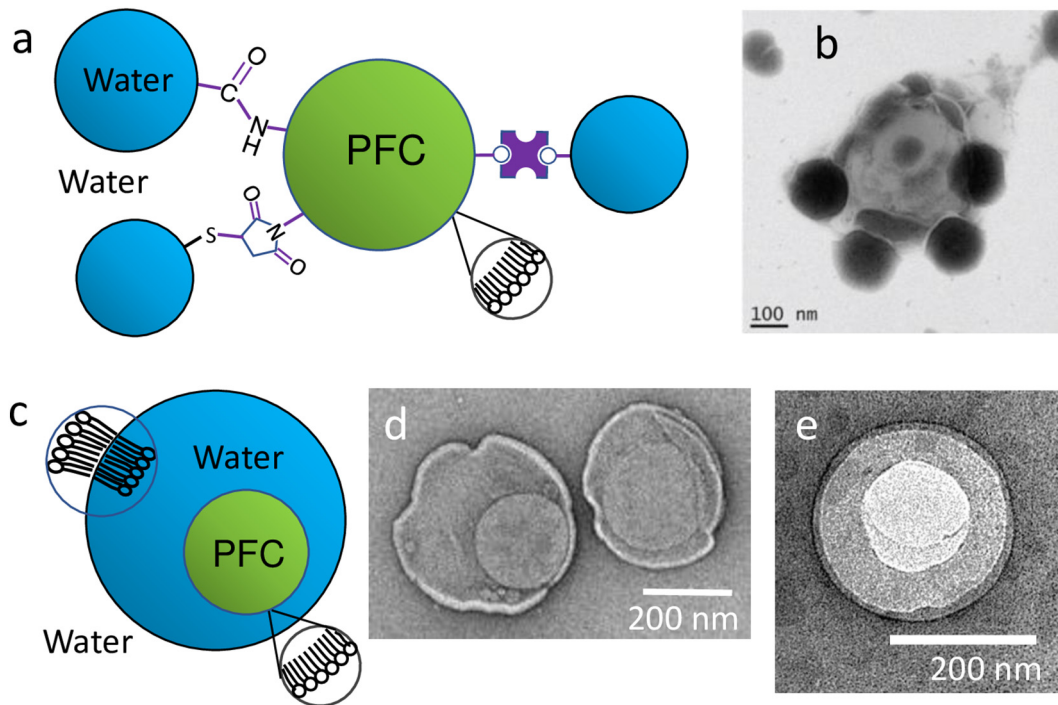


**Fig. 8.** a) Liposomes tethered to PFC MBs (schematic), also illustrating popular carbodiimide, maleimide and avidin-biotin coupling methods; b) transmission electron micrograph of a SF<sub>6</sub> nanobubble/paclitaxel liposome conjugate; c) a lipid-coated PFC MB nested in a liposome (schematic); TEM images of d) nested *F*-butane MBs, and e) a nested *F*-pentane phase-shift NE. Adapted from b) [244], d) [246] and e) [248].

US-triggered drug delivery [242–244]. Magnetically targeted doxorubicin-loaded liposome-*F*-propane MB conjugates allowed US-enhanced delivery [245].

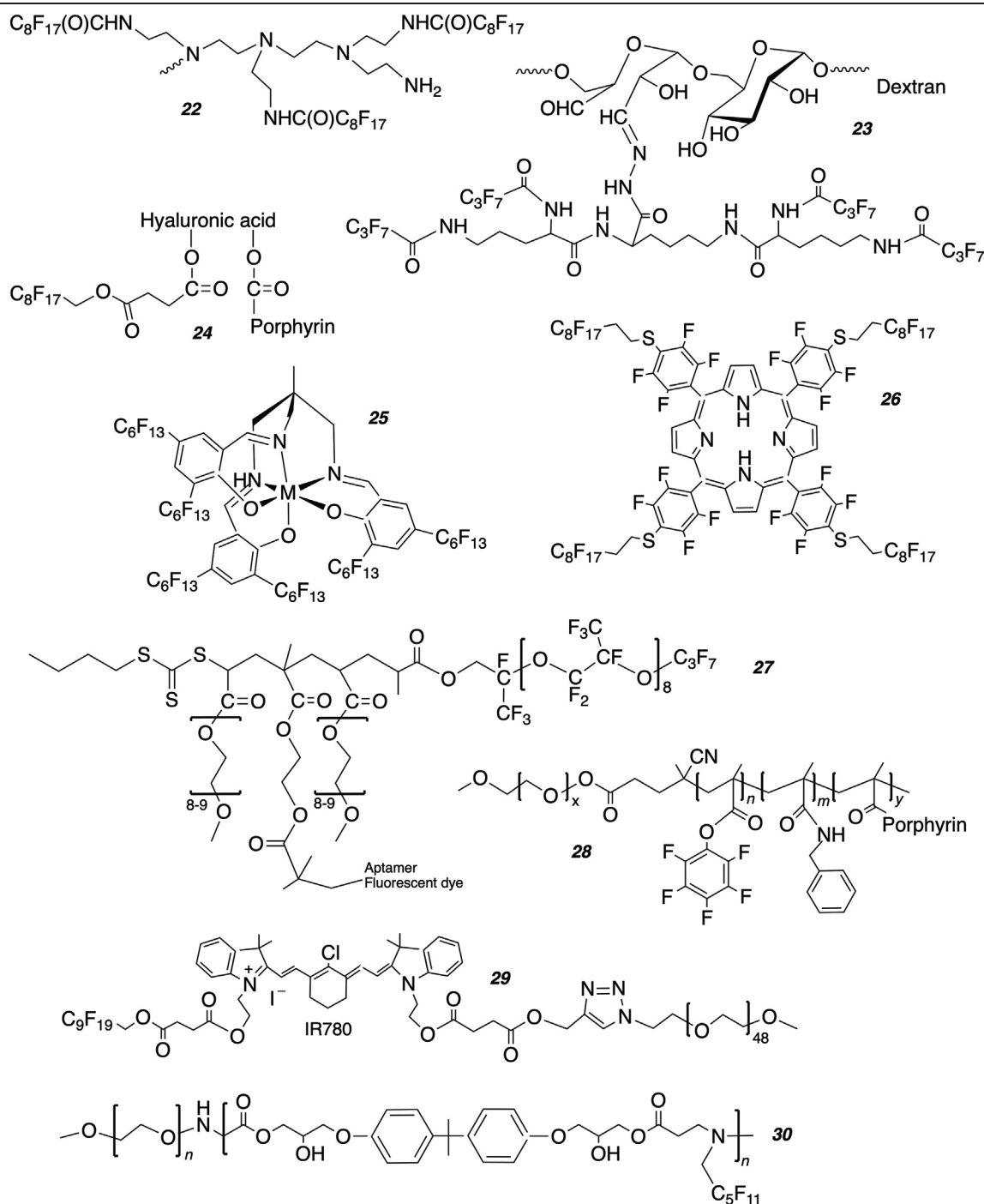
*F*-butane NBs [246] and *F*-hexane or *F*-pentane P-SNEs [247,248] nested within liposomes allowed US-triggered drug release (Fig. 8b). Tumor-targeted fusogenic liposomes were loaded with a *F*-pentane P-SNE [249]. *F*-propane and recombinant tissue plasminogen activator protein (rtPA)-loaded liposomes destined for treatment of ischemic stroke by sonothrombolysis actually comprised a variety of structures including liposomes (with and without gas) and lipid-shelled MBs

[250]. *F*-propane “bubble liposomes” enabled US-activated antisense oligonucleotide therapy of muscular dystrophy in mice [251].

### 3.5.4. Polymer micelles and nanoparticles with perfluoroalkylated or arylated components

Further colloids have been investigated that, without incorporating PFCs per se, contain components that contain sufficient *F*-alkyl or *F*-aryl moieties (Table 7) for them to acquire some of the properties and functions of PFCs such as gas dissolving capacity, solubility in PFCs, <sup>19</sup>F MRI probing ability, or control of cargo release. The capacity

**Table 7**  
Examples of functional *F*-alkylated or *F*-arylated colloid components that can also contribute to oxygen delivery for cancer therapies.





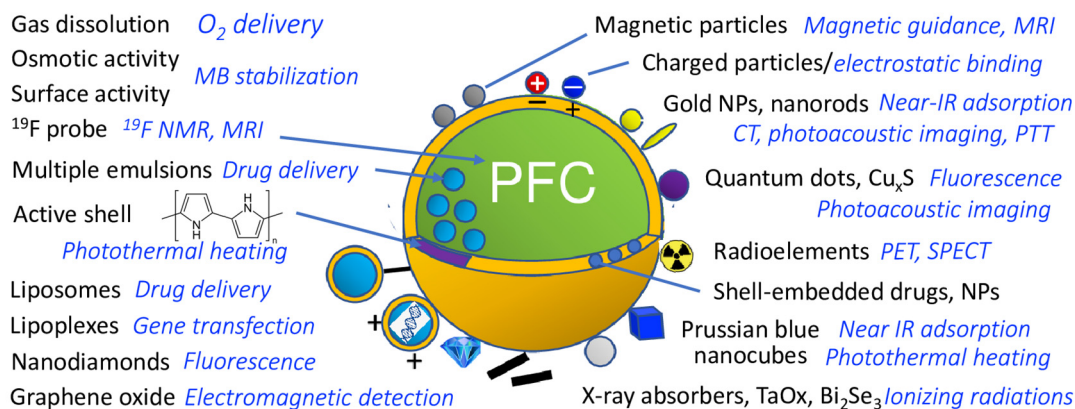
for such systems to facilitate O<sub>2</sub> delivery, when investigated, actually appears rather remarkable. For example, O<sub>2</sub>-carrying micelles of *F*-octanoic acid-grafted poly(ethylene imine) **22**, also loaded with a photosensitizer, improved photodynamic glioma tumor growth inhibition [252]. A tumor-targeted, pH- and light-sensitive poly(lysine) dendron fitted with several *F*-propyl groups **23** provided the O<sub>2</sub>-carrying NP component needed for photodynamic therapy (PDT) enhancement [57]. Micelles made of *F*-nonanoic acid- and porphyrin photosensitizer-conjugated hyaluronic acid **24**, designed for targeted O<sub>2</sub>-enhanced PDT, increased singlet oxygen (<sup>1</sup>O<sub>2</sub>) production [58]. *F*-octyl chain grafting imparted US-triggered O<sub>2</sub> delivery capacity to a sonosensitized porous silica shell [253]. *F*-alkylated siloxane/polystyrene NPs incorporating a *F*-arylated zinc phthalocyanine photosensitizer were also produced [254].

*F*-alkylation has often been used to increase the solubility in PFCs of dyes for fluorescence imaging [255], sensitizers for PDT, or paramagnetic metal chelates for MRI as in **25** [256,257]. Four *F*-octyl chains bound via tetrafluorophenyl-based linkers onto a porphyrin **26** ensured its solubility in PFC NEs for concurrent O<sub>2</sub> delivery and photosensitizing [258]. The photosensitizer could thus be dissolved in a *F*-decalin/*F*-tributylamine NE, in which its undesirable aggregation was reduced, leading to superior <sup>1</sup>O<sub>2</sub> production and melanoma cell killing. Targeted *F*-polyether-based hyperbranched polymer NPs **27**, conjugated with a fluorescent dye, provided fluorescence imaging and sensitive <sup>19</sup>F MRI detection of breast cancer in a mouse model [259]. Further examples of *F*-alkylated or *F*-arylated NPs can be found in Section 6.

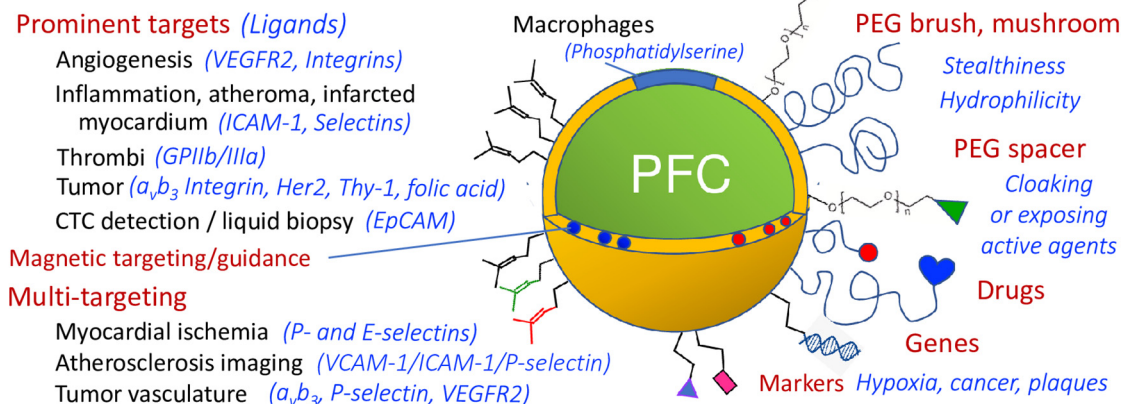
### 3.6. Functionalization and targeting of perfluorocarbon colloids

Surface modification, functionalization and targeting (Scheme 6) can expand the range of indications for PFC colloids well beyond O<sub>2</sub> delivery and help augment their efficacy and safety. Functionalization involves attachment (as through carbodiimide, maleimide, pyridyl disulfide or avidin/biotin coupling, see Fig. 8) [260,261], or incorporation, adsorption or electrostatic binding of fluorescent dyes, photo- and sonosensitizers, radiopaque elements, magnetic NPs, radiotracers, etc. New binding techniques based on biorthogonal click chemistry are emerging [262,263]. Poly(2-oxazoline) amphiphiles were used to control PFC nanoemulsion surface chemistry [264]. Such additions authorize fluorescence, photoacoustic and sono-photoacoustic imaging, computed tomography (CT), X-ray phase contrast imaging, positron emission tomography (PET) or single-photon emission computed tomography (SPECT), or MR imaging or guidance, as well as labeling and tracking of circulating cells. Incorporation of photo- and sonosensitizers also enables energy conversion (e.g. light or sound into thermal or mechanical energy) therapies, as well as reactive oxygen species (ROS)-based therapies. Still further functions can be conferred to PFC nanocarriers, such as: -responsiveness to environmental stimuli, including pH, temperature, O<sub>2</sub> level, redox potential, presence of specific enzymes, markers or ROS; -control of vaporization energy threshold for P-SNEs; -capacity for evading opsonization and phagocytosis by coating with hydrophilic surface brushes or RBC membrane components; -increase of drug cargo space, as by binding or incorporating drug-loaded liposomes and carrier NPs; -competency for condensing and

#### a PFC colloid functionalization



#### b PFC colloid targeting and decoration



**Scheme 6.** Schematic illustration of multiple a) functionalization and b) targeting possibilities of PFC colloids.

preserving genetic material; —control of in vivo drug cargo protection or presentation; —capacity for on-demand, externally triggered or stimuli-dependent focused cargo release or even projection into tissues [100,107,108,265–267]. Fluorination of the functionalizing agent can enable its dissolution in the PFC core [255–258].

PFC colloids have also been fitted with a range of targeting implements (Scheme 6b). Targeting is critical for such applications as molecular imaging or precisely disease-focused O<sub>2</sub>, energy or drug delivery. PFC-based nanocarriers loaded with magnetic NPs can be directed to their target by applying an external magnetic field [245,268–270]. Different strategies for magnetic functionalization have been examined [271]. Dendronized iron oxide loaded-*F*-hexane MBs could serve as versatile, magnetically targetable multimodal imaging and drug delivery systems [34]. Detection of inflammation sites can be obtained by inclusion of phosphatidylserine in the nanocarrier shell, which promotes uptake by activated macrophages [100,272,273]. *Sonazoid*, with a phosphatidylserine-containing shell can thus act as a marker of phagocytosis [274]. Dual P/E-selectin-targeted MBs allowed US monitoring of anti-inflammatory treatment response in acute ileitis [275]. Active targeting to specific diseased tissues can be achieved by surface conjugation of appropriate monoclonal antibodies, peptides, peptidomimetics, oligosaccharides or folic acid. Privileged targets include infarcted myocardium, atheroma plaques, thrombi and activated platelets, sites of inflammation, or sites of angiogenesis related to malignant tumor growth [100,105,107,108,261,267,276–279]. A folate-targeted *F*-pentane P-SNE loaded with a chemotherapeutic drug and Fe<sub>3</sub>O<sub>4</sub> provided multimodal imaging and treatment of ovarian cancer in mice [280]. Hyaluronic acid has also been used as a targeting moiety [58]. *F*-alkylated lipopeptides that are precursors of targeting lipopeptide conjugates have been synthesized and their incorporation in the phospholipid shell of *F*-hexane-stabilized MBs investigated [281]. Targeting can be assisted by US-generated radiation forces [282]. The development of targeted PFC-based devices for detection of circulating tumor cells (liquid biopsy) is also focusing considerable interest [283]. Multiple functionalization and targeting foster multimodal imaging, enhanced therapeutic efficacy, increased safety, and opens an endless range of theranostic possibilities.

#### 4. Oxygen delivery by PFC nanoemulsions

The early objective of developing PFC-based O<sub>2</sub>-delivering “blood substitutes” has not been forsaken. Further evidence of O<sub>2</sub> delivery efficacy by means of PFC NEs has been secured. New, highly stable size-controlled NEs have been developed. The alternative option of using MBs or P-SNE-derived MBs for O<sub>2</sub> delivery is being actively investigated. Additional indications for O<sub>2</sub>-delivering therapeutics have emerged. Potentiation of the foremost O<sub>2</sub>-dependent cancer treatment strategies, including radiotherapy, chemotherapy, photo- and sonodynamic therapy, and now immunotherapy, is also an important goal.

##### 4.1. Basics of oxygen transport and delivery by perfluorocarbon nanoemulsions

The basics of O<sub>2</sub> transport and delivery by PFC NEs have been reviewed and compared to those that support hemoglobin-based carriers [1,7]. Briefly, PFCs dissolve O<sub>2</sub> physically, typically 20 times more than water or blood serum. Such solubility relies on weak non-specific van der Waals-type interactions. Contrary to hemoglobin, the O<sub>2</sub> content of PFCs is a linear function of O<sub>2</sub> partial pressure and there is no saturation. Full benefit for patients will thus be gained when the fraction of inspired oxygen (FiO<sub>2</sub>) is 1 or close to 1. PFCs do not bind O<sub>2</sub> through strong directional chemical bonds as hemoglobin does, and O<sub>2</sub> release requires no allosteric factor. Oxygen is therefore immediately and close-to-totally available to tissues, with extraction ratios typically reaching 90% of the dissolved O<sub>2</sub>. Administration of a PFC NE is comparable to increasing the O<sub>2</sub> content of the plasma compartment of blood.

High FiO<sub>2</sub> produces a large O<sub>2</sub> tension gradient, and hence, a potent driving force for O<sub>2</sub> diffusion into tissues. Additionally, the much more numerous, much smaller-sized PFC droplets relative to RBCs offer a huge interface for gas exchange and circulate more easily through capillary beds, thus further facilitating O<sub>2</sub> diffusion. Even when blood cell circulation is hindered, perfusion of tissues by the PFC nanodroplets is expected to persist along with residual plasma flow. When both PFC and hemoglobin are present, the PFC will release its dissolved O<sub>2</sub> first, while the hemoglobin-bound O<sub>2</sub> remains in reserve. As transport and delivery rely on physical dissolution, the same principles apply to other gases, including N<sub>2</sub>, CO<sub>2</sub>, NO, CO, Xe, and volatile anesthetics. The large solubility of CO<sub>2</sub> in PFCs should be noted. Also notable is that, contrary to Hb, PFCs do not scavenge nitric oxide and therefore do not cause vasoconstriction.

A multiparameter mathematical model allows calculation of the “hemoglobin equivalency” of a PFC NE. In typical clinical conditions, the patient’s hemoglobin level being about 8 g/dL, a 2.7 g PFC/kg body weight dose of *Oxygent* (110 mL of NE) was found equivalent to about 4 g/dL of hemoglobin [284]. This value was validated by clinical data from a Phase III study in general surgery.

Further, much needed insight into the mechanism of O<sub>2</sub> delivery in the microcirculation has been gained [285]. In a case of extreme hemodilution in a hamster model, infusion of 4.2 g/kg body weight of a PFC NE (*Oxyocyte*) increased systemic and microvascular O<sub>2</sub> delivery by 25% when the animals breathed air and by 400% when they breathed pure O<sub>2</sub>, as compared to a hydroxyethylstarch solution [286]. The PFC NE produced a significant increase of the amount of O<sub>2</sub> transported and consumed. Acid-base balance, mean arterial pressure and cardiac output were restored. No evidence for vasoconstriction or microvascular perfusion impairment was noted. Further studies of the physiology of microcirculation and its regulation mechanisms, the role of the vascular endothelium, and the effects of O<sub>2</sub> carriers on them, were encouraged [285].

A meaningful advance in the utilization of O<sub>2</sub>-carrying *F*-colloids is the realization that release of O<sub>2</sub> from NEs could be triggered or accelerated and focused using external stimuli. On-demand local release of O<sub>2</sub> from PFC NEs to specific tissues has, in particular, been triggered by focused US (Fig. 9) [111,214,287,288].

##### 4.2. Development status of O<sub>2</sub>-carrying PFC nanoemulsion products

No satisfactory PFC NE has so far gained approval and substantial acceptance. As indicated previously, the early commercial product *Fluosol* could not be successful in view of its poor user-friendliness. *Oxygent* development did not survive Alliance’s financial debacle. The emulsion *Perforan* (Perforan, Pushchino, Russia), despite requiring frozen transportation and storage, and notwithstanding a long organ-dwelling component (*F*-methylcyclohexylpiperidine **10**, 30% of total PFC; MW 595; organ half-life of at least 3 months), is available in former Soviet Union Countries and has been used in Mexico [289–291]. Introduction in North America under the brand name *Vidaphor* (FluorO2 Therapeutics, Inc. Boca Raton, FL) is being sought. Development of *Oxyfluor* (HemaGen Corp., CA), a *F*- $\alpha,\omega$ -dichlorooctane NE [292], with a misconstrued stabilization principle involving safflower oil supplementation that actually form separate droplets rather than the expected stabilizing oily sub-shell [293], was discontinued following funding problems. *Oxyocyte* (Tenax Therapeutics, Morrisville, NC), an emulsion of “*F*-*t*-butylcyclohexane” **11** with poorly documented purity, organ retention (estimated at about 2 weeks) and emulsion characteristics, has experienced a futile clinical trial in 2014 [14]. On the other hand, several PFC NEs are commercially available for research purposes, including a *F*-poly(ethylene) NE (CS-1000, Celsense, Pittsburg, PA) that is used in several FDA-approved clinical trials involving <sup>19</sup>F MRI tracking of circulating cells.

Yet, there is at this point no factual reason to discard the PFC NE-based O<sub>2</sub>-delivery approach. Previous endeavors have suffered from



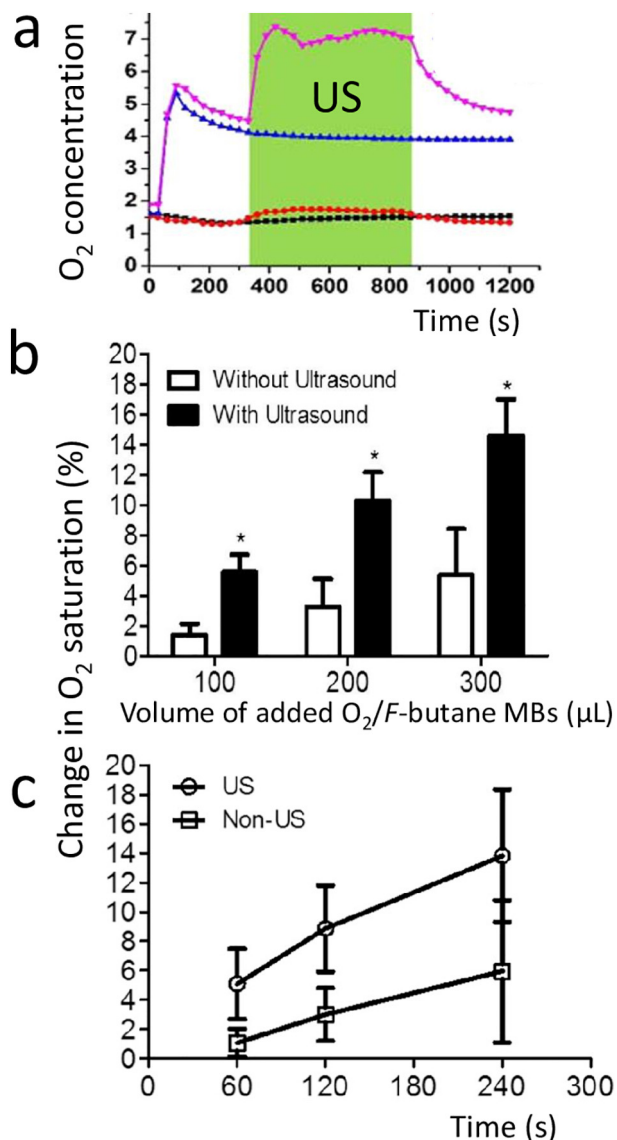


**Fig. 9.** Oxygen release from PFC colloids can be stimulated by exposure to US. a) Changes in dissolved O<sub>2</sub> concentration over time in deoxygenated water without (black) or with (blue) addition of an O<sub>2</sub>-loaded F-15-crown-5-ether NE; US treatment was applied during the period highlighted in green (water: red; pink: with PFC). b) Change in O<sub>2</sub> saturation using O<sub>2</sub>/F-butane-filled MBs with (black bars) and without (white bars) exposure to US after addition of 100, 200, and 300 µL of MB dispersion (10<sup>10</sup> MBs per mL, \* *p* < 0.05); c) effect of US exposure duration on O<sub>2</sub> release from MBs: change in O<sub>2</sub> concentration following US treated (circles) or untreated (squares) injection of 300 µL of MBs dispersion. Adapted from a) [288], b) and c) [111]. (For interpretation of the references to colour in this figure legend, the reader is referred to the web version of this article.)

ill-conceived component selection, sub-optimal emulsion characteristics, clinical evaluation blunders, and/or funding issues. The capacity for well-designed, properly engineered PFC emulsions to deliver O<sub>2</sub> has been proven. Large-scale, industrial production of high purity, readily excretable PFCs, and of reproducible small and narrowly-dispersed sterile NEs with long-term shelf stability has been established. Side effects related to PFC NEs appear limited to short-lived flu-like symptoms and mild transient thrombocytopenia, which could likely be further reduced.

Moreover, advanced fluorocarbon-hydrocarbon diblock-stabilized, size-controlled NEs have been obtained that have a shelf-life of over two years at room temperature (Fig. 3) [1,22,49,50]. These emulsions effectively delivered O<sub>2</sub> to cells [294], isolated organs [66], animal models [295,296], and also proved advantageous for <sup>19</sup>F MRI imaging [297,298].

#### 4.3. Further demonstration of oxygen delivery efficacy by PFC nanoemulsions

Additional demonstrations of effective O<sub>2</sub> delivery by PFC NEs are continuously being reported. They support the ability of such O<sub>2</sub> therapeutics to protect organs and salvage tissues at risk of hypoxia, enhance O<sub>2</sub>-dependent cancer therapies, assist regeneration of damaged tissues, preserve organs for transplantation, help regulate gas supply in biotechnology, and more. The early goal of a “blood substitute” to replace blood or RBC transfusion has all but vanished, primary due to rather short intravascular persistence. The potential of PFC-based O<sub>2</sub>-carriers in emergency medicine and more generally while waiting for blood transfusion still holds. Some of the examples provided below also illustrate the concurrent (theranostic) capacity of PFC NEs for both diagnostic imaging and therapeutic performance.

##### 4.3.1. Protecting and salvaging tissues from hypoxia

Administration of PFC NEs can help counteract hypoxia, a deficit in O<sub>2</sub> supply versus consumption. Notably, gut perfusion and oxygenation were significantly improved in a group of patients instrumented for gut tonometry during the cardiac surgery phase III trial of *Oxygent*, indicating protection of the gastrointestinal tract against hypoxia (Fig. 10) [299]. This could constitute a valuable indication for PFC NE products and an acceptable endpoint for clinical trials. Administration of *Perftoran* along with moderate ANH reduced the need for allogeneic RBCs in cardiac surgical valvuloplasty patients [300]. *Oxycyte* delayed the need for blood transfusion in acutely anemic hamsters [301]. Systemic and microvascular O<sub>2</sub> delivery was considerably augmented in hemodiluted, O<sub>2</sub>-breathing hamsters by administration of this product; acid-base balance, mean arterial pressure and cardiac output went back to normal; no vasoconstriction was observed [285]. A F-octylbromide NE improved myocardial oxygenation and cardiac function in the isolated working rabbit heart [302]. *Oxygent* enhanced cerebral blood flow and tissue oxygenation in hemodiluted rats [303]. A Fm-stabilized F-octylbromide NE allowed survival of “bloodless” rats after near-total exchange-transfusion, enabling high-resolution imaging of brain astrocytes and neurons by two-photon laser-scanning microscopy [296]. The same NE resuscitated rabbits exposed to acute hemorrhagic shock [295]. An intravenously administered *Oxygent*-type formulation alleviated acute lung injury in rats [304]. A (F-hexyl)octane NE lessened brain tissue hypoxia, preventing irreversible brain damage in an ischemic rat model [305]. *Oxycyte* improved cognitive function and reduced neuronal cell loss in rats subjected to percussion brain injury [306], and

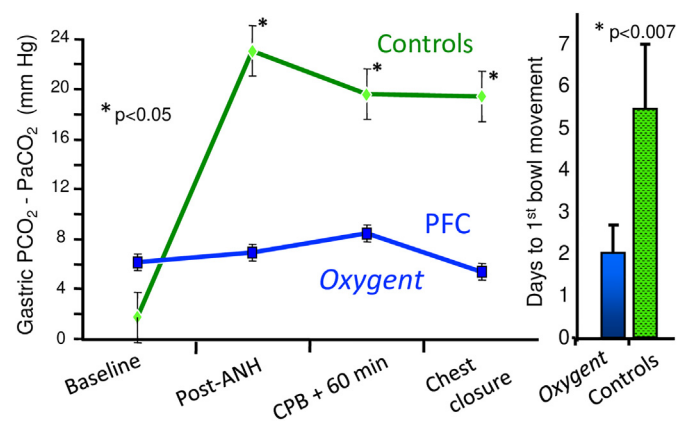


**Fig. 10.** Prevention of gastro-intestinal tract hypoxia and organ protection by a F-octylbromide NE during surgery. Gut tonometry data collected during a Phase III clinical trial of *Oxygent* in coronary artery bypass graft surgery patients (ANH: acute normovolemic hemodilution; CPB: cardiopulmonary bypass). The gastric pCO<sub>2</sub> gap (PCO<sub>2</sub> - PaCO<sub>2</sub>), a marker of hypoxia, was preserved in the *Oxygent* group, while it increased dramatically when no emulsion was administered. Adapted from [299].

markedly reduced lesion area and cell death after traumatic spinal cord injury in rats [307]. The NE also reduced infarct size and improved functional recovery after acute ischemic stroke in the rat [308]. Resuscitation of mice from hemorrhagic shock using *F*-octylbromide emulsified with RBC membrane proteins was deemed comparable to that obtained with whole blood [51,54]. Reduction of tissue hypoxia with *Perftoran* in cats with post-hemorrhagic anemia was reported [309]. Blood from sickle cell disease patients, when mixed with a PFC emulsion in vitro, showed increased O<sub>2</sub> extraction, indicating facilitated O<sub>2</sub> transport [310].

Pulmonary administration of an aerosolized *F*-octylbromide NE achieved effective O<sub>2</sub> delivery in rats [311] and in a rabbit model of acute lung injury [312]. Topically applied 2H,3H-decafluoropentane NE droplets enhanced transdermal O<sub>2</sub> release under US-exposure for hypoxic wound healing [48,234,235].

#### 4.3.2. Enabling oxygen-dependent cancer therapies

Hypoxia within solid tumors is a major impediment to most current cancer therapies, including radio-, photo(sono)dynamic-, chemo- and immunotherapies, most of which require a supply of O<sub>2</sub> for production of singlet oxygen and other ROS that are the actual cancer cell-killing agents [313–316]. These therapies themselves consume O<sub>2</sub>, which aggravates hypoxia and further impedes tumor response. The damage caused to the microvasculature of the tumor can also hamper O<sub>2</sub> delivery. In addition, hypoxia confers immunosuppressive attributes to the tumor microenvironment that allow tumors to escape detection by the immune system [317,318]. PFC-based O<sub>2</sub> carriers can help overcome tumor hypoxia and deliver the O<sub>2</sub> required for potentiating O<sub>2</sub>-dependent cancer therapies [288,315,316]. Of note, radicals such as <sup>1</sup>O<sub>2</sub> benefit from considerably prolonged lifetimes in PFCs [319]. Moreover, small O<sub>2</sub>-loaded NE (or P-SNE) droplets can extravasate from leaky tumor vessels and accumulate in tumor tissue; O<sub>2</sub> release can then be actuated on demand, for example with focused US.

Radiosensitization was, for example, achieved using an *Oxygent*-type emulsion that suppressed hypoxia-associated radio-resistance in brain tumors in mice [320]. Hypoxic xenograft prostate tumors were re-oxygenated, even without augmented O<sub>2</sub> breathing, due to accumulation of a *F*-octylbromide NE in the tumor in mice [321]. Decoration of *F*-hexane NE droplets with TaO<sub>x</sub> NPs improved tumor oxygenation, augmented the X-ray absorbing capacity and increased local radiation energy density in tumor tissue [322]. *F*-15-crown-5-ether NE droplets encapsulated in a polymer shell, then coated with RBC membrane proteins, accumulated in tumor tissue, reduced tumor hypoxia and enhanced radiotherapy in mice [51,54]. NEs of *F*-tributylamine and of a *F*-tripropylamine/*F*-decalin mixture delivered O<sub>2</sub> for radiotherapy enhancement and also augmented RBC infiltration in murine colon and breast tumors, which was deemed to provide a second-stage O<sub>2</sub> delivery [323]. However, clinical use of *F*-tributylamine and even tripropylamine can hardly be envisaged due to overlong organ retention; the former may also raise environmental issues [324]. Use of PFC-based O<sub>2</sub>-carrying systems and other nanomaterials to enhance radiotherapy has been reviewed [325].

There is also renewed interest in PFC-assisted photodynamic therapy (PDT) and sonodynamic therapy (SDT). PDT uses a photosensitizer such as porphyrins, cyanines, plasmonic gold NPs or quantum dots that, upon excitation by light, usually near-infrared laser light, assists generation of the ROS that destroy tumor cells. Numerous photosensitizer-loaded, O<sub>2</sub>-carrying PFC NEs have demonstrated their capacity to significantly reduce tumor hypoxia, enhance <sup>1</sup>O<sub>2</sub> production upon irradiation and inhibit tumor growth in animal models (Fig. 11) [258,287,326–333]. A *F*-15-crown-5-ether/albumin emulsion achieved focused ultrasound (FUS)-activated local O<sub>2</sub> delivery for enhanced radio- and photodynamic therapy (Fig. 12) [288]. A NE comprising *F*-tributylamine and indocyanine green, and coated with RBC membrane fragments, accumulated in tumors and enhanced PDT efficacy in mice [52]. Dissolution of a fluorinated photosensitizer in PFC NEs led

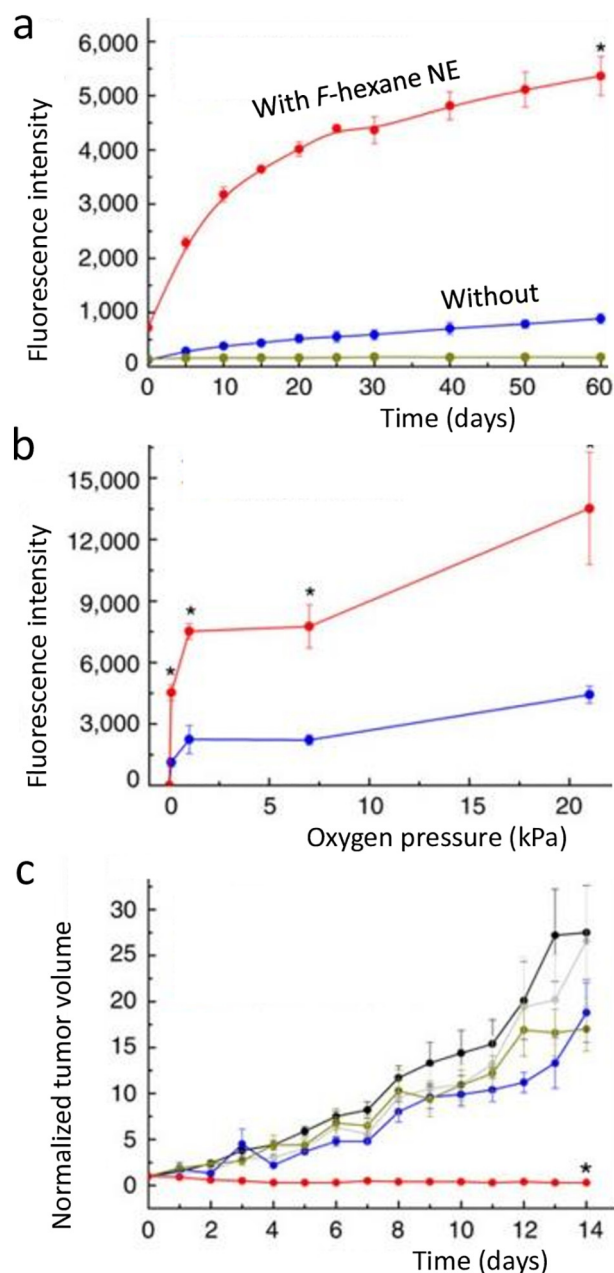


**Fig. 11.** Singlet oxygen (<sup>1</sup>O<sub>2</sub>) production under near-infrared irradiation, a) as measured by singlet oxygen sensor green fluorescence intensity over time for water (green), heptamethine (IR780) dye-loaded liposomes (blue) and a dye-loaded, O<sub>2</sub>-carrying *F*-hexane NE (red); b) fluorescence intensity as a function of O<sub>2</sub> pressure for dye-loaded liposomes (blue) and dye-loaded *F*-hexane emulsion (red), and c) changes in tumor volume during photodynamic treatment of tumor-bearing mice receiving saline (controls, black), dye-loaded liposomes (light green), the same under near-infrared irradiation (blue), the *F*-hexane emulsion with the liposomal dye (green), and the latter under irradiation (red) [287]. (For interpretation of the references to colour in this figure legend, the reader is referred to the web version of this article.)

to superior PDT production of <sup>1</sup>O<sub>2</sub> and caused more melanoma cell death in vitro upon irradiation [258]. A *F*-octylbromide emulsion doped with a heptamethine photosensitizer and functionalized with a small tumor-penetrating peptide enhanced PDT efficacy in mice [331]. A *F*-hexane NE loaded with a redox-responsive tetrapyrrole photosensitizer provided fluorescence/photoacoustic imaging-guided enhanced PDT in tumor-bearing mice [332]. O<sub>2</sub>-carrying *F*-hexane NE droplets loaded with an inorganic photosensitizer consisting of hybrid gold/SiO<sub>2</sub>/Cu<sub>2</sub>O NPs for enhanced plasmon-induced resonance energy

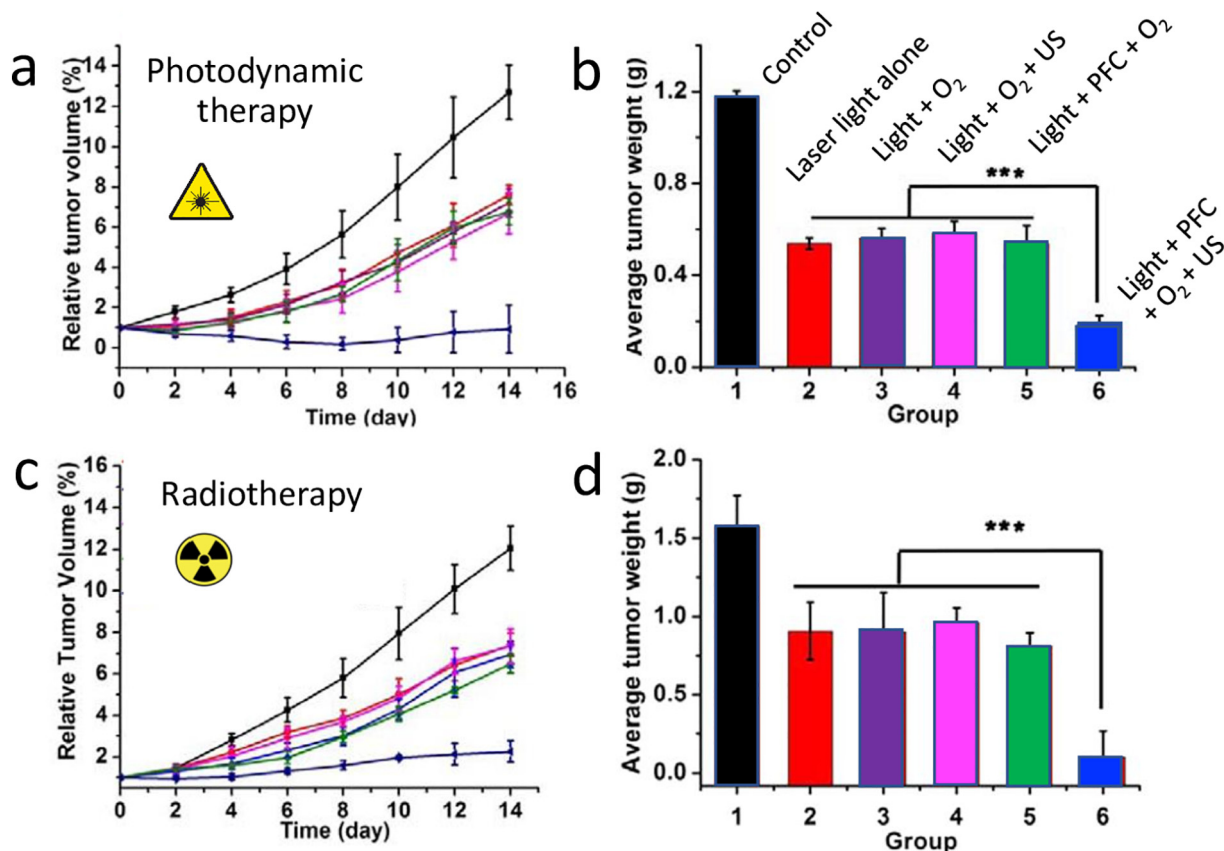


**Fig. 12.** US-triggered tumor oxygenation-enhanced photodynamic therapy (a and b) and radiotherapy (c and d) using a photosensitized F-15-crown-5-ether NE; the color code is provided in frame b). a) Tumor growth over time in mice under various photodynamic treatments; b) average tumor weight after these treatments; c) tumor growth, and d) average tumor weight after radiotherapy treatments. Adapted from [288].

transfer, led to deeper light penetration in tissues and improved PDT efficacy against tumor growth [334]. A tumor pH-responsive, photosensitive *F*-hexane NE permitted O<sub>2</sub>-potentiated PDT and US/fluorescence imaging [330]. A *F*-polyether NE loaded with a photosensitizer also improved PDT in tumor-bearing mice [335]. Indocyanine green-loaded *F*-octylbromide “nanoliposomes”, more likely a PFC-in-water NE, delivered O<sub>2</sub> for synergistic photodynamic and photothermal tumor growth inhibition in mice while also providing fluorescence, photoacoustic and CT contrast imaging [336]. A *F*-hexane NE with a perylene diimide polymer shell provided O<sub>2</sub> for PDT promotion, as well as enhanced PTT, and US and photoacoustic imaging [329].

Sonodynamic therapy, an emerging modality that relies on US activation of sonosensitizers for converting O<sub>2</sub> into ROS, and operates via US-induced MB cavitation to produce the free radicals, can treat tumors at much greater depth than PDT and may elicit lesser side-effects (photo-toxicity) [337–339]. SDT, like PDT, is hampered by tumor hypoxia and can thus benefit from O<sub>2</sub>-carrying PFCs. The mechanisms of PDT, SDT and combined PDT and SDT have recently been reviewed [340]. Diverse photosensitizer-loaded NEs demonstrated significantly reduced hypoxia, enhanced <sup>1</sup>O<sub>2</sub> generation by SDT, and inhibited tumor growth in animals. A *F*-tributylamine NE with a PLGA shell that incorporated an heptamethine dye and doxorubicin, improved combined SDT/chemotherapy treatment of hypoxic breast tumor in mice [341].

Response to many major chemotherapeutics (e.g. cisplatin, doxorubicin, paclitaxel, docetaxel) also relies on ROS generation, and hence, on O<sub>2</sub> supply. Several tumor hypoxia-induced chemoresistance mechanisms could be counteracted with PFC-based oxygenating nanocarriers. Hypoxia-induced resistance to cisplatin was overcome by administration of a *F*-octylbromide NE (Fig. 13) [342]. High-intensity focused

US-responsive tumor-targeted NEs of various PFCs (*F*-pentane, *F*-hexane, *F*-octylbromide and *F*-poly(ether)), stabilized by poly (organosiloxane)-derivatized phospholipids, were investigated for O<sub>2</sub> and doxorubicin co-delivery [343]. The *F*-hexane product produced the best results in terms of tumor hypoxia relief, multidrug resistance alleviation and tumor metastasis inhibition. A *F*-tributylamine/albumin NE displayed platelet inhibiting abilities, resulting in PFC accumulation in the tumor and decreased tumor hypoxia [344].

Immunotherapy, which boosts the body's natural defenses to fight disease, emerges as a highly promising novel cancer therapy. However, a main obstacle to its effectiveness is again that hypoxia can depress certain functions of immune cells. In particular, hypoxic tumor cells over-produce adenosine, which is a potent suppressor of T cells and natural killer (NK) cells [318]. Oxygenation of the tumor microenvironment can thus greatly help stimulate immunotherapy [315–317]. It was also noted that PFC NE-mediated platelet inhibition stimulated intratumoral infiltration of T cells, resulting in enhanced immunotherapy [345]. After exposure to focused US, bone marrow-derived monocytes loaded with a *F*-pentane NE and doxorubicin-containing poly(acrylic acid-co-distearin acrylate) NPs were used as a cellular Trojan horse that accumulated in the tumor and induced apoptosis of cancer cells in tumor-bearing mice [346].

#### 4.3.3. Regenerating bones, nerves, and engineering tissues

O<sub>2</sub>-delivering PFC products also appear promising for repairing damaged nerves, tendons and bones, as well as for culture of cells and tissues and diverse biotechnological productions. For example, a *F*-tributylamine-based O<sub>2</sub>-carrying fibrin hydrogel injected into collagen-chitosan conduits seeded with cells of the peripheral nervous system provided O<sub>2</sub> for sciatic nerve regeneration and functional



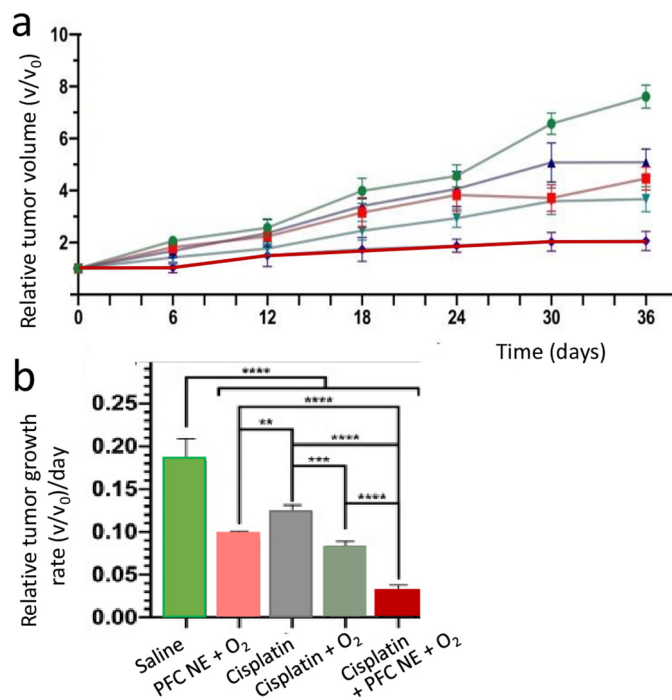


**Fig. 13.** An O<sub>2</sub>-carrying *F*-octylbromide NE helps overcome hypoxia-induced resistance to cisplatin therapy. a) Tumor growth in mice treated with saline (green circles), the PFC NE + O<sub>2</sub> (red squares), cisplatin (grey triangles), cisplatin + O<sub>2</sub> (green triangles) or cisplatin + PFC NE + O<sub>2</sub> (diamonds); b) relative tumor growth rate for the same treatment. Adapted from [342].

recovery in rats [232]. *F*-octane NE droplets loaded in hollow polymeric microparticles delivered O<sub>2</sub>, thereby extending the survival and preserving the osteogenic differentiation potency of hypoxic human periosteal-derived cells; new bone formation was accelerated and bone density was increased in cultured cells and in minipigs with mandibular osteomyelitis [347,348]. Degenerative intervertebral disc repair was realized using a simvastatin-loaded *F*-pentane phase-shift double emulsion, along with US, in isolated rabbit spinal discs [215]. Diverse biotechnological culture systems for enzyme, hormone, anticancer drug, monoclonal antibody, genetic material, or tissue graft production have investigated use of neat or emulsified PFCs, or PFC-enriched gels or scaffolds for transfer of O<sub>2</sub>, CO<sub>2</sub> and other gases for improving

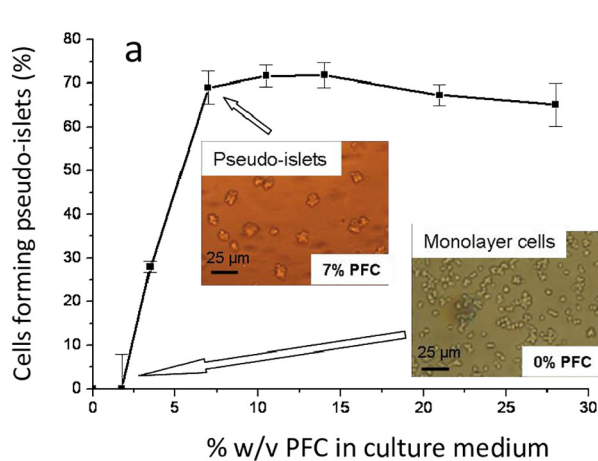


**Fig. 14.** Contact with an O<sub>2</sub>-delivering *F**nHm*-stabilized PFC NE increased cell viability and a) prevented adhesion of  $\beta$ -cells to the Petri dish and promoted formation of insulin-secreting pseudo-islets; b) stimulation of insulin production showing the beneficial effect on pseudo-islet functionality (the stimulation index is the ratio of insulin concentration at high versus low glucose concentration). Adapted from [352].

biomass yields [349]. Incorporation of *F*-octylbromide in an alginate gel resulted in a substantial increase in O<sub>2</sub> permeability and transport for tissue engineering [350].

#### 4.3.4. Preserving isolated organs and tissues

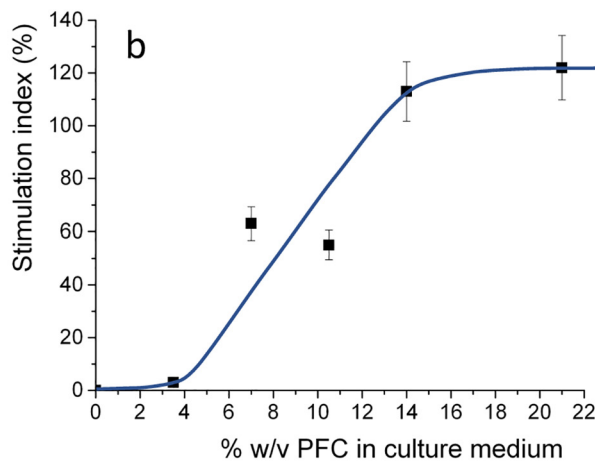
Oxygen is indispensable for the preservation of organ grafts destined for transplantation. Advances in organ and tissue preservation could substantially increase the number of receivers. *Oxygent*-type NEs improved liver-transplantation survival in rats [351]. A *F**nHm* diblock-stabilized *F*-octylbromide NE prevented hypoxia of pancreatic rat Langerhans islets and preserved their insulin production capacity (Fig. 14) [294,352,353]. Ex vivo lung reconditioning and transplantation with this NE was deemed safe and improved tissue preservation and graft function in a pig model [66]. Such a reconditioning strategy could help mitigate graft shortages. The pharmaceutical design and development of PFC nanocolloids for O<sub>2</sub> delivery in regenerative medicine has been reviewed [354].

### 5. The O<sub>2</sub> microbubble delivery option—a change in paradigm

An alternate option for O<sub>2</sub> delivery relies on the direct administration of PFC-stabilized O<sub>2</sub> micro- or nanobubbles rather than emulsion droplets. This represents a definite change in paradigm since in the former case the PFC does no longer act as a solvent for physical dissolution of O<sub>2</sub>, but as a gaseous stabilizer of an O<sub>2</sub> microbubble. Such MBs can also be generated through vaporization of NE droplets. US exposure can prompt on-demand O<sub>2</sub> delivery from MBs located at the disease site.

#### 5.1. Injectable PFC-stabilized micro- and nanobubbles

O<sub>2</sub>-loaded PFC-stabilized MBs can be fabricated *de novo* and administered as such. In addition, they offer the possibility of US image-guided and triggered O<sub>2</sub> delivery. Thus, focused US-triggered destruction of lipid-shelled O<sub>2</sub> MBs osmotically stabilized by a small amount of *F*-butane significantly enhanced image-guided local O<sub>2</sub> delivery (Fig. 9b,c) [111]. In some instances perfluorochemical MBs have served as templates for the preparation of O<sub>2</sub> MBs: PFC-stabilized MBs are prepared first, after which the PFC is exchanged for O<sub>2</sub> [112,113,355]. US-targeted destruction of *F*-butane MBs sparged with O<sub>2</sub> and coupled to a sonosensitizer (Rose Bengal) and chemotherapeutics potentiated simultaneous chemo- and sonodynamic treatment of pancreatic [113,356] or breast [355] cancer in xenografted tumor-bearing mice. Similar MBs with superparamagnetic iron oxide NPs loaded in their shell allowed magnetic targeting [357]. *F*-propane-stabilized



O<sub>2</sub>-loaded MBs substantially elevated pO<sub>2</sub> in a rabbit breast tumor model upon US-triggered burst [358]. *F*-propane enabled the formation of Span-60-shelled MBs that, after freeze-drying, were laden with O<sub>2</sub>, allowing US-assisted sensitization of hypoxic breast tumors to radiotherapy in mice [359,360]. US-mediated local O<sub>2</sub> release from *F*-propane/O<sub>2</sub> MBs inhibited hypoxia and accomplished vascular normalization for enhanced tumor perfusion and doxorubicin delivery and penetration [361]. O<sub>2</sub> delivery by MBs and NBs for effective reversal of hypoxia and photo-triggered cancer theranostics has been thoroughly reviewed [99,140]. SF<sub>6</sub> MBs (*SonoVue*) enhanced the antitumor effects of sinoporphyrin sodium-mediated SDT in vitro and in mice [362]. Intraperitoneal administration of O<sub>2</sub>/paclitaxel-loaded, folate-targeted *F*-propane MBs allowed US-mediated MB destruction for delivery of O<sub>2</sub> and paclitaxel to ovarian cancer cells and tumor-associated macrophages in a murine model [363,364].

## 5.2. Microbubbles generated through acoustic nanoemulsion droplet vaporization

A still further possibility is to generate O<sub>2</sub>-delivering MBs by in vivo vaporization of previously infused P-SNEs of volatile PFCs. Acoustic droplet vaporization is most commonly used. P-SNEs of *F*-pentane, with its boiling point at 28–30 °C, i.e. somewhat below human body temperature, are the most thoroughly investigated. Dextran-shelled *F*-pentane nanobubbles showed US-enhanced O<sub>2</sub> delivery in vitro [165]. Small doses of the *Echogen F*-pentane P-SNE effectively protected O<sub>2</sub>-breathing rats from severe anemia [365], and significantly reduced hypoxia caused by right-to-left shunt in the lung of pigs [366].

These early demonstrations were consolidated by studies using the *F*-pentane/*F*-surfactant P-SNE *NVX-108* for overcoming the tumor hypoxia barrier to cancer radio-, chemo- & immunotherapy [198]. O<sub>2</sub> delivery by this P-SNE protected the ischemic brain in a rabbit stroke model, reducing stroke volume and improving neurological outcome [367]. It extended the “golden hour” time window for recombinant tissue plasminogen activator (rtPA) thrombolysis treatment (Fig. 15) [368]. The product also reduced the extent of infarction in a murine stroke model [369], and of myocardial ischemia-reperfusion injury in acutely infarcted rat hearts [370]. Its administration increased cerebral O<sub>2</sub> tension and lessened post-traumatic brain injury hypoxia in rats [371], and substantially reduced infarct size in a murine model of cardiac ischemia [372]. Use of *NVX-108* as a resuscitation fluid for management of hemorrhagic shock and traumatic brain injury has been reviewed [373]. Its O<sub>2</sub> offloading behavior was studied in vitro [374]. O<sub>2</sub> delivery decreased ischemic stroke infarct volume in a rabbit model [375]. The emulsion markedly enhanced tumor pO<sub>2</sub> and radiotherapy efficacy in pancreatic tumor xenografts in mice [376]. The O<sub>2</sub> carried by another multifunctional *F*-pentane P-SNE contributed to enhanced

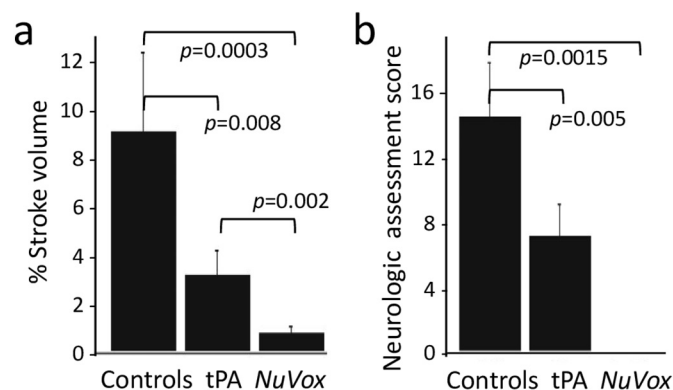


**Fig. 15.** Administration of an O<sub>2</sub>-delivering *F*-pentane P-SNE (*NuVox*) extended the window for tissue plasminogen activator (tPA) therapy in a rabbit stroke model: a) % stroke volumes at 24 h for animals treated with the PFC emulsion and tPA alone, and vs. controls; b) neurologic assessment scores at 24 h. Adapted from [368].

photodynamic treatment, leading to glioblastoma tumor eradication in mice (Fig. 16) [329]. A similar emulsion reduced brain damage after traumatic brain injury-related hypoxia in swine [196].

Clinical Phase Ib/II studies of the safety, tolerability and effectiveness of *NVX-108* in overcoming tumor hypoxia have been conducted in primary glioblastoma multiforme patients, in combination with radiation and temozolomide chemotherapy [197,198]. No significant adverse effects were noted in this initial dose exploration phase. The product has received Orphan Drug Designation as an O<sub>2</sub> providing radiosensitizer for chemoradiation treatment of glioblastoma. A randomized prospective phase II trial is on-going. A small dose-escalation study in acute ischemic stroke patients concluded that the product was safe at the dose tested and may improve clinical outcomes [377].

A paclitaxel and indocyanine green-loaded *F*-pentane P-SNE provided combined photo(sono)dynamic therapy and chemotherapy as well as dual US and photoacoustic imaging [378]. A similar P-SNE loaded with oxaliplatin, when subjected to near-infrared and ultrasound, augmented the anti-tumor effect, enhanced immunological potency and provided dual-mode imaging in mice [379]. Other examples of uses of *F*-pentane and heavier PFCs for O<sub>2</sub>-dependant cancer therapy enabling are provided in Section 4.3.2; it is sometimes difficult to appreciate whether phase shift is implicated.

## 6. O<sub>2</sub> delivery by further PFC-based colloids

A few recent studies that investigate O<sub>2</sub> transport by fluorinated colloids other than PFC NEs, MBs or P-SNEs, in which O<sub>2</sub> delivery is either a

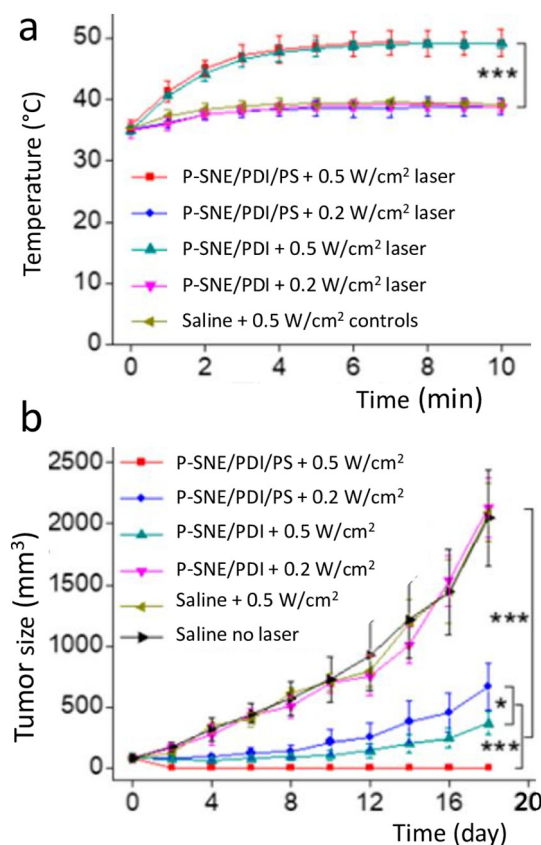


**Fig. 16.** Photoacoustic and US imaging-guided combined photothermal (PTT) and O<sub>2</sub>-enhanced photodynamic (PDT) cancer therapy in mice using a *F*-pentane P-SNE with a perylene diimide photoabsorber shell (P-SNE/PDI) that can include a fluorinated zinc phthalocyanine photosensitizer (PS), under 0.5 or 0.2 W/cm<sup>2</sup> laser light irradiation. a) Temperature curves at tumor region; b) tumor growth curves; complete tumor eradication was observed in the O<sub>2</sub>-supplying *F*-pentane P-SNE/PTT + PDT group subjected to 0.5 W/cm<sup>2</sup> laser irradiation. Adapted from [329].



deliberate part of a theranostic strategy, or that pursue other goals, but inevitably also provide an O<sub>2</sub> reservoir, are illustrated here. Examples of *F*-alkylated or *F*-arylated components of fluorinated polymeric micelles formed for this purpose are provided in Table 7. <sup>1</sup>O<sub>2</sub> production and PDT efficacy of micelles made of PEGylated copolymers bearing pending pentafluorophenyl groups and photosensitizing porphyrins **28** increased when the *F*-phenyl/porphyrin ratio increased [380]. Augmented ROS production for PDT therapy was also obtained with O<sub>2</sub>-carrying, photosensitizer-doped micelles made from *F*-octyl chain-bearing branched poly(ethylene imine) **22** [252]. Doxorubicin-loaded micelles made of a polymer with PEG chains outside, a central photosensitive heptamethine dye, and C<sub>9</sub>F<sub>19</sub> chains inside **29**, were reported to enhance O<sub>2</sub> delivery, resulting in synergistic PDT and chemotherapy in mice [381]. O<sub>2</sub>-carrying photosensitive NPs of pegylated poly(β-amino ester) polymer with pending *F*-pentyl chains **30**, co-loaded with a specific oxydoreductase inhibitor (NLG919) involved in tumor escape from immuno-surveillance, relieved immune suppression and enhanced PDT

efficacy through alleviation of tumor hypoxia (Fig. 17) [382]. Fluorinated, hyaluronic acid-based polymeric micelles made of compound **24** showed O<sub>2</sub>-enhanced PDT efficacy against choroidal melanoma [58].

*F*-hexane was encaged in targeted porous Fe<sub>3</sub>O<sub>4</sub> NPs loaded with etoposide for MRI-monitored O<sub>2</sub>-enhanced chemotherapy in mice [223]. *F*-hexane loaded in hollow MoS NPs surface-modified with a phthalocyanine and with human serum albumin, served as O<sub>2</sub> carriers for PDT as well as for fluorescence, photoacoustic and CT imaging in mice [221]. *F*-hexane-loaded PEGylated hollow Bi<sub>2</sub>Se<sub>3</sub> NPs provided augmented near IR and X-ray absorbing capacity, and achieved enhanced light-induced O<sub>2</sub> delivery to fight hypoxia-associated radio-resistance in tumors in mice [224]. O<sub>2</sub> diffusion, hypoxia alleviation and enhanced radiotherapy were also obtained with *F*-pentane-loaded, <sup>64</sup>Cu-labeled mesoporous organosilica NPs, as well as US/photoacoustic and PET imaging (Fig. 18) [228].

*F*-octyl chains were grafted onto sonosensitizer-carrying hollow silica NPs for US-promoted O<sub>2</sub> delivery for enhanced SDT efficacy in

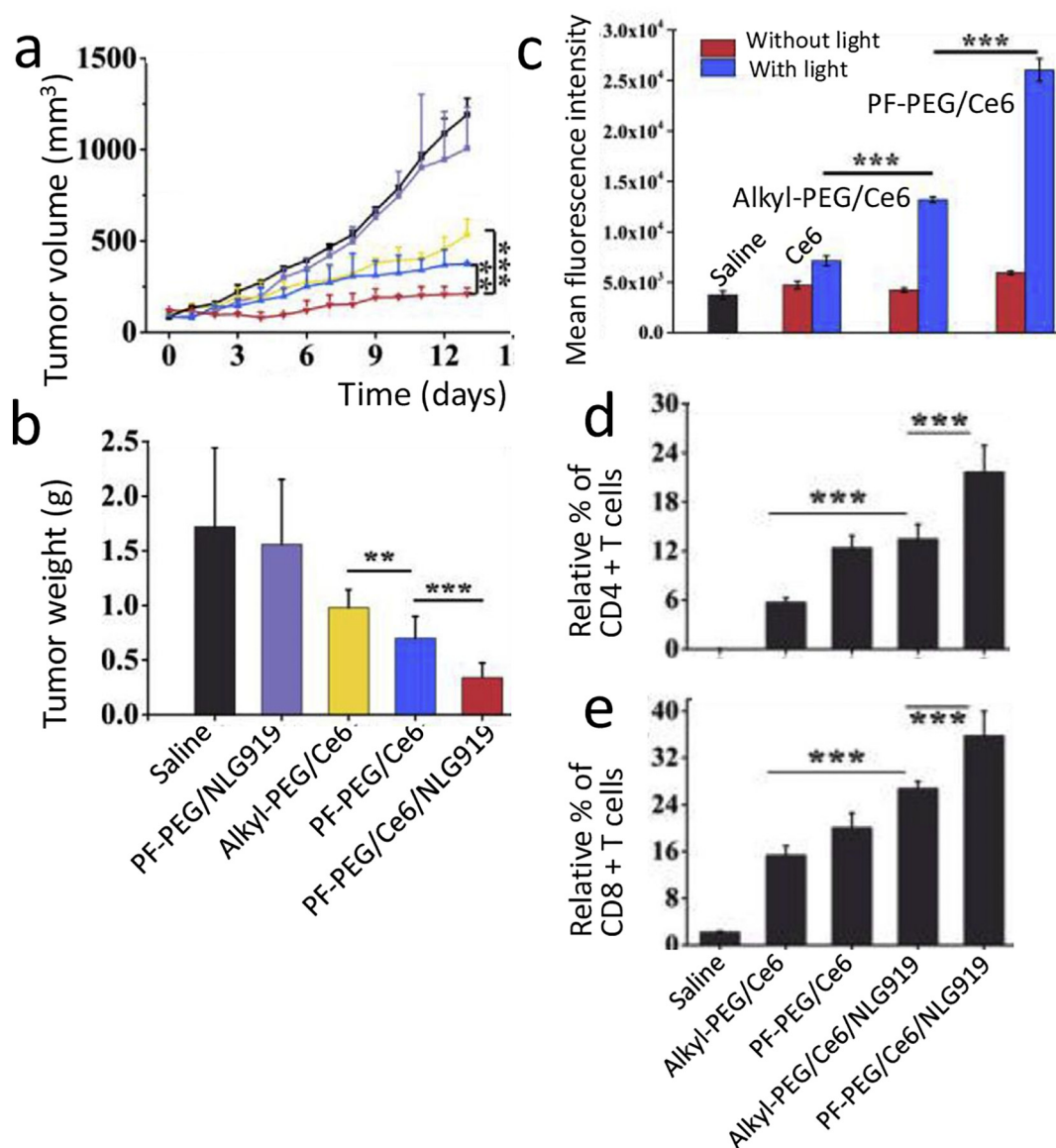


**Fig. 17.** Simultaneous O<sub>2</sub>-enhanced photodynamic therapy and boosted antitumor immune response obtained in mice with O<sub>2</sub>-carrying micelles of a pending *F*-pentyl chain-fitted PEG-polymer (PF-PEG) loaded with a chlorin (Ce6) photosensitizer and an inhibitor (NLG919) of indoleamine-2,3-dioxygenase (IDO), a tumor-expressed enzyme that is involved in tumor immune escape; a non-fluorinated analog (alkyl-PEG) polymer was also investigated. a) Inhibition of tumor growth (tumor volume over time) by various treatments (laser light was 55 W/cm<sup>2</sup>; same color code as in b); b) tumor weight at the last day of treatment; c) mean fluorescence intensity, denoting ROS generation capacity using singlet oxygen sensor green for various formulations, with and without laser light; d) percentage of tumor infiltrating CD4+ T cells, and e) CD8+ T cells. Adapted from [382].

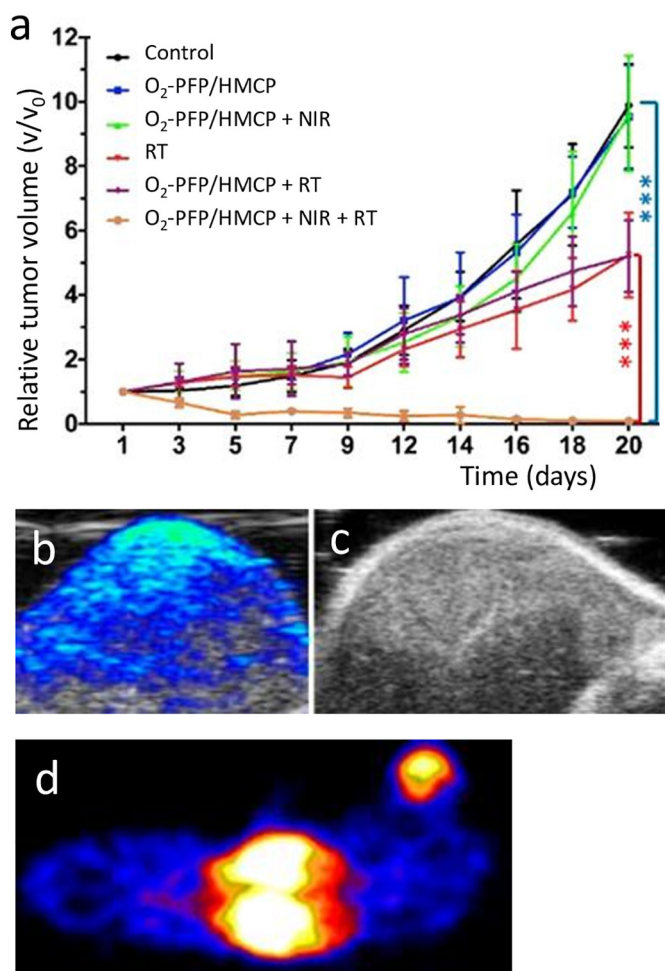


**Fig. 18.** *F*-pentane (PFP)-loaded pegylated biodegradable hollow mesoporous organosilica NPs with surface-bound CuS (designated as HMCP) for laser light-induced MB-enhanced, O<sub>2</sub>-sensitized radiotherapy. a) Relative tumor volume over time in mice for various treatments (NIR: near-infrared, RT: radiotherapy); b-d) photoacoustic, US and PET images, respectively; the latter was obtained by <sup>64</sup>Cu labeling of the NPs. Adapted from [228].

pancreatic tumor cells and tumor xenografts in mice (Fig. 19) [253]. *F*-sebacic acid-bridged tetra(hydroxyphenyl)porphyrin-cross-linked porous PEGylated polymeric NPs filled with *F*-15-crown-5-ether provided O<sub>2</sub> for hypoxia relief and enhanced PDT in mice; <sup>99m</sup>Tc radioisotope-chelating enabled SPECT imaging [383]. Tumor-targeted, pH-sensitive dextran NPs, grafted with *F*-propyl poly(*L*-lysine) dendrons and doped with a cyanine photosensitizer, was used for PDT and inhibited breast tumor growth and reduced lung and liver metastasis in mice [57]. Enhanced <sup>1</sup>O<sub>2</sub> production and PDT were also reported with O<sub>2</sub>-carrying hybrid *F*-alkylated siloxane-polystyrene NPs doped with a *F*-arylated zinc phthalocyanine photosensitizer [254].

## 7. Perfluorocarbon colloids can also deliver other gases, contrast, energy, drugs, genes, and have a clear vocation for theranostics

The recent years have witnessed an outburst of prospective PFC-based nanomedicines for an increasing number of indications other than O<sub>2</sub> delivery. Objectives include increasingly sophisticated diagnostic imaging modalities, focused delivery of energy in various forms, controlled as and when required delivery of therapeutics, ... and even control of urinary stress. Even when the primary goal is different, the *F*-colloids put to work predictably do carry, and can release a certain amount of O<sub>2</sub>. Multiple functionalization can lead to theranostic

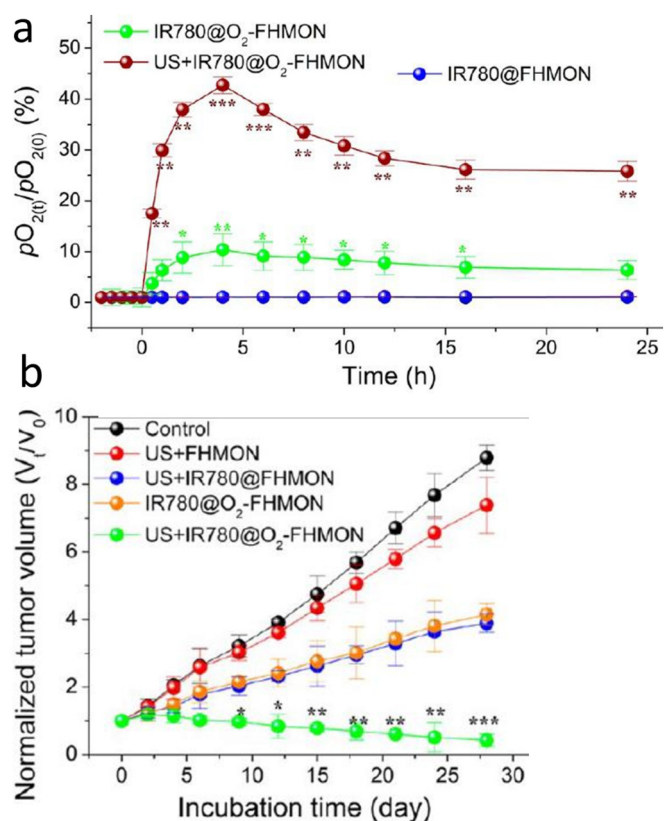


**Fig. 19.** *F*-octyl chain-functionalized hollow mesoporous organosilica NPs (named FHMON) loaded with a sonosensitizer (IR780) for alleviating hypoxia-induced resistance to sonodynamic pancreatic cancer therapy. a) Hypoxia reversion in solid pancreatic tumor implanted in mice, as indicated by relative pO<sub>2</sub> variation over time, for diverse treatments; b) reduction of hypoxia-induced resistance to treatment, as reflected by tumor volume changes over time. Adapted from [253].

procedures and synergistic effects. Safely crossing the blood-brain barrier for delivery of O<sub>2</sub>, energy and other therapeutics is a major challenge that could be met by appropriate MB or P-SNE/US combinations. The capacity of PFC colloids for simultaneous diagnostic imaging/monitoring/assessing functions and O<sub>2</sub>, energy and drug delivery open countless theranostic opportunities.

### 7.1. Delivery, or removal, of therapeutic gases other than oxygen

Gases other than O<sub>2</sub> can also be delivered by PFC NPs, MBs and other PFC constructs. A *F*-octane NP delivered, for example, nitric oxide as an antibacterial agent [384]. Likewise for *F*-propane/NO MBs [385]. Pulsed US-induced release of NO from *F*-propane-stabilized MBs induced vasorelaxation in porcine carotid artery tissue [386]. Complementing graphene oxide sheets with an *F*-alkylated PEG improved the preservation of dissolved NO gas, thereby enhancing antibacterial activity against *E. coli* and *S. aureus* [387,388]. Mixed hydrogen/*F*-propane MBs delivered H<sub>2</sub> as an antioxidant against myocardial ischemia-reperfusion injury in a rat model [389]. Xe-containing *F*-propane MBs were prepared for US-triggered neuroprotective Xe release for treatment of stroke [390].

PFCs may also help retrieve undesired gases, such as N<sub>2</sub> for prevention and treatment of decompression sickness, but the results obtained under diverse conditions were uncertain. Administration of a *F*-pentane P-SNEs (*Echogen*) increased central venous O<sub>2</sub> tension and effectively enhanced tissue denitrogenation under O<sub>2</sub> breathing in pigs [391]. Another study with a *F*-pentane P-SNE found no effectiveness in rodents [392]. An undesirable increase of pulmonary artery pressure and no

effect on survival were observed with *Oxycyte*, also in swine [393]. Further options are being discussed [394]. Removal of arterial gas embolism-causing air bubbles formed during use of cardiovascular bypass machines has been demonstrated with PFC NEs [395]. PFCs can also help eliminate the excess  $O_2$  that inhibits cell growth in certain bioprocesses. The aid of a *F*-octylbromide/*F*-surfactant NE led, for example, to a 5-fold increase in biomass production in microalgae cultivation [396]. The rapid scavenging of  $O_2$  dissolved in an air-saturated fluid during US-activated droplet vaporization of a *F*-pentane/albumin P-SNE was investigated in vitro and modeled [397,398].

## 7.2. $^{19}\text{F}$ MRI, ultrasound and multimodal imaging for diagnosis of disease, guidance for procedure, assessment of treatment outcome

As noted, PFC NEs provide ideal  $^{19}\text{F}$  NMR and MRI probes, including for labeling and tracking of circulating cells, while soft-shell MBs are ideal contrast agents for diagnostic US imaging. Targeting provides molecular imaging, and functionalization (Section 3.6) opens numerous other imaging modalities, including fluorescence, photoacoustic, sonophotoacoustic imaging, CT, PET and SPECT,  $^1\text{H}$  MR imaging or guidance, many of which can be acquired simultaneously.

$^{19}\text{F}$  magnetic resonance benefits from high sensitivity, second only to  $^1\text{H}$ , from a broader range of chemical shifts, and from high specificity owing to the lack of endogenous molecular fluorine in the body.  $^{19}\text{F}$  MRI originally required use of PFCs having numerous magnetically equivalent fluorine atoms, such as *F*-poly(ethylethers) **12** (e.g.  $\text{CF}_3(\text{OCF}_2\text{CF}_2)_n\text{OCF}_3$ ), *F*-15-crown-5-ether **13**, PERFECTA, and other *F*-alkylated polymers and dendrimers [19,399–403]. Technical progress in equipment (RF coils) and MR sequences now permits use of more rapidly excreted and less expensive PFCs, such as *F*-octylbromide, although they have fewer equivalent  $^{19}\text{F}$  nuclei [297,298,403,404]. Incorporation of paramagnetic elements can further enhance the sensitivity of  $^{19}\text{F}$  probes [256,257,405]. Being paramagnetic, the  $O_2$  dissolved in PFCs also impacts MR relaxation parameters, enabling quantitative mapping of tissue oxygenation [406].  $^{19}\text{F}$  MRI is thus emerging as a powerful imaging modality for detection of inflammation, myocardial infarct, thrombi, angiogenesis, ischemia, allograft rejection, quantification of tissue oxygenation (oxymetry), temperature, pH and other parameters [19,297,402,404,405,407]. For example,  $^{19}\text{F}$  MR imaging and spectroscopy with *F*-octylbromide or *F*-15-crown-5-ether NEs allowed quantification of vascular damage in kidney following ischemia-reperfusion injury, as well as assessment of treatment with an anti-thrombin agent-loaded PFC NE [408].

PFC probes and  $^{19}\text{F}$  MRI could also help advance the development and clinical translation of immune and stem cell-based therapies, a promising up-and-coming strategy for cancer treatment, by providing critical quantitative in vivo information on circulating immune cell status [409,410]. Labeling of circulating cells by internalization of PFC NE droplets, as through phagocytosis, allows direct  $^{19}\text{F}$  MRI tracking of immune cells, such as inflammation macrophages for visualizing inflammatory processes, or adoptive transfer of T lymphocytes, NK cells, dendritic cells or peripheral blood mononuclear cells for cell-based therapies and vaccines [24,399,411,412]. In oncology, the main objective is to realize separation, identification and destruction of circulating tumor cells shed by primary tumors [413–417]. As noted, a series of commercial *F*-15-crown-5-ether and *F*-poly(ethylether) NE tracer agents is available from Celsense Inc. (Pittsburg) for cell labeling, including the FDA-approved *F*-polyether NE, CS-1000, simplifying cell-tracking investigations by  $^{19}\text{F}$  MRI [412,414,418]. Uptake of *F*-15-crown-5-ether nanodroplet by cardiac progenitor cells was significantly enhanced when the cells were labeled with *FuGENE*, a reagent frequently used for DNA transfection [419]. Use of a *F*-*t*-butylcyclohexane emulsion as a tracer has also been suggested [420].

Concerning standard  $^1\text{H}$  MRI probe capacity, it is easily conferred to PFC NEs by incorporation of paramagnetic metal complexes, such as gadolinium(III) chelate- or superparamagnetic iron oxide-based agents

[421,422]. Dendronized iron oxide NPs inserted in the phospholipid shell of *F*-hexane-stabilized MBs are being proposed for combined MRI/US imaging [34].

Overlaying  $^{19}\text{F}$  and  $^1\text{H}$  images provides detection and quantification of the  $^{19}\text{F}$ -probe as “hot spots” in a specific site, while  $^1\text{H}$  MRI depicts the anatomic context [423], allowing, for example, detection and localization of inflammation [424], or of venous thrombosis and diagnosis of pulmonary thromboembolism [425].

Elastic soft-shelled gas bubbles are ideal sound reflectors (Scheme 3). When subjected to US waves, soft-shelled MBs alternatively expand and contract, and resonate at a frequency that is inversely proportional to their radius and also depends on shell elasticity. Nonlinear MB expansion and contraction generate harmonic and sub-harmonic frequencies that can be filtered out and constitute the very signature of the MBs. Their detection and localization enable contrast-enhanced US imaging. Higher energy US pulses engender inertial MB cavitation and, eventually, can lead to disruption and release of energy (either thermal or mechanical) and cargo [67,107,108,115,277,426–428]. The capacity for manipulating MBs by US is unique and has reached utmost accuracy. Conversely, the advent of MBs has stimulated the development of numerous novel MB-specific imaging modes and procedures, such as cavitation imaging, harmonic power Doppler, pulse inversion, or amplitude modulation imaging that improve diagnostic sensitivity, specificity and reliability [428–431]. In view of their size, usually 1–4  $\mu\text{m}$ , standard intravascularly administered contrast MBs are restricted to the vasculature and are therefore basically blood pool agents [87,88,107,137,278,431–434]. Several MB contrast agents have been in clinical practice for 20 years (Section 3.3). The initially approved indication concerned essentially left ventricular opacification and endocardial border delineation. Over the years, the range of indications has expanded, while most of the FDA's initial restrictions have been lifted. In Europe (and off-label in the US), contrast agents are also utilized for liver and breast masses characterization and other uses, including assessment of pancreatic masses, of the neovascularization of carotid plaques and detection of vulnerable ones, and evaluation of the gastrointestinal and urinary tracts [435–437].

Several clinical studies explore the use of these agents for further indications, especially tumor characterization. MB-delivered contrast can also help monitor and assess treatment efficacy [434,438–441]. A pilot study indicated that  $\text{SF}_6$  MBs (*SonoVue*)-enhanced US could be as effective as contrast CT for evaluating radiotherapy efficacy in patients with liver metastasis [442]. The safety of PFC-based MB products has been surveyed in a meta-analysis involving over 200,000 patients, which found that contrast echocardiography was actually associated with a lower mortality than for control patients! [426,443] Use of contrast-enhanced US in emergency and critical care situations has been reviewed [444], and guidelines for clinical use of US contrast agents are regularly published [445,446].

As mentioned earlier, MBs can also, when fitted with appropriate implements, provide fluorescence [447] or photoacoustic [448,449] imaging, PET [228,450,451] or SPECT [383,452,453], or proton MRI imaging or guidance. For example,  $\text{SF}_6$  MBs with gold NPs in their shell, when destroyed by US, enhanced the photoacoustic signal, allowing background-free photoacoustic imaging of tumor-bearing mice [448]. *F*-butane MBs (*Vevo MicroMarker*), along with focused US, enabled delivery of silica-coated gold nanorods across the BBB for photoacoustic diagnostic imaging and therapeutic monitoring of neurological conditions in mice [449]. Magnetically guidable iron oxide-loaded *F*-pentane NBs provided  $^1\text{H}$  MRI/US contrast imaging [454]. *Definity* was used for US/ $\text{Gd}^{3+}$ -enhanced MRI-guided BBB opening [455].

Molecular imaging detects, characterizes and quantifies molecular markers of diseases. It reveals specific biochemical changes produced at the cellular level. Therefore, the PFC NE droplet or MB is fitted with ligands that can target one or more biomarkers specific of the disease (Scheme 6b) [100,101,278,279,426,456–461]. Favored targets include atherosclerosis, microvascular inflammation, thrombosis, ischemic



injury and tumor neovascularization [277,278,462–468]. Molecular imaging should be particularly valuable for early cancer diagnosis and therapy. It could also help detect acute rejection after cardiac transplantation [469] and should provide precious means of monitoring treatment efficacy. US molecular imaging with BR55 could provide a predictive tool of anti-angiogenic mammary tumor treatment efficacy through early assessment of individual patient response [470]. Dual-targeted MBs enhance diagnosis specificity and reliability [471,472].

A clinical trial explores the use of macrophage-aiming phosphatidylserine-containing MBs (*Sonazoid*) for imaging of sentinel lymph nodes in breast cancer patients [473]. NEs could have an advantage over MBs in molecular imaging because of their much longer intravascular persistence, which increases the probability for binding to the targeted tissue.

Detection of metastases grown from circulating tumor cells (CTCs) shed by a primary tumor is key to diagnosis and prognosis of cancer. Properly targeted PFC NEs and MBs can provide effective ways for early detection, isolation, characterization and targeted treatment of such cells [283,474–477]. This technique offers a non-invasive liquid biopsy approach for metastatic cancer staging and treatment. PFC-labeled MBs can thus help biopsy sentinel lymph nodes in breast cancer, potentially replacing axillary surgery [478,479], and has entered routine practice in certain medical centers [480]. Targeted *USpheres* MBs were used for in vivo characterization of programmed death ligand-1 (PD-L1)-expressing cells in a mouse model [481].

### 7.3. Controlled delivery and channeling of therapeutic energy

Using PFC NEs, MBs or P-SNEs, controlled focalized US- or light-actuated delivery of thermal and/or mechanical therapeutic energy can be achieved in various forms, including heat, acoustic streaming and radiation force, stable and inertial cavitation and, for higher US intensities, MB explosion sound waves and jet of particles (Scheme 3). Energy can be focused, targeted and delivered on-demand at specific sites, thereby enabling a panoply of minimally invasive procedures such as thermal or mechanical tissue ablation, sonothrombolysis, embolotherapy, revascularization, sonoporation, sonobactericide and other procedures. MBs provide cavitation nuclei, help control the conversion of acoustic pressure into thermal and/or mechanical energy, reduce the level of energy required to initiate cavitation and reduce the duration of the intervention, thereby decreasing damage on nearby healthy tissues. *F*-colloids can help direct the procedure either towards production of heat as for coagulative thermal ablation, or towards mechanical tissue destruction (histotripsy).

One objective of high-intensity focused US is to raise the temperature of a specific targeted tissue volume above 55 °C to generate coagulative necrosis and tumor death. PFC-based SNEs increased the efficacy of focal energy deposition in a tissue-mimicking phantom study [482]. Another phantom study with a *F*-hexane P-SNE coated with human serum albumin, or with a fluorinated surfactant, provided controlled thermal ablation [483]. In a further phantom study, micron-sized *F*-octylbromide NEs stabilized with *F*-surfactants were proposed for focused US thermotherapy [191]. A *F*-pentane P-SNE allowed in vivo MR-guided focused US ablation of tumors in rabbit [484]. The efficacy of *F*-butane MBs and of *F*-pentane/*F*-butane P-NEs in rat liver ablation was compared [485]. A *F*-15-crown-5-ether NE enabled precise <sup>19</sup>F MRI-guided thermal ablation of tumors in mice [486]. Lipid and poloxamer-shelled *F*-propane nanobubbles provided image-guided delivery of Pluronic L10 as a thermal sensitizer for facilitating radiofrequency tumor ablation [487]. Tumor ablation can also be achieved photothermally. Thus, *F*-pentane P-SNEs with a PLGA shell loaded with magnetic NPs allowed MRI/US imaging and photothermal tumor ablation in mice [488,489]. A *F*-pentane P-SNE loaded with gold nanorods produced cavitation effects that enhanced sonoporation and improved delivery of photothermal tumor treatment in mice [490]. A clinical study of MB (*SonoVue*)-assisted ablation of uterine fibroid

found that significantly lesser acoustic power and shorter exposure time were needed than in the absence of MBs [491].

Histotripsy is a non-invasive image-guided US technology that mechanically destroys targeted tissues. Unlike thermal ablative forms of therapeutic US, histotripsy relies on the mechanical action of bubble clouds for tissue destruction [492]. Applying short high pressure histotripsy pulses to *F*-pentane or *F*-hexane NEs effectively ablated prostate cancer spheroids embedded in tissue-mimicking gel phantoms [493]. Transcranial MRI-guided focused US with *Optison* MBs allowed ablation of tissue volumes in rat brain without long-term undesirable effects [494]. Phospholipid-shelled *F*-butane MBs under US were used for myocardial reduction therapy in a rat model of hypertrophic cardiomyopathy [495].

Sonothrombolysis, the destruction of vessel-obstructing blood clots, is being intensively investigated [496–498]. *Definity*, combined with US, enhanced the lytic activity of rtPA in an in vitro model of ischemic stroke [250]. US-induced inertial cavitation, but not stable cavitation, of *F*-butane MBs (*BR38*, Bracco), in combination with rtPA, achieved clot lysis and fibrin degradation in vitro [499]. Sonothrombolysis using *BR38* or *SonoVue* improved microvascular patency in a rat model of stroke [500]. A *F*-pentane P-SNE achieved clot lysis at reduced acoustic powers in rat [501]. A comparison of in vitro sonothrombolysis of aged clots with *F*-butane P-SNEs and MBs is available [502].

Clinical advances in sonothrombolysis have been reviewed [497,503]. A phase III clinical MB (*SonoVue*)-assisted sonothrombolysis study in acute stroke patients is ongoing in Norway [504]. A clinical trial using *Definity* improved recanalization rates and reduced infarct size, resulting in sustained improvements in systolic function in patients with acute ST-segment elevation myocardial infarction undergoing a percutaneous coronary intervention [505].

Embolotherapy aims mainly at the deliberate occlusion of tumor-feeding blood vessels. *F*-butane MBs were, for example, used to produce an antivasular effect that led to tumor inhibition in mice [506]. A potent reduction of tumor perfusion, accompanied by intratumoral immune activation, was obtained with *Definity*-assisted US under MRI monitoring in murine melanoma [507]. US vaporization of an integrin  $\alpha_v\beta_3$ -targeted, phospholipid-shelled *F*-pentane P-SNE halted growth and induced necrosis in a rodent model of hepatocellular carcinoma [508]. Synergistic antitumor and antivasular effects were observed when US-stimulated MBs (*Definity*) were combined with radiation for breast tumor treatment in mice [509]. The effect of low-frequency low-intensity, MBs (*SonoVue*)-assisted US irradiation parameters on xenograft prostate cancer hypoxia were investigated in mice [510].

Safe blood-brain barrier crossing is another intensely pursued goal. MB (*Definity*)-assisted transcranial focused US alone may, without drug adjunction, help reduce amyloid plaque formed in neurodegenerative diseases and increase endogenous immunoglobulin levels and glial activation [511–513]. Improvement in spatial memory was noted [512,513], as well as a short term antidepressant effect in rodents [514]. Small pilot safety studies with *Definity*- or *SonoVue*-enabled, MR-guided focused US indicated that transient BBB opening in Alzheimer's patients [515] or amyotrophic lateral sclerosis patients [516] could be safe. Blood-spinal cord barrier opening using MB/US combinations has been investigated in rabbits with *Optison* [517] and *SonoVue* [518].

Tissue oxygenation can also be enhanced by dilating blood vessels, which can be produced by mechanical stimulation of NO synthesis. This was achieved by combining *F*-butane/lipid MBs and US exposure, and facilitated reperfusion of ischemic tissue after microvascular obstruction [519]. Likewise, US-mediated cavitation of such MBs markedly increased blood flow and reversed hind limb ischemia in a mouse model [520]. In both cases, the US-induced MB oscillations produced shear stress that caused endothelial mechanotransduction and NO release.

The compressibility of PFCs was put at work in “shock absorbers” consisting of large, centimeter-size polymer-enclosed PFC capsules (*Vesair* bladder control system, Solace Therapeutics, Framingham MA)



that are introduced in the bladder and are in advanced clinical trial for alleviating urinary stress incontinence [521,522].

#### 7.4. Delivery of drugs, genes, tracers, nanoparticles, cells

PFC-based colloids can be loaded with drugs, genes, markers, nanoparticles, cells and other therapeutic devices for controlled delivery. This delivery approach has potential for image-guided, externally triggered, repeatable release of therapeutic cargo at an elected site in diseased tissues, thereby increasing drug efficacy whilst minimizing undesired effects for healthy tissues. Targeting and sonoporation are essential facets of this strategy, as well as concomitant contrast imaging for guidance and monitoring of treatment. Only a limited number of references, mainly reviews, can be given here [95,98,108,137,149,157,523–527]. PFC-promoted recognition, recruitment and transport of drugs, biomarkers and NPs, with enhanced efficacy for the fluorinated ones, could further contribute to safe and efficacious delivery [23,528,529].

Sonoporation, that is, forcing transient openings through the vascular endothelium or blood-brain barrier for passage of drugs, genes, markers, NPs, etc., can be achieved using US of sufficient intensity. Adjunction of MBs can greatly increase sonoporation efficiency, lower the acoustic energy required and mitigate untoward effects [530–534]. The mechanisms of sonoporation have been discussed [535–537]. Sonoporation with clusters associating negatively charged *Sonazoid* MBs and positively charged P-SNE droplets improved therapeutic efficacy of paclitaxel in a pancreatic tumor model in mice [538]. *MicroMarker* MBs, as well as polymer capsules, enhanced US-assisted sonoporation of drug-loaded liposomes [539]. A small clinical study indicated that MB (*SonoVue*)-mediated US applied during chemotherapy in patients with tumors in the digestive system was safe and could restrict tumor progression [540].

Safely crossing the tight blood-brain barrier to deliver therapeutics to specific targets within the brain is a major challenge. PFC colloids could assist focused US-induced BBB opening in a minimally invasive way by reducing and controlling the energy required for the process, while also providing the imaging, guiding and monitoring tools needed for efficacy and safety assessment [159,541–545]. The vaporization efficiency of *F*-propane and *F*-butane nanodroplets was investigated in relation with delivery of a protein-sized dextran [546]. A SF<sub>6</sub> MB/liposome complex delivered O<sub>2</sub> and brain-derived neurotrophic factor, showed neuroprotective effects and improved behavioral deficits in a mouse model of Parkinson's disease [547]. The use of MB-assisted focused US for BBB opening in experimental models of Parkinson's disease has been reviewed [548].

Cardiovascular drug and gene delivery with US and MBs has been reviewed [267,525]. Intraplaque neovascularization-targeting MBs (*Targestar*-derived), loaded with *Endostar* (a recombinant human endostatin, a broad-spectrum anti-angiogenesis agent), inhibited atherosclerotic plaque growth in a mouse model [549]. Antibody-targeted, resveratrol-loaded *F*-propane NBs slowed down intervertebral disk degeneration in rabbits [550].

Cancer treatment involving *F*-colloids is the focus of many reviews [117,551–554]. Permeabilization of cell membrane by MB/low intensity US treatment can facilitate drug penetration in tumors [555], and synergistic (mechanical) antiangiogenic and (chemical) antitumor effects [556]. Examples of cancer treatment studies implying PFC colloids include [346,557–561]. A US-responsive doxorubicin-loaded *F*-hexane NE released Na<sub>2</sub>CO<sub>3</sub> for alleviation of lactic acidosis-mediated doxorubicin resistance [562]. A doxorubicin-loaded *F*-octylbromide NE, encapsulated in brain-targeting peptide-modified PLGA, increased intratumoral accumulation and allowed on-demand high intensity focused US-triggered drug release at the glioblastoma site in mice [563]. A *F*-pentane P-SNE with a shell of PLGA decorated with gold NPs for photothermal therapy, and fitted with a peptide ligand directed at a membrane receptor of melanoma cells for activating the immune system in the tumor microenvironment, enhanced anti-programmed

death-1 (anti-PD-1) antibody treatment efficacy [564]. Sequential release of a chemotherapeutic drug at different acoustic pressure levels from a mixture of soft and hard-shell *F*-pentane P-SNEs is also feasible [167]. Doxorubicin was loaded in a multifunctional *F*-hexane P-SNE that also incorporated Fe<sub>3</sub>O<sub>4</sub> NPs and was folic acid-targeted, allowing MRI and US imaging-guided combined chemotherapy and high intensity focused US tumor ablation (Fig. 20) [565]. O<sub>2</sub>-sparged, doxorubicin and paclitaxel-loaded *F*-butane MBs, which also incorporated the Rose Bengal sonosensitizer, demonstrated US-mediated, combined chemosensitization efficacy on a spheroid model of human breast cancer and on a murine model of the disease [355]. Such *F*-butane MBs, functionalized with the antimetabolite gemcitabine, proved efficacy in the treatment of pancreatic cancer in mice [356].

Several clinical studies involve PFC-assisted focused US-induced BBB opening for treatment of central nervous system diseases. The MBs used are usually the commercially available ones. A small Phase I study in pancreatic cancer patients found that combining PFC MBs (*SonoVue*) with low intensity focused US to enhance gemcitabine delivery through sonoporation was safe [566]. Clinical Phase I/IIa trials revealed that an implantable US device (*SonoCloud*), in combination with *SonoVue*, allowed carboplatin treatment of patients with glioblastoma [567,568]. MR-guided low intensity focused US BBB opening with *Definity* combined with chemotherapy was deemed accurate, safe, reversible and repeatable in patients with glioma [569].

Gene delivery can be achieved either by gene-loaded, usually cationic *F*-colloids, or by co-administration of genes along with sonoporation-promoting MBs. Reviews on enhanced gene delivery using MBs and US are available [90,570,571]. SF<sub>6</sub> MB/liposome complexes were proposed for site- and time-specific plasmid DNA and doxorubicin delivery to tumor cells [559]. The effect of *F*-butane MB-enhanced sonoporation on the delivery of DNA was studied in mice [572]. RNA was delivered to the heart for cardiac gene expression knockdown in mice [573]. MR-guided focused US with *Definity* allowed targeted delivery of a gene silencing viral vector for Parkinson's disease treatment in mice [574]. Aptamer tumor-targeted *F*-propane/lipid siRNA-loaded NBs were effective for prostate cancer treatment in mice [575]. siRNA biotin-streptavidin bound to the surface of *F*-propane/lipid NBs, when subjected to US, enhanced siRNA transfection and reduced glioma tumor growth in mice [576]. Combined siRNA and doxorubicin loaded, targeted SF<sub>6</sub> MB-liposome complexes were investigated for US-guided prostate cancer treatment in mice [560]. Site-specific MB (*SonoVue*)-mediated delivery of a bone remodeling gene was investigated for bone fracture healing in mice [577]. Gene delivery for acute spinal cord injury treatment was achieved by US destruction of cationic *F*-propane NBs in rats [578].

Inhibiting immune checkpoints that block T-cell function is a promising cancer therapy approach. Delivery across the BBB of targeted natural killer (NK) cells to specific regions in the brain, using *Definity* MBs and MRI-guided focused US, improved survival in early treatment of brain tumors in rodents [579]. Likewise, the use of *USpheres* helped improve adoptively transferred NK cell infiltration in a mouse model of ovarian cancer [580]. An anti-vascular US-stimulated *F*-propane MB treatment, combined with anti-PD-1 therapy, increased tumor growth inhibition and survival in mice [581]. Numerous articles report use of *F*-15-crown-5-ether NEs for dendritic cell tracking.

Fighting bacterial infection by combining MBs or P-SNEs with US and antimicrobial drugs is an emerging strategy (sonobactericide) that could be particularly valuable in the context of increasing drug resistance of bacteria [582–584].

#### 7.5. Pulmonary, ophthalmic and other applications

Neat liquid or gaseous PFCs are routinely being used in ophthalmic indications [585] and investigated for pulmonary ones [20]. A review on US-mediated ocular delivery of therapeutics cites a few studies on PFC MB-assisted gene transfer [586]. Aerosolized PFCs, primarily

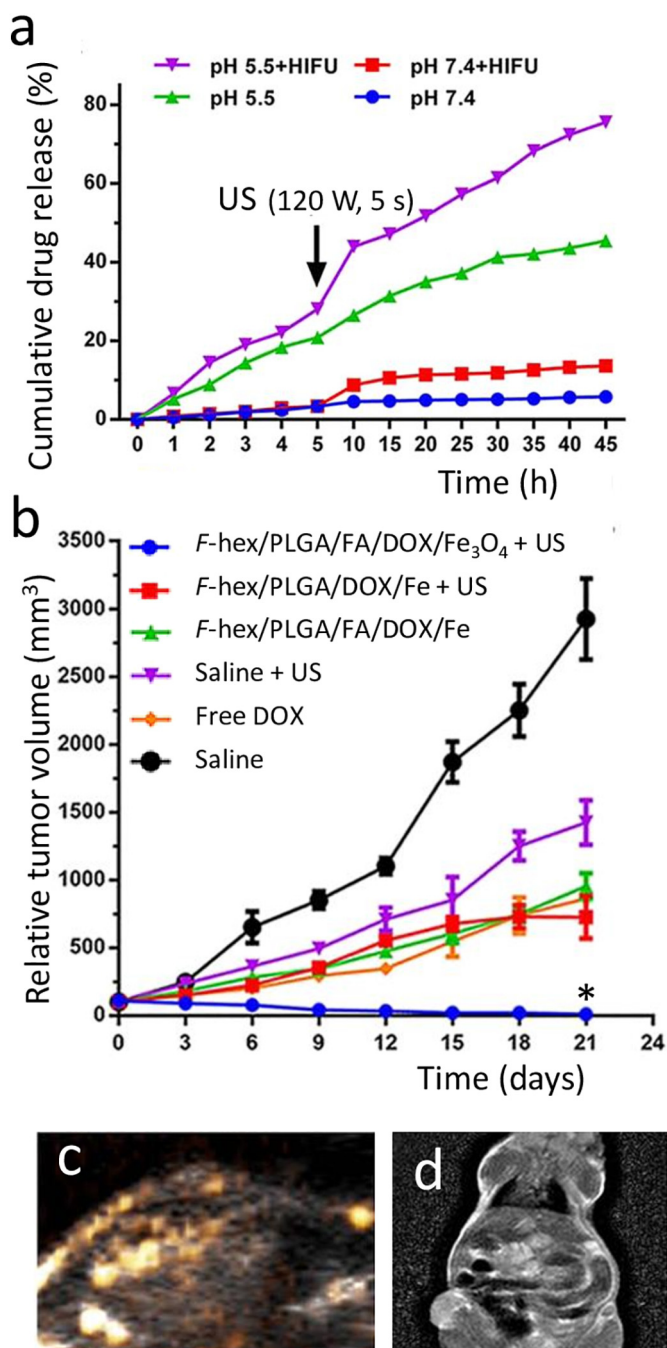


**Fig. 20.** Combined (theranostic) tumor ablation and chemotherapy using a US-triggerable phase-shift PLGA-shelled *F*-hexane composite loaded with doxorubicin (DOX) and superparamagnetic  $\text{Fe}_3\text{O}_4$  NPs (Fe), and fitted with folic acid (FA) for targeting. a) Stimuli-responsive DOX-release at different pH and high-intensity focused US exposure conditions; b) variation of relative tumor volume with time after diverse treatments, (\* $p < 0.01$  vs. other treatment groups); c) and d) contrast US imaging and MRI, respectively, for image guidance. Adapted from [565].

*F*-hexane, were investigated as anti-inflammatory agents in acute lung injury models [20,587,588]. Pulmonary delivery of neat PFCs is being investigated for liquid ventilation and hypothermic organ protection after cardiac arrest [589], and as lung surfactant substitutes [30]. Intratracheal *F*-hexane is also being tested for attenuation of inflammation in smoke inhalation injury patients [590].

Pulmonary delivery of a *F*-decalin NE containing a fluorinated antagonist of a chemokine receptor and a siRNA was more effective than intravenous injection in the treatment of metastatic lung cancer in a

mouse model [591]. A *F*-octylbromide/ $\text{CO}_2$  combination is undergoing clinical trials as a bronchodilator for treatment of acute asthma [592]. Water-in-PFC reverse emulsions are effective systems for delivery of hydrophilic drugs through the pulmonary route [20,199,203]. Pulmonary delivery of vasodilators was achieved via aerosolization of drug-loaded water-in-*F*-octylbromide NEs in rats, providing a potential treatment of high-altitude pulmonary edema and pulmonary artery hypertension [205].

In addition to delivering  $\text{O}_2$  for alleviating isolated Langerhans islet necrosis, an *F*-octylbromide emulsion was found to prevent adhesion of Langerhans cells to Petri dishes, favoring pseudo-islet formation and preserving insulin production (Fig. 14) [352].

A notable use of a PFC as a processing aid in pharmaceutical engineering is that of a phospholipid/ $\text{CaCl}_2$ -shelled *F*-octylbromide emulsion for manufacturing spray-dried hydrophobic porous particles, *Pulmospheres*<sup>TM</sup> (initially developed by Alliance Pharm. Corp.) that enable uniform suspension and consistent aerosol delivery of a large variety of drugs as dry powders [593,594]. Commercially developed *Pulmosphere*-based formulations include inhalable insulin (*Exubera*, Pfizer, New York, USA) and tobramycin (*TOBY Podhaler*, Novartis, Basel, Switzerland). A ciprofloxacin antibiotic dry powder inhaler product (Bayer Healthcare, Berlin, Germany) for chronic lung infection treatment is in late-stage clinical development [595]. *Re*-branded *Aerospheres*, *Pulmospheres* are used to deliver fixed dose combinations of long-acting beta-agonist and muscarinic antagonist, or of corticosteroid budesonide/anticholinergic glycopyrrolate/long-acting beta-agonist formoterol fumarate from pressurized metered-dose inhalers for chronic obstructive pulmonary disease treatment (*Bevespi* and *Breztri Aerospheres*, AstraZeneca, London, UK).

#### 7.6. A vocation for theranostics

As seen above, PFC colloids can fulfill multiple duties, often simultaneously (Table 8). Therapeutic delivery of  $\text{O}_2$ , energy or drugs is, owing to the specific properties of PFCs, accompanied by an aptitude for  $^{19}\text{F}$  or US imaging. Theranostic approaches have become trendy. They often involve several functionalization and targeting devices, multiple components, sophisticated preparation procedures and increasingly complex colloidal structures. These theranostic approaches will not be reviewed here. A profusion of recent reviews, a few of which are mentioned here, attests the attention raised by PFC-based theranostics. These reviews bear largely on cancer treatment and cover design of new PFC materials [269,554,596,597];  $\text{O}_2$  delivery for photo-triggered theranostics [99,314,316]; photoacoustic imaging and photothermal therapy [598]; focused US/targeted MB destruction for tissue permeation and image-guided local drug delivery [117,159,599]; MB dynamics and multiparameter interactions with US, cells and tissues, with implications for clinical translation [115,137]; MB-mediated BBB-opening and PET-monitored drug delivery [451]; use of targeted, stimuli-responsive  $^{19}\text{F}$  MRI probes [403,600]; and more. Examples of theranostic *F*-colloids can be found in papers cited earlier, such as [221,228,329,336,378,383,565], as well as in Figs. 16–20.

## 8. Prospects

The past decade has witnessed an amazing surge of the number of new PFC-based  $\text{O}_2$ -carrying colloids and medical indications investigated. Our knowledge of PFC colloid preparation, stabilization, physics and in vivo behavior has considerably progressed. Substantial  $\text{O}_2$  delivery efficacy data further support the capacity of PFC nanoemulsions to help relieve tissue hypoxia, potentiate  $\text{O}_2$ -dependent cancer treatment, regenerate damaged tissues, preserve isolated organs, etc. In view of these data, we believe that the PFC NE-based  $\text{O}_2$  delivery approach retains its assets. However, many of the NEs presently used for experimental and clinical investigations were designed in the late 1990s or earlier, when our understanding in the matter was still elementary.

**Table 8**  
PFC-based nanomedicines: a vocation for theranostics.

<b>Diagnostic</b> ± triggering	<i>Anatomic, dynamic</i> ± <i>Molecular imaging</i>	Multiple ultrasound imaging modes: B-mode, harmonics, Doppler, cavitation.... <sup>19</sup> F MRI ± <sup>1</sup> H MRI, hot spot detection ± Photoacoustic imaging ± Computed X-ray tomography ± PET, SPECT ± Fluorescence imaging ....	<i>Angiogenesis</i> <i>Inflammation</i> <i>Thrombi, plaques</i> <i>Infarcted myocardium</i> <i>Tumors</i> <i>Circulating tumor cells</i> <i>Liquid biopsy</i>
	± <i>O<sub>2</sub> delivery</i>	Bridging/emergency O <sub>2</sub> supply Relieving hypoxia, protecting organs Enhancing O <sub>2</sub> -dependent cancer therapies: radiotherapy, photo- & sonodynamic therapies chemo- & immunotherapies	<i>Resuscitation</i> <i>Emergency; trauma</i> <i>Stroke</i> <i>Myocardial infarction</i> <i>Cancer therapy</i> <i>Tissue regeneration</i> <i>Graft preservation</i>
	± <i>Energy delivery</i>	High intensity focused ultrasound radiation force, microstreaming, microjets, shock waves Photothermal therapy	<i>Tissue ablation</i> <i>Histotripsy</i> <i>Thrombolysis</i> <i>Embolotherapy</i> <i>Revascularization</i> <i>Sonoporation</i>
	± <i>Drug/gene delivery</i>	On-demand localized release Membrane permeation Barrier crossing: blood/brain/tumor/retina Tumor extravasation and retention effect Fluorine-fluorine recognition effect ....	<i>Focused drug delivery</i> <i>Transfection</i>
→ <b>F-colloids offer countless functional combinations and theranostic opportunities</b>		Disease detection & characterization ± Image-guided procedures ± Enabling O <sub>2</sub> , energy and drug-based therapies ± Monitoring/assessing therapy efficacy ↑ Personalized and precision medicine	

Clearly, further progress in the field commands that any new product development effort takes into account and capitalizes on the vast amount of knowledge and experience, positive and negative, that has since been gained. Unfortunately, this has not always been the case, including for research projects and clinical trials bearing on otherwise innovative applications. Inappropriate selection of PFCs, formulations, emulsification techniques, characterization methods, has often led to suboptimal NEs, calling for suboptimal results. O<sub>2</sub>-carrying NEs should obviously use the shortest dwelling time, highest O<sub>2</sub>-carrying capacity PFCs, and should definitely avoid need for frozen storage. Much could also be learned from studies directed at other indications for PFC colloids than O<sub>2</sub> delivery, but that could help solve O<sub>2</sub> delivery issues. Investigation of advanced, re-formulated NEs is warranted.

In addition to NEs, the option of delivering O<sub>2</sub> through PFC-stabilized MBs and P-SNEs appears very promising. The commercially available MBs that were approved for US contrast imaging have demonstrated their safety and their ability to deliver O<sub>2</sub> to tissues. Use of approved MB products certainly encouraged and facilitated exploration of other uses and could ease clinical translation for O<sub>2</sub> delivery-based indications. But here again, most of these agents have been developed (and licensed) some 20 years ago. Numerous new MB systems investigated for various indications could also ensure focused, on-demand relief of tissue hypoxia. Integration of more recently accrued knowledge, and development of MBs more specifically adapted to the O<sub>2</sub> delivery function, are warranted. Modeling of MB behavior has progressed considerably. Theoretical models are now available to predict the behavior of MBs, facilitating the understanding and characterization of their physical properties, as well as their interactions with the ultrasound field and their environment. Nanobubbles provide further possibilities, although theoretical basis needs to be developed.

The P-SNE-based O<sub>2</sub> delivery approach is particularly interesting, in particular for tumor tissue penetration and blood-brain barrier crossing. PFCs constitute ideal phase-change agents. This option implicates, however, that the complex in vivo vaporization (phase-shift) process be

wholly mastered so that the size of the MBs generated upon activation be properly determined. Thorough consistent control of the phase-change event remains one of the major challenges of this desirable approach, and a key to product safety. Surmounting this challenge appears achievable through suitable PFC selection and shell formulation.

The findings that O<sub>2</sub> delivery from F-colloids can be manipulated non-invasively using US waves, laser light, or other stimuli, and that O<sub>2</sub> release can be image-guided and focused on selected tissues and triggered when ever required represent a precious advance. Most PFC-based colloids, in addition to carrying O<sub>2</sub>, have other assets, such as <sup>19</sup>F probe quality for NEs, or US contrast imaging attributes for MBs, illustrating their outstanding aptitude for theranostic functions. Conversely, even when designed for other purposes, PFC-based colloids will constantly carry and help diffuse some amount of O<sub>2</sub>. PFC-based colloids will thus always offer a O<sub>2</sub> delivery component. F-colloid functionalization and/or targeting (and multi-functionalization and multi-targeting) provide further tools for controlled in vivo colloid efficacy, augmented versatility, expanded theranostic capacities, and enhanced safety. The PFC can perform several tasks concurrently, including dissolving gases, generating bubbles, ensuring their stability, providing cavitation nuclei for phase shift, a sensitive probe for MRI, a protective environment for fragile species, thermal and mechanical energy transfer capacity, pressure buffering effects, and more. Some F-colloids can provide, simultaneously or successively, detection and characterization of illness, image guidance for surgical procedures, delivery of O<sub>2</sub>, drug and gene, including across the blood-brain barrier, delivery of therapeutic energy, monitoring and assessment of treatment efficacy, and eventually, the prospect for personalized treatment. The abundance of recent reviews attests the proficiency of F-colloids for breeding multi-functionalized PFC-based theranostic nanomedicines.

The present surge of medically oriented PFC colloid research is characterized by a marked trend towards increased complexity, implicating numerous components and sophisticated design and engineering processes for the eventual generation of multiple simultaneous diagnostic



and therapeutic (theranostic) functions. One may wonder whether such complexity, and the manifold manufacturing, regulatory and marketing constraints that such constructs implicate may not accumulate obstacles on the road to timely pharmaceutical development, clinical translation and regulatory acceptance. Each component, and their association, each industrial process involved, each claimed function or indication will likely require demonstration of safety and efficacy. Although the cleverness of certain approaches is appealing, the downsides of increased complexity cannot be ignored.

### Declaration of Competing Interest

The authors declare that they have no known competing financial interests or personal relationships that could have appeared to influence the work reported in this paper.

### Acknowledgments

We acknowledge the European INTERREG V Program (Nanotransmed) for financial support.

### References

- Riess JG. Oxygen carriers ("blood substitutes") – raison d'être, chemistry, and some physiology. *Chem Rev.* 2001;101:2797–919.
- Riess JG. Understanding the fundamentals of perfluorocarbons and perfluorocarbon emulsions relevant to *in vivo* oxygen delivery. *Artif Cells Blood Substit Immobil Biotechnol.* 2005;33:47–63.
- Keipert PE. Oxygent<sup>TM</sup>, a perfluorochemical-based oxygen therapeutic for surgical patients. In: Winslow RM, editor. *Blood Substitutes*. Amsterdam: Elsevier; 2006. p. 312–23 Chapter 28.
- Spahn DR, Waschke KF, Standl T, Motsch J, Van Huynegem L, Welte M, et al. Use of perflubron emulsion to decrease allogeneic blood transfusion in high-blood-loss non-cardiac surgery: results of a European phase 3 study. *Anesthesiology.* 2002; 97:1338–49.
- Spahn DR, Keipert PE. An overview of two human trials of perfluorocarbon emulsions in noncardiac surgery. *Shock.* 2019;52:116–8.
- Hill SE, Leone BJ, Faithfull NS, Flaim KE, Keipert PE, Newman MF. Perflubron emulsion (AF0144) augments harvesting of autologous blood: a phase II study in cardiac surgery. *J Cardiothorac Vasc Anesth.* 2002;16:555–60.
- Riess JG. Perfluorocarbon-based oxygen delivery. *Artif Cells Blood Substit Immobil Biotechnol.* 2006;34:567–80.
- Keipert PE, Stehling L. The concept of augmented acute normovolemic hemodilution: using a perfluorochemical-based intravenous oxygen carrier to decrease allogeneic blood transfusion in elective surgery. *Transf Alt Transf Med.* 2001;3:11–6.
- Bryson GL, Laupacis A, Wells GA. Does acute normovolemic hemodilution reduce perioperative allogeneic transfusion? A meta-analysis. *The international study of perioperative transfusion. Anesth Analg.* 1998;86:9–15.
- Messmer K, Kemming G. Clinical hemodilution. In: Winslow RM, editor. *Blood Substitutes*. Amsterdam: Elsevier; 2006. p. 178–87 Chapter 16.
- Homi HM, Yang H, Pearlstein RD, Grocott HP. Hemodilution during cardiopulmonary bypass increases cerebral infarct volume after middle cerebral artery occlusion in rats. *Anesth Analg.* 2004;99:974–81.
- Karkouti K, Djalani G, Borger MA, Beattie WS, Fedorko L, Wijeyesundera D, et al. Low hematocrit during cardiopulmonary bypass is associated with increased risk of postoperative stroke in cardiac surgery. *Ann Thorac Surg.* 2005;80:1381–7.
- Mathew JP, Mackensen GB, Phillips-Bute B, Stafford-Smith M, Podgoreanu MV, Grocott HP, et al. Effects of extreme hemodilution during cardiac surgery on cognitive function in the elderly. *Anesthesiology.* 2007;107:577–84.
- Hill SE. Perfluorocarbons: knowledge gained from clinical trials. *Shock.* 2019;52 (Suppl. 1):60–4.
- Spahn DR, Chassot P-G. Clinical trials in cardiac surgery. In: Winslow RM, editor. *Blood Substitutes*. Amsterdam: Elsevier; 2006. p. 163–77 Chapter 14.
- Banks RE. Fluorine chemistry at the Millennium. *Fascinated by fluorine*. Oxford: Elsevier; 2000.
- Riess JG. Fluorous micro- and nanophases with a biomedical perspective. *Tetrahedron.* 2002;58:4113–31.
- Krafft MP, Riess JG. Selected physicochemical aspects of poly- and perfluoroalkylated substances relevant to performance, environment and sustainability—part one. *Chemosphere.* 2015;129:4–19.
- Tirotta I, Dichiarante V, Pigliacelli C, Cavallo G, Terraneo G, Bombelli FB, et al. <sup>19</sup>F magnetic resonance imaging (MRI): from design of materials to clinical applications. *Chem Rev.* 2015;115:1106–29.
- Krafft MP. Perfluorocarbons and perfluorocarbon emulsions for pulmonary indications. In: Seppelt K, editor. *The curious world of fluorinated molecules*. Amsterdam: Elsevier; 2020. p. 219–39 Chapter 7.
- Siegemund G, Schwertfeger W, Feiring A, Smart B, Behr F, Vogel H, et al. Fluorine compounds, organic. *Ullmann's encyclopedia of industrial chemistry*. Weinheim: Wiley-VCH Verlag; 2012. p. 443–94.
- Krafft MP, Riess JG. Chemistry, physical chemistry and uses of molecular fluorocarbon-hydrocarbon diblocks, triblocks and related compounds - unique apolar components for self-assembled colloid and interface engineering. *Chem Rev.* 2009;109:1714–92.
- Yang G, O'Duill M, Gouverneur V, Krafft MP. Recruitment and immobilisation of a fluorinated biomarker across an interfacial phospholipid film using a fluorocarbon gas. *Angew Chem Int Ed.* 2015;54:8402–6.
- Koshkina O, Lajoinie G, Baldelli Bombelli F, Swider E, Cruz LJ, White PB, et al. Multicore liquid perfluorocarbon-loaded multimodal nanoparticles for stable ultrasound and <sup>19</sup>F MRI applied to *in vivo* cell tracking. *Adv Funct Mater.* 2019;29: 1806485.
- Ullmann K, Poggemann L, Nirschl H, Leneweit G. Adsorption process for phospholipids of different chain lengths at a fluorocarbon/water interface studied by Du Noüy ring and spinning drop. *Colloid Polym Sci.* 2020;298:407–17.
- Nguyen PN, Trinh Dang TT, Waton G, Vandamme T, Krafft MP. A nonpolar, nonamphiphilic molecule can accelerate adsorption of phospholipids and lower their surface tension at the air/water interface. *ChemPhysChem.* 2011;12:2646–52.
- Nguyen PN, Veschini M, Tanaka M, Waton G, Vandamme T, Krafft MP. Counteracting the inhibitory effect of proteins towards lung surfactant substitutes: a fluorocarbon gas helps displace albumin at the air/water interface. *Chem Commun.* 2014;50:11576–9.
- Shi D, Liu X, Counil C, Krafft MP. Fluorocarbon exposure mode markedly affects phospholipid monolayer behavior at the gas/liquid interface: impact on size and stability of microbubbles. *Langmuir.* 2019;35:10025–33.
- Gerber F, Krafft MP, Vandamme TF, Goldmann M, Fontaine P. Fluidization of a dipalmitoylphosphatidylcholine monolayer by fluorocarbon gases: potential use in lung surfactant therapy. *Biophys J.* 2006;90:3184–92.
- Krafft MP. Overcoming inactivation of the lung surfactant by serum proteins: a potential role for fluorocarbons? *Soft Matter.* 2015;11:5982–94.
- Krafft MP, Fainerman VB, Miller R. Modeling of the effect of fluorocarbon gases on the properties of phospholipid monolayers and the adsorption dynamics of their aqueous solutions or dispersions. *Colloid Polym Sci.* 2015;293:3091–7.
- Liu X, Counil C, Shi D, Mendoza-Ortega EE, Vela-Gonzalez AV, Maestro A, et al. First quantitative assessment of the adsorption of a fluorocarbon gas on phospholipid monolayers at the air/water interface. *J Colloid Interface Sci.* 2021;593:1–10.
- Gazzera L, Milani R, Pirrie L, Schmutz M, Blanck C, Resnati G, et al. Design of highly stable echogenic microbubbles through controlled assembly of their hydrophobic shell. *Angew Chem Int Ed.* 2016;55:10263–7.
- Shi D, Wallyn J, Nguyen D-V, Perton F, Felder-Flesch D, Bégin-Colin S, et al. Microbubbles decorated with dendronized magnetic nanoparticles for biomedical imaging. Effective stabilization via fluororous interactions. *Beilstein J Nanotechnol.* 2019;10:2103–15.
- Counil C, Krafft MP. When fluorocarbon gases attract molecules and induce their adsorption at interfaces: Implications for therapeutic microbubble design and engineering. In: Ojima I, editor. *Frontiers of Organofluorine chemistry*. Singapore: World Scientific; 2019.
- Riess JG. Reassessment of criteria for the selection of perfluorochemicals for second-generation blood substitutes: analysis of structure/property relationships. *Artif Organs.* 1984;8:44–56.
- Riess JG. Fluorocarbon emulsions - Designing an efficient shuttle service for the respiratory gases - the so-called "blood substitutes". In: Banks RE, editor. *Fluorine at the millennium*. Amsterdam: Elsevier; 2000. p. 385–431 Chapter 23.
- Krafft MP, Riess JG, Weers JG. The design and engineering of oxygen-delivering fluorocarbon emulsions. In: Benita S, editor. *Submicronic emulsions in drug targeting and delivery*. Amsterdam: Harwood Academic Publ.; 1998. p. 235–333 Chapter 10.
- Kabalnov A, Klein D, Pelura T, Schutt E, Weers J. Dissolution of multicomponent microbubbles in the blood stream: 1 Theory. *Ultrasound Med Biol.* 1998;24: 739–49.
- Wesseler EP, Iltis R, Clark L. The solubility of oxygen in highly fluorinated liquids. *J Fluorine Chem.* 1977;9:137–46.
- Riess JG, Le Blanc M. Solubility and transport phenomena in perfluorochemicals relevant to blood substitution and other biomedical applications. *Pure Appl Chem.* 1982;54:2383–406.
- Correas J-M, Meuter AR, Singlas E, Kessler DR, Worah D, Quay SC. Human pharmacokinetics of a perfluorocarbon ultrasound contrast agent evaluated with gas chromatography. *Ultrasound Med Biol.* 2001;27:565–70.
- Miller HC, Verdelli LS, Gall JF. Some physical properties of sulfur hexafluoride. *Ind Eng Chem.* 1951;43:1126–9.
- Brown JA. Physical properties of perfluoropropane. *J Chem Eng Data.* 1963;8: 106–8.
- Stiles VE, Cady GH. Physical properties of perfluoro-n-hexane and perfluoro-2-methylpentane. *J Am Chem Soc.* 1952;74:3771–3.
- Sarkar K, Katiyar A, Jain P. Growth and dissolution of an encapsulated contrast microbubble: effects of encapsulation permeability. *Ultrasound Med Biol.* 2009; 35:1385–96.
- Kabalnov A, Weers J, Arlauskas R, Tarara T. Phospholipids as emulsion stabilizers: 1. Interfacial tensions. *Langmuir.* 1995;11:2966–74.
- Magnetto C, Prato M, Khadjavi A, Giribaldi G, Fenoglio I, Jose J, et al. Ultrasound-activated decafluoropentane-cored and chitosan-shelled nanodroplets for oxygen delivery to hypoxic cutaneous tissues. *RSC Adv.* 2014;4:38433.



- [49] Riess JG, Cornélus C, Follana R, Krafft MP, Mahé AM, Postel M, et al. Novel fluorocarbon-based injectable oxygen-carrying formulations with long-term room-temperature storage stability. *Adv Exp Med Biol*. 1994;345:227–34.
- [50] Marie-Bertilla S, Thomas J-L, Marie P, Krafft MP. Co-surfactant effect of a semifluorinated alkane at a fluorocarbon/water interface. Impact on the stabilization of fluorocarbon-in-water emulsions. *Langmuir*. 2004;20:3920–4.
- [51] Gao M, Liang C, Song X, Chen Q, Jin Q, Wang C, et al. Erythrocyte-membrane-encapsulated perfluorocarbon as nanoscale artificial red blood cells to relieve tumor hypoxia and enhance cancer radiotherapy. *Adv Mater*. 2017;29:1701429.
- [52] Ren H, Liu J, Li Y, Wang H, Ge S, Yuan A, et al. Oxygen self-enriched nanoparticles functionalized with erythrocyte membranes for long circulation and enhanced phototherapy. *Acta Biomater*. 2017;59:268–82.
- [53] Wrobeln A, Laudien J, Groß-Heitfeld C, Linders J, Mayer C, Wilde B, et al. Albumin-derived perfluorocarbon-based artificial oxygen carriers: a physico-chemical characterization and first in vivo evaluation of biocompatibility. *Eur J Pharm Biopharm*. 2017;115:52–64.
- [54] Zhuang J, Ying M, Spiekermann K, Holay M, Zhang Y, Chen F, et al. Biomimetic nanoemulsions for oxygen delivery in vivo. *Adv Mater*. 2018;30:1804693.
- [55] Zhang F, Zhuang J, Esteban-Fernández de Ávila B, Tang S, Zhang Q, Fang RH, et al. A nanomotor-based active delivery system for intracellular oxygen transport. *ACS Nano*. 2019;13:11996–2005.
- [56] Cavalli R, Argenziano M, Vigna E, Giustetto P, Torres E, Aime S, et al. Preparation and in vitro characterization of chitosan nanobubbles as theranostic agents. *Colloids Surf B Biointerfaces*. 2015;129:39–46.
- [57] Ma S, Zhou J, Zhang Y, Yang B, He Y, Tian C, et al. An oxygen self-sufficient fluorinated nanoplateform for relieved tumor hypoxia and enhanced photodynamic therapy of cancers. *ACS Appl Mater Interfaces*. 2019;11:7731–42.
- [58] Li J, Xue Y, Tian J, Liu Z, Zhuang A, Gu P, et al. Fluorinated-functionalized hyaluronic acid nanoparticles for enhanced photodynamic therapy of ocular choroidal melanoma by ameliorating hypoxia. *Carbohydr Polym*. 2020;237:116119.
- [59] Yang Q, Chen H, Bai Y, Cao Y, Hu W, Zhang L. Facile synthesis of lipid-perfluorocarbon nanoemulsion coated with silica shell as an ultrasound imaging agent. *Adv Healthc Mater*. 2018;7:1700816.
- [60] de Leon A, Perera R, Hernandez C, Cooley M, Jung O, Jeganathan S, et al. Contrast enhanced ultrasound imaging by nature-inspired ultrastable echogenic nanobubbles. *Nanoscale*. 2019;11:15647.
- [61] Day RA, Estabrook DA, Wu C, Chapman JO, Togle AJ, Sletten EM. Systematic study of perfluorocarbon nanoemulsions stabilized by polymer amphiphiles. *ACS Appl Mater Interfaces*. 2020;12:38887–98.
- [62] Laudien J, Groß-Heitfeld C, Mayer C, de Groot H, Kirsch M, Ferenz KB. Perfluorodecalin-filled poly(*n*-butylcyanoacrylate) nanocapsules as potential artificial oxygen carriers: preclinical safety and biocompatibility. *J Nanosci Nanotechnol*. 2015;15:5637–48.
- [63] Nolte D, Pickelmann S, Lang M, Keipert P, Messmer K. Compatibility of different colloid plasma expanders with perflubron emulsion: An intravital microscopic study in the hamster. *Anesthesiology*. 2000;93:1261–70.
- [64] Joann-Hureaux V, Audonnet-Blaise S, Lacatusu D, Krafft MP, Dewachter P, Cauchois G, et al. Effects of a new perfluorocarbon emulsion on human plasma and whole-blood viscosity in the presence of albumin, hydroxyethyl starch, or modified fluid gelatin: An in vitro rheologic approach. *Transfusion*. 2006;46:1892–8.
- [65] Vásquez DM, Ortiz D, Alvarez OA, Briceño JC, Cabrales P. Hemorheological implications of perfluorocarbon based oxygen carrier interaction with colloid plasma expanders and blood. *Biotechnol Prog*. 2013;29:796–807.
- [66] Inci I, Arni S, Iskender I, Citak N, Rodriguez JM, Weisskopf M, et al. Functional, metabolic and morphologic results of ex vivo donor lung perfusion with a perfluorocarbon-based oxygen carrier nanoemulsion in a large animal transplantation model. *Cells*. 2020;9:2501.
- [67] Upadhyay A, Dalvi SV. Microbubble formulations: synthesis, stability, modeling and biomedical applications. *Ultrasound Med Biol*. 2019;45:301–43.
- [68] Abou-Saleh RH, Swain M, Evans SD, Thomson NH. Poly(ethylene glycol) lipid-shelled microbubbles: abundance, stability, and mechanical properties. *Langmuir*. 2014;30:5557–63.
- [69] Eisenbrey JR, Albala L, Kramer MR, Daroshefski N, Brown D, Liu J-B, et al. Development of an ultrasound sensitive oxygen carrier for oxygen delivery to hypoxic tissue. *Int J Pharm*. 2015;478:361–7.
- [70] Paeßen V, Doleschel D, Kiessling F. Evolution of contrast agents for ultrasound imaging and ultrasound-mediated drug delivery. *Front Pharmacol*. 2015;6:197.
- [71] Kissa E. Fluorinated surfactants and repellents. New York: Marcel Dekker; 2001.
- [72] Gladysz JA, Curran DP, Horváth I. Handbook of Fluorous Chemistry. Wiley-VCH: Weinheim; 2004.
- [73] Riess JG, Krafft MP. Fluorocarbons and fluorosurfactants for *in vivo* oxygen transport (blood substitutes), imaging and drug delivery. *Mater Res Soc Bull*. 1999;24:42–8.
- [74] Riess JG, Greiner J. Carbohydrate- and related polyol-derived fluorosurfactants - An update. *Carbohydr Res*. 2000;327:147–68.
- [75] Holtz C, Rowat AC, Agresti JJ, Hutchinson JB, Angilè FE, Schmitz CHJ, et al. Biocompatible surfactants for water-in-fluorocarbon emulsions. *Lab Chip*. 2008;8:1632–9.
- [76] Reznik N, Lajoinie G, Shpak O, Gelderblom EC, Williams R, de Jong N, et al. On the acoustic properties of vaporized submicron perfluorocarbon droplets. *Ultrasound Med Biol*. 2014;40:1379–84.
- [77] Fernandes DA, Kolios MC. Intrinsically absorbing photoacoustic and ultrasound contrast agents for cancer therapy and imaging. *Nanotechnology*. 2018;29:505103.
- [78] Zhang S, Xu T, Cui Z, Shi W, Wu S, Zong Y, et al. Time and frequency characteristics of cavitation activity enhanced by flowing phase-shift nanodroplets and lipid-shelled microbubbles during focused ultrasound exposures. *Ultrasound Med Biol*. 2019;45:2118–32.
- [79] Krafft MP, Riess JG. Highly fluorinated amphiphiles and colloidal systems, and their applications in the biomedical field - a contribution. *Biochimie*. 1998;80:489–514.
- [80] Krafft MP, Riess JG. Perfluorocarbons, life sciences and biomedical uses. *J Polym Sci Part A: Polym Chem*. 2007;45:1185–98.
- [81] Chowdhury MS, Zheng W, Kumari S, Heyman J, Zhang X, Dey P, et al. Dendronized fluorosurfactant for highly stable water-in-fluorinated oil emulsions with minimal inter-droplet transfer of small molecules. *Nat Commun*. 2019;10:4546.
- [82] Corvis Y, Manta S, Thebault C, Couture O, Dhote H, Michel J-P, et al. Novel perfluorinated triblock amphiphilic copolymers for lipid-shelled microbubble stabilization. *Langmuir*. 2018;34:9744–53.
- [83] Salama IE, Paul A. Emulsions of fluorinated oils stabilised by fluorinated silica nanoparticles. *Colloids Surf A: Physicochem Eng Aspects*. 2016;494:125–38.
- [84] Krafft MP, Riess JG. Per- and polyfluorinated substances (PFASs): environmental challenges. *Curr Opin Colloid Interface Sci*. 2015;20:192–212.
- [85] Flaim SF. Pharmacokinetics and side effects of perfluorocarbon-based blood substitutes. *Artif Cells Blood Substit Immobil Biotechnol*. 1994;22:1043–54.
- [86] Riess JG, Dalfors JL, Hanna GK, Klein DH, Krafft MP, Pelura TJ, et al. Development of highly fluid, concentrated and stable fluorocarbon emulsions for diagnosis and therapy. *Biomater Artif Cells Immobil Biotechnol*. 1992;20:839–42.
- [87] Schutt ES, Klein DH, Mattrey RM, Riess JG. Injectable microbubbles as contrast agents for diagnostic ultrasound imaging: the key role of perfluorochemicals. *Angew Chem Int Ed*. 2003;42:3218–35.
- [88] Lindner JR. Microbubbles in medical imaging: current applications and future directions. *Nat Rev Drug Discov*. 2004;3:527–32.
- [89] Gerber F, Waton G, Krafft MP, Vandamme TF. Long-lived microbubbles for oxygen delivery. *Artif Cells Blood Substit Immobil Biotechnol*. 2007;35:119–24.
- [90] Hernot S, Klibanov AL. Microbubbles in ultrasound-triggered drug and gene delivery. *Adv Drug Deliv Rev*. 2008;60:1153–66.
- [91] Stride E, Edirisinghe M. Novel microbubble preparation technologies. *Soft Matter*. 2008;4:2350–9.
- [92] Rossi S, Waton G, Krafft MP. Phospholipid-coated gas bubble engineering - key parameters for size and stability control as determined by an acoustic method. *Langmuir*. 2010;26:1649–55.
- [93] Rossi S, Szijártó C, Gerber F, Waton G, Krafft MP. Fluorous materials in microbubble engineering science and technology - design and development of new bubble preparation and sizing technologies. *J Fluorine Chem*. 2011;132:1102–9.
- [94] Szijártó C, Rossi S, Waton G, Krafft MP. Effects of perfluorocarbon gases on the size and stability characteristics of phospholipid-coated microbubbles - osmotic effect versus interfacial film stabilization. *Langmuir*. 2012;28:1182–9.
- [95] Sirsi SR, Borden MA. State-of-the-art materials for ultrasound-triggered drug delivery. *Adv Drug Deliv Rev*. 2014;72:2–14.
- [96] Goodwin AP, Nakatsuka MA, Mattrey RF. Stimulus-responsive ultrasound contrast agents for clinical imaging: motivations, demonstrations, and future directions. *Wiley Interdiscip Rev Nanomed Nanobiotechnol*. 2015;7:111–23.
- [97] Daeichin V, van Rooij T, Skachkov I, Ergin B, Specht PAC, Lima A, et al. Microbubble composition and preparation for high-frequency contrast-enhanced ultrasound imaging: in vitro and in vivo evaluation. *IEEE Trans Ultrason Ferroelectr Freq Control*. 2017;64:555–67.
- [98] Mulvana H, Browning RJ, Luan Y, de Jong N, Tang M-X, Eckersley RJ, et al. Characterization of contrast agent microbubbles for ultrasound imaging and therapy research. *IEEE Trans Ultrason Ferroelectr Freq Control*. 2017;64:232–51.
- [99] Khan MS, Hwang J, Lee K, Choi Y, Kim K, Koo H-J, et al. Oxygen-carrying micro/nanobubbles: composition, synthesis techniques and potential prospects in photo-triggered theranostics. *Molecules*. 2018;23:2210.
- [100] Wang S, Hossack J, Klibanov AL. Targeting of microbubbles: contrast agents for ultrasound molecular imaging. *J Drug Target*. 2018;26:420–34.
- [101] Brown E, Lindner JR. Ultrasound molecular imaging: principles and applications in cardiovascular medicine. *Curr Cardiol Rep*. 2019;21:30.
- [102] Chattaraj R, Blum NT, Goodwin AP. Design and application of stimulus-responsive droplets and bubbles stabilized by phospholipid monolayers. *Curr Opin Colloid Interface Sci*. 2019;40:14–24.
- [103] Khan MS, Hwang J, Lee K, Choi Y, Jang J, Kwon Y, et al. Surface composition and preparation method for oxygen nanobubbles for drug delivery and ultrasound imaging applications. *Nanomaterials*. 2019;9:48.
- [104] Lee L, Cavalieri F, Ashokkumar M. Exploring new applications of lysozyme-shelled microbubbles. *Langmuir*. 2019;35:9997–10006.
- [105] Unnikrishnan S, Du Z, Diakova GB, Klibanov AL. Formation of microbubbles for targeted ultrasound contrast imaging: practical translation considerations. *Langmuir*. 2019;35:10034–41.
- [106] Al-Jawadi S, Thakur SS. Ultrasound-responsive lipid microbubbles for drug delivery: a review of preparation techniques to optimise formulation size, stability and drug loading. *Int J Pharm*. 2020;585:119559.
- [107] Stride E, Segers T, Lajoinie G, Cherkaoui S, Bettinger T, Versluis M, et al. Microbubble agents: new directions. *Ultrasound Med Biol*. 2020;46:1326–43.
- [108] Kooiman K, Roovers S, Langeveld SAG, Kleven RT, Dewitte H, O'Reilly MA, et al. Ultrasound-responsive cavitation nuclei for therapy and drug delivery. *Ultrasound Med Biol*. 2020;46:1296–325.
- [109] Dalvi SV, Joshi JR. Modeling of microbubble dissolution in aqueous medium. *J Colloid Interface Sci*. 2015;437:259–69.
- [110] Kabalnov A, Bradley J, Flaim S, Klein D, Pelura T, Peters B, et al. Dissolution of multicomponent microbubbles in the blood stream: 2 Experiment. *Ultrasound Med Biol*. 1998;24:751–60.
- [111] Kwan JJ, Kaya M, Borden MA, Dayton PA. Theranostic oxygen delivery using ultrasound and microbubbles. *Theranostics*. 2012;2:1174–84.

- [112] McEwan C, Owen J, Stride E, Fowley C, Nesbitt H, Cochrane D, et al. Oxygen carrying microbubbles for enhanced sonodynamic therapy of hypoxic tumours. *J Control Release*. 2015;203:51–6.
- [113] McEwan C, Kamila S, Owen J, Nesbitt H, Callan B, Borden M, et al. Combined sonodynamic and antimetabolite therapy for the improved treatment of pancreatic cancer using oxygen loaded microbubbles as a delivery vehicle. *Biomaterials*. 2016; 80:20–32.
- [114] Sridhar S, Patel A, Dalvi SV. Estimation of storage stability of aqueous microbubble suspensions. *Colloids Surf A*. 2016;489:182–90.
- [115] Versluis M, Stride E, Lajoinie G, Dollet B, Segers T. Ultrasound contrast agent modeling: a review. *Ultrasound Med Biol*. 2020;46:2117–44.
- [116] Unger EC, Porter T, Culp W, Labell R, Matsunaga T, Zutshi R. Therapeutic applications of lipid-coated microbubbles. *Adv Drug Deliv Rev*. 56; 2004; 1291–314.
- [117] Wischhusen J, Padilla F. Ultrasound-targeted microbubble destruction (UTMD) for localized drug delivery into tumor tissue. *IRBM*. 2019;40:10–5.
- [118] Feshitan JA, Chen CC, Kwan JJ, Borden MA. Microbubble size isolation by differential centrifugation. *J Colloid Interface Sci*. 2009;329:316–24.
- [119] Segers T, Versluis M. Acoustic bubble sorting for ultrasound contrast agent enrichment. *Lab Chip*. 2014;14:1705–14.
- [120] Kok MP, Segers T, Versluis M. Bubble sorting in pinched microchannels for ultrasound contrast agent enrichment. *Lab Chip*. 2015;15:3716–22.
- [121] Lin H, Chen J, Chen C. A novel technology: microfluidic devices for microbubble ultrasound contrast agent generation. *Med Biol Eng Comput*. 2016;54:1317–30.
- [122] Pulsipher KW, Hammer DA, Lee D, Sehgal CM. Engineering theranostic microbubbles using microfluidics for ultrasound imaging and therapy: a review. *Ultrasound Med Biol*. 2018;44:2441–60.
- [123] Segers T, de Rond L, de Jong N, Borden M, Versluis M. Stability of monodisperse phospholipid-coated microbubbles formed by flow-focusing at high production rates. *Langmuir*. 2016;32:3937–44.
- [124] Hyvelin J-M, Gaud E, Costa M, Helbert A, Bussat P, Bettinger T, et al. Characteristics and echogenicity of clinical ultrasound contrast agents: An in vitro and in vivo comparison study. *J Ultrasound Med*. 2017;36:941–53.
- [125] Smeenge M, Tranquart F, Mannaerts CK, de Reijke TM, van de Vijver MJ, Laguna MP, et al. First-in-human ultrasound molecular imaging with a VEGFR2-specific ultrasound molecular contrast agent (BR55) in prostate cancer: a safety and feasibility pilot study. *Invest Radiol*. 2017;52:419–27.
- [126] Willmann JK, Bonomo L, Testa AC, Rinaldi P, Rindi G, Keerthi S, Valluru, et al. Ultrasound molecular imaging with BR55 in patients with breast and ovarian lesions: first-in-human results. *J Clin Oncol*. 2017;35:2133–40.
- [127] Turco S, El Kaffas A, Zhou J, Lutz AM, Wijkstra H, Willmann JK, et al. Pharmacokinetic modeling of targeted ultrasound contrast agents for quantitative assessment of anti-angiogenic therapy: a longitudinal case-control study in colon cancer. *Mol Imaging Biol*. 2019;21:633–43.
- [128] Rojas JD, Lin F, Chiang Y-C, Chytil A, Chong DC, Bautch VL, et al. Ultrasound molecular imaging of VEGFR-2 in clear-cell renal cell carcinoma tracks disease response to antiangiogenic and notch-inhibition therapy. *Theranostics*. 2018;8:141–55.
- [129] Thomas DH, Sboros V, Emmer M, Vos H, de Jong N. Microbubble oscillations in capillary tubes. *IEEE Trans Ultrason Ferroelectr Freq Control*. 2013;60:105–14.
- [130] Shpak O, Verweij M, de Jong N, Versluis M. Droplets, bubbles and ultrasound interactions. In: Escoffre J-M, Bouakaz A, editors. *Therapeutic Ultrasound, Advances in Experimental Medicine and Biology*. Springer; 2016. p. 157–74 Chapter 9.
- [131] Upadhyay A, Dalvi SV, Gupta G, Khanna N. Effect of PEGylation on performance of protein microbubbles and its comparison with lipid microbubbles. *Mater Sci Eng C*. 2017;71:425–30.
- [132] Segers T, Gaud E, Versluis M, Frinking P. High-precision acoustic measurements of the nonlinear dilatational elasticity of phospholipid coated monodisperse microbubbles. *Soft Matter*. 2018;14:9550–61.
- [133] Helfield B. A review of phospholipid encapsulated ultrasound contrast agent microbubble physics. *Ultrasound Med Biol*. 2019;45:282–300.
- [134] Izadifar Z, Babyn P, Chapman D. Ultrasound cavitation/microbubble detection and medical applications. *J Med Biol Engineer*. 2019;39:259–76.
- [135] Mannaris C, Bau L, Grundy M, Gray M, Lea-Banks H, Seth A, et al. Microbubbles, nanodroplets and gas-stabilizing solid particles for ultrasound-mediated extravasation of unencapsulated drugs: An exposure parameter optimization study. *Ultrasound Med Biol*. 2019;45:954–67.
- [136] Presset A, Bonneau C, Kazuyoshi S, Nadal-Desbarats L, Mitsuyoshi T, Bouakaz A, et al. Endothelial cells, first target of drug delivery using microbubble-assisted ultrasound. *Ultrasound Med Biol*. 2020;46:1565–83.
- [137] Roovers S, Segers T, Lajoinie G, Deprez J, Versluis M, De Smedt SC, et al. The role of ultrasound-driven microbubble dynamics in drug delivery: from microbubble fundamentals to clinical translation. *Langmuir*. 2019;35:10173–91.
- [138] Alheshibri M, Qian J, Jehannin M, Craig VSJ. A history of nanobubbles. *Langmuir*. 2016;32:11086–100.
- [139] Cavalli R, Soster M, Argenziano M. Nanobubbles: a promising efficient tool for therapeutic delivery. *Ther Deliv*. 2016;7:117–38.
- [140] Khan MS, Hwang J, Seo Y, Shin K, Lee K, Park C, et al. Engineering oxygen nanobubbles for the effective reversal of hypoxia. *Art Cells Nanomed Biotechnol*. 2018;46:S318–27.
- [141] Krupka TM, Solorio L, Wilson RE, Wu H, Azar N, Exner AA. Formulation and characterization of echogenic lipid-Pluronic Nanobubbles. *Mol Pharm*. 2010;7:49–59.
- [142] Yi X, Abenojar EC, Zhu J, Zheng Y, Exner AA. In vitro preparation and characterization of magnetic Nanobubbles. *IEEE Int Ultrasonics Symp Glasgow*. Oct 2019;2019:392–5.
- [143] Zullino S, Argenziano M, Ansari S, Cipriani R, Nasi L, Albertini F, et al. Superparamagnetic oxygen-loaded nanobubbles to enhance tumor oxygenation during hyperthermia. *Front Pharmacol*. 2019;10:1001.
- [144] Craig V, Krafft MP, editors Zemb T. Hot topics special issue nanodroplets and nanobubbles. *Curr Opin Colloid Interface Sci*. 2021:56.
- [145] Kripfgans OD, Fowlkes JB, Woydt M, Eldevik OP, Carson PL. In vivo droplet vaporization for occlusion therapy and phase aberration correction. *IEEE Trans Ultrason Ferroelectr Freq Control*. 2002;49:726–38.
- [146] Rapoport N. Phase-shift, stimuli-responsive perfluorocarbon nanodroplets for drug delivery to cancer. *Wiley Interdiscip Rev Nanomed Nanobiotechnol*. 2012;4:492–510.
- [147] Zhou Y. Application of acoustic droplet vaporization in ultrasound therapy. *J Ther Ultrasound*. 2015;3:20.
- [148] Mountford PA, Borden MA. On the thermodynamics and kinetics of superheated fluorocarbon phase-change agents. *Adv Colloid Interface Sci*. 2016;237:15–27.
- [149] Rapoport N. Drug-loaded perfluorocarbon nanodroplets for ultrasound-mediated drug delivery. In: Escoffre J-M, Bouakaz A, editors. *Therapeutic Ultrasound, Advances in Experimental Medicine and Biology*. Switzerland: Springer; 2016. p. 221–41 Chapter 13.
- [150] Yu J, Chen X, Villanueva FS, Kim K. Vaporization and recondensation dynamics of indocyanine green-loaded perfluoropentane droplets irradiated by a short pulse laser. *Appl Phys Lett*. 2016;109:243701.
- [151] Sheeran PS, Matsuura N, Borden MA, Williams R, Matsunaga TO, Burns PN, et al. Methods of generating submicrometer phase-shift perfluorocarbon droplets for applications in medical ultrasonography. *IEEE Trans Ultrason Ferroelectr Freq Control*. 2017;64:252–63.
- [152] Chen Q, Yu J, Kim K. Review: optically-triggered phase-transition droplets for photoacoustic imaging. *Biomed Eng Lett*. 2018;8:223–9.
- [153] Li M, Luo H, Zhang W, He K, Chen Y, Liu J, et al. Phase-shift, targeted nanoparticles for ultrasound molecular imaging by low intensity focused ultrasound irradiation. *Int J Nanomedicine*. 2018;13:3907–20.
- [154] Zullino S, Argenziano M, Stura I, Guiot C, Cavalli R. From micro- to nano-multifunctional theranostic platform: effective ultrasound imaging is not just a matter of scale. *Mol Imaging*. 2018;17 1536012118778216.
- [155] Burgess MT, Porter TM. Control of acoustic cavitation for efficient sonoporation with phase-shift nanoemulsions. *Ultrasound Med Biol*. 2019;45:846–58.
- [156] Kee ALY, Teo BM. Biomedical applications of acoustically responsive phase shift nanodroplets: current status and future directions. *Ultrasound Sonochem*. 2019;56:37–45.
- [157] Lea-Banks H, O'Reilly MA, Hynynen K. Ultrasound-responsive droplets for therapy: a review. *J Control Release*. 2019;293:144–54.
- [158] Loskutova K, Grishenkov D, Ghorbani M. Review on acoustic droplet vaporization in ultrasound diagnostics and therapeutics. *Biomed Res Int*. 2019;2019:9480193.
- [159] Yildirim A, Blum NT, Goodwin AP. Colloids, nanoparticles, and materials for imaging, delivery, ablation, and theranostics by focused ultrasound (FUS). *Theranostics*. 2019;9:2572–94.
- [160] Brambila CJ, Lux J, Mattrey RF, Boyd D, Borden MA, De Gracia Lux C. Bubble inflation using phase-change perfluorocarbon nanodroplets as a strategy for enhanced ultrasound imaging and therapy. *Langmuir*. 2020;36:2954–65.
- [161] Duan L, Yang L, Jin J, Yang F, Liu D, Hu K, et al. Micro/nano-bubble-assisted ultrasound to enhance the EPR effect and potential theranostic applications. *Theranostics*. 2020;10:462–83.
- [162] Shi Y, van der Meel R, Chen X, Lammers T. The EPR effect and beyond: strategies to improve tumor targeting and cancer nanomedicine treatment efficacy. *Theranostics*. 2020;10:7921–4.
- [163] Chen CC, Sheeran PS, Wu S-Y, Olumolade OO, Dayton PA, Konofagou EE. Targeted drug delivery with focused ultrasound-induced blood-brain barrier opening using acoustically-activated nanodroplets. *J Control Release*. 2013;172:795–804.
- [164] Zhang X, Hu J, Zhao G, Huang N, Tan Y, Pi L, et al. PEGylated PLGA-based phase shift nanodroplets combined with focused ultrasound for blood brain barrier opening in rats. *Oncotarget*. 2017;8:38927–36.
- [165] Cavalli R, Bisazza A, Giustetto P, Civra A, Lembo D, Trotta G, et al. Preparation and characterization of dextran nanobubbles for oxygen delivery. *Int J Pharm*. 2009; 381:160–5.
- [166] Mannaris C, Yang C, Carugo D, Owen J, Lee JY, Nwokeoha S, et al. Acoustically responsive polydopamine nanodroplets: a novel theranostic agent. *Ultrasound Sonochem*. 2020;60:104782.
- [167] Cao Y, Chen Y, Yu T, Guo Y, Liu F, Yao Y, et al. Drug release from phase-changeable nanodroplets triggered by low-intensity focused ultrasound. *Theranostics*. 2018;8:1327–39.
- [168] Li Y, Liu R, Liu L, Zhang Y, Sun J, Ma P, et al. Study on phase transition and contrast-enhanced imaging of ultrasound responsive nanodroplets with polymer shells. *Colloids Surf B Biointerfaces*. 2020;189:110849.
- [169] Hannah AS, Luke GP, Emelianov SY. Blinking phase-change nanocapsules enable background-free ultrasound imaging. *Theranostics*. 2016;16:1866–76.
- [170] Yoon H, Yarmoska SK, Hannah AS, Yoon C, Hallam KA, Emelianov SY. Contrast-enhanced ultrasound imaging in vivo with laser-activated nanodroplets. *Med Phys*. 2017;44:3444–9.
- [171] Teston E, Hingot V, Faugeras V, Errico C, Bezagu M, Tanter M, et al. A versatile and robust microfluidic device for capillary-sized simple or multiple emulsions production. *Biomed Microdevices*. 2018;20:94.
- [172] Sheeran PS, Luo S, Dayton PA, Matsunaga TO. Formulation and acoustic studies of a new phase-shift agent for diagnostic and therapeutic ultrasound. *Langmuir*. 2011;27:10412–20.
- [173] Dove JD, Mountford PA, Murray TW, Borden MA. Engineering optically triggered droplets for photoacoustic imaging and therapy. *Biomed Opt Express*. 2014;5:4417–27.



- [174] Porter TR, Arena C, Sayyed S, Lof J, High RR, Xie F, et al. Targeted transthoracic acoustic activation of systemically administered nanodroplets to detect myocardial perfusion abnormalities. *Circ Cardiovasc Imaging*. 2016;9:e003770.
- [175] Choudhury SA, Xie F, Dayton PA, Porter TR. Acoustic behavior of a reactivated, commercially available ultrasound contrast agent. *J Am Soc Echocardiogr*. 2017;30:189–97.
- [176] Lin S, Shah A, Hernández-Gil J, Stanzola A, Harris BI, Matsunaga TO, et al. Optically and acoustically triggerable sub-micron phase-change contrast agents for enhanced photoacoustic and ultrasound imaging. *Photoacoustics*. 2017;6:26–36.
- [177] Sheeran PS, Yoo K, Williams R, Yin M, Foster FS, Burns PN. More than bubbles: creating phase-shift droplets from commercially available ultrasound contrast agents. *Ultrasound Med Biol*. 2017;43:531–40.
- [178] Borden MA, Song K-H. Reverse engineering the ultrasound contrast agent. *Adv Colloid Interface Sci*. 2018;262:39–49.
- [179] Choudhury SA, Xie F, Kutty S, Lof J, Stolz E, Porter TR. Selective infarct zone imaging with intravenous acoustically activated droplets. *PLoS One*. 2018;13:e0207486.
- [180] Chattaraj R, Goldscheiter GM, Yildirim A, Goodwin AP. Phase behavior of mixed lipid monolayers on perfluorocarbon nanoemulsions and its effect on acoustic contrast. *RSC Adv*. 2016;6:111318–25.
- [181] Aliabouzar M, Kumar KN, Sarkar K. Acoustic vaporization threshold of lipid-coated perfluoropentane droplets. *J Acoust Soc Am*. 2018;143:2001–12.
- [182] Lacour T, Guédrá M, Valier-Brasier T, Coulouvrat F. A model for acoustic vaporization dynamics of a bubble/droplet system encapsulated within a hyperelastic shell. *J Acoust Soc Am*. 2018;143:23–37.
- [183] Rojas JD, Borden MA, Dayton PA. Effect of hydrostatic pressure, boundary constraints and viscosity on the vaporization threshold of low-boiling-point phase-change contrast agents. *Ultrasound Med Biol*. 2019;45:968–79.
- [184] Aliabouzar M, Kumar KN, Sarkar K. Effects of droplet size and perfluorocarbon boiling point on the frequency dependence of acoustic vaporization threshold. *J Acoust Soc Am*. 2019;145:1105–16.
- [185] Rapoport NY, Kennedy AM, Shea JE, Scaife CL, Nam K-H. Controlled and targeted tumor chemotherapy by ultrasound activated nanoemulsions/microbubbles. *J Control Release*. 2009;138:268–76.
- [186] Mountford PA, Thomas AN, Borden MA. Thermal activation of superheated lipid-coated perfluorocarbon drops. *Langmuir*. 2015;31:4627–34.
- [187] Kripfgans OD, Fabiilli ML, Carson PL, Fowlkes JB. On the acoustic vaporization of micrometer-sized droplets. *J Acoust Soc Am*. 2004;116:272–81.
- [188] Schad KC, Hynynen K. In vitro characterization of perfluorocarbon droplets for focused ultrasound therapy. *Phys Med Biol*. 2010;55:4933–47.
- [189] Shpak O, Verweij M, Vos HJ, de Jong N, Lohse D, Versluis M. Acoustic droplet vaporization is initiated by superharmonic focusing. *PNAS*. 2014;111:1697–702.
- [190] de Gracia Lux C, Vezeridis AM, Lux J, Armstrong AM, Sirsi SR, Hoyt K, et al. Novel method for the formation of monodisperse superheated perfluorocarbon nanodroplets as activatable ultrasound contrast agents. *RSC Adv*. 2017:48561–8.
- [191] Desgranges S, Lorton O, Gui-Lévy L, Guillemin P, Celicanin Z, Hyacinthe J-N, et al. Micron-sized PFOB liquid core droplets stabilized with tailored-made perfluorinated surfactants as a new class of endovascular sono-sensitizers for focused ultrasound thermotherapy. *J Mater Chem B*. 2019;7:927–39.
- [192] Szablowski JO, Bar-Zion A, Shapiro MG. Achieving spatial and molecular specificity with ultrasound-targeted biomolecular nanotherapeutics. *Acc Chem Res*. 2019;52:2427–34.
- [193] Vlaisavljevich E, Durmaz YY, Maxwell A, ElSayed M, Xu Z. Nanodroplet-mediated histotripsy for image-guided targeted ultrasound cell ablation. *Theranostics*. 2013;3:851–64.
- [194] Abdalkader R, Unga J, Yamashita F, Maruyama K, Hashida M. Evaluation of the theranostic potential of perfluorohexane-based acoustic nanodroplets. *Biol Pharm Bull*. 2019;42:2038–44.
- [195] Beppu S, Matsuda H, Shishido T, Matsumura M, Miyatake K. Prolonged myocardial contrast echocardiography via peripheral venous administration of QW3600 injection (EchoGen): its efficacy and side effects. *J Am Soc Echocardiogr*. 1997;10:11–24.
- [196] Arnaud F, Haque A, Morris E, Moon-Massat P, Auken C, Biswajit S, et al. Treatment of swine closed head injury with perfluorocarbon NVX-428. *Med Sci*. 2020;8:41.
- [197] Unger EC, Stea B. Randomized prospective phase II clinical trial of NVX-108 in association with chemoradiation of glioblastoma. NIH; 2017 <https://grantome.com/grant/NIH/R44-CA144817-03>.
- [198] Graham K, Unger E. Overcoming tumor hypoxia as a barrier to radiotherapy, chemotherapy and immunotherapy in cancer treatment. *Int J Nanomedicine*. 2018;13:6049–58.
- [199] Sadtler VM, Krafft MP, Riess JG. Achieving stable, reverse water-in-fluorocarbon emulsions. *Angew Chem Int Ed Engl*. 1996;35:1976–8.
- [200] Sadtler VM, Krafft MP, Riess JG. Reverse water-in-fluorocarbon emulsions as a drug delivery system: An *in vitro* study. *Colloids Surf A*. 1999;147:309–15.
- [201] Krafft MP, Chittofrati A, Riess JG. Emulsions and microemulsions with a fluorocarbon phase. *Curr Opin Colloid Interface Sci*. 2003;8:251–8.
- [202] Courrier HM, Krafft MP, Butz N, Porté C, Frossard N, Rémy-Kristensen A, et al. Evaluation of cytotoxicity of new semi-fluorinated amphiphiles derived from dimorpholinophosphate. *Biomaterials*. 2003;24:689–96.
- [203] Courrier HM, Vandamme TF, Krafft MP. Reverse water-in-fluorocarbon emulsions and microemulsions obtained with a fluorinated surfactant. *Colloids Surf A: Physicochem Eng Aspects*. 2004;244:141–8.
- [204] Orizondo RA, Nelson DL, Fabiilli ML, Cook KE. Effects of fluorosurfactant structure and concentration on drug availability and biocompatibility in water-in-perfluorocarbon emulsions for pulmonary drug delivery. *Colloid Polym Sci*. 2017;295:2413–22.
- [205] Ferguson SK, Pak DJ, Hopkins JL, Harral JW, Redinius KM, Loomis Z, et al. Pre-clinical assessment of a water-in-fluorocarbon emulsion for the treatment of pulmonary vascular diseases. *Drug Deliv*. 2019;26:147–57.
- [206] Sadtler VM, Jeanneaux F, Krafft MP, Rabai J, Riess JG. Perfluoroalkylated amphiphiles with a monomorpholinophosphate or dimorpholinophosphate polar head group. *New J Chem*. 1998;22:609–13.
- [207] Chevalier Y, Zemb T. The structure of micelles and microemulsions. *Rep Prog Phys*. 1990;53:279–371.
- [208] Guo MT, Rotem A, Heyman JA, Weitz DA. Droplet microfluidics for high-throughput biological assays. *Lab Chip*. 2012;12:2146–55.
- [209] Klein AM, Mazutis L, Akartuna I, Tallapragada N, Veres A, Li V, et al. Droplet barcoding for single-cell transcriptomics applied to embryonic stem cells. *Cell Transplant*. 2015;161:1187–201.
- [210] Shembekar N, Chaipan C, Utharala R, Merten CA. Droplet-based microfluidics in drug discovery, transcriptomics and high-throughput molecular genetics. *Lab Chip*. 2016;16:1314–31.
- [211] Clausell-Tormos J, Lieber D, Baret J-C, El-Harrak A, Miller OJ, Frenz L, et al. Droplet-based microfluidic platforms for the encapsulation and screening of mammalian cells and multicellular organisms. *Chem Biol*. 2008;15:427–37.
- [212] Pan M, Rosenfeld L, Kim M, Xu M, Lin E, Derda R, et al. Fluorinated Pickering emulsions impede interfacial transport and form rigid interface for the growth of anchorage-dependent cells. *ACS Appl Mater Interfaces*. 2014;6:21446–53.
- [213] Duncanson WJ, Arriaga LR, Ung WL, Kopeček JA, Porter TM, Weitz DA. Microfluidic fabrication of perfluorohexane-shelled double emulsions for controlled loading and acoustic-triggered release of hydrophilic agents. *Langmuir*. 2014;30:13765–70.
- [214] Lee YH, Ma YT. Synthesis, characterization, and biological verification of anti-HER2 indocyanine green-doxorubicin-loaded polyethyleneimine-coated perfluorocarbon double nanoemulsions for targeted phototherapy of breast cancer cells. *J Nanobiotechnol*. 2017;15:41.
- [215] Nguyen K, Pan H-Y, Haworth K, Mahoney E, Mercado-Shekhar KP, Lin C-Y, et al. Multiple exposure drug release from stable nanodroplets by high-intensity focused ultrasound for a potential degenerative disc disease treatment. *Ultrasound Med Biol*. 2019;45:160–9.
- [216] Aliabouzar M, Lu X, Kripfgans OD, Fowlkes JB, Fabiilli ML. Acoustic droplet vaporization in acoustically responsive scaffolds: effects of frequency of excitation, volume fraction and threshold determination method. *Ultrasound Med Biol*. 2019;45:3246–60.
- [217] Lee H, Choi C-H, Abbaspourrad A, Wesner C, Caggioni M, Zhu T, et al. Fluorocarbon oil reinforced triple emulsion drops. *Adv Mater*. 2016;28:8425–30.
- [218] Krafft MP, Riess JG. Stable highly concentrated fluorocarbon gels. *Angew Chem Int Ed Engl*. 1994;33:1100–1.
- [219] Qian X, Han X, Chen Y. Insights into the unique functionality of inorganic micro/nanoparticles for versatile ultrasound theranostics. *Biomaterials*. 2017;142:13–30.
- [220] Zhang N, Cai X, Gao W, Wang R, Xu C, Yao Y, et al. A multifunctional theranostic nanoagent for dual-mode image-guided HIFU/chemo- synergistic cancer therapy. *Theranostics*. 2016;6:404–17.
- [221] Wang J, Liu L, You Q, Song Y, Sun Q, Wang Y, et al. All-in-one theranostic nanoplatfrom based on hollow MoS<sub>2</sub> for photothermally-manuevered oxygen self-enriched photodynamic therapy. *Theranostics*. 2018;8:955–71.
- [222] Zhou Y, Wang R, Teng Z, Wang Z, Hu B, Kolios M, et al. Magnetic nanoparticle-promoted droplet vaporization for in vivo stimuli-responsive cancer theranostics. *NPG Asia Mater*. 2016;8:e313.
- [223] Zhou J, Xue C, Hou Y, Li M, Hu Y, Chen Q, et al. Oxygenated theranostic nanoplatforms with intracellular agglomeration behavior for improving the treatment efficacy of hypoxic tumors. *Biomaterials*. 2019;197:129–45.
- [224] Song G, Liang C, Yi X, Zhao Q, Cheng L, Yang K, et al. Perfluorocarbon-loaded hollow Bi<sub>2</sub>Se<sub>3</sub> nanoparticles for timely supply of oxygen under near-infrared light to enhance the radiotherapy of cancer. *Adv Mater*. 2016;28:2716–23.
- [225] Ke H, Wang J, Tong S, Jin Y, Wang S, Qu E, et al. Gold nanoshelled liquid perfluorocarbon magnetic nanocapsules: a nanotheranostic platform for bimodal ultrasound/magnetic resonance imaging guided photothermal tumor ablation. *Theranostics*. 2014;4:12–23.
- [226] Lee AL, Gee CT, Weegman BP, Einstein SA, Juelfs AR, Ring HL, et al. Oxygen sensing with perfluorocarbon-loaded ultraporos mesostructured silica nanoparticles. *ACS Nano*. 2017;11:5623–32.
- [227] Pochert A, Vernikouskaya I, Pascher F, Rasche V, Lindén M. Cargo-influences on the biodistribution of hollow mesoporous silica nanoparticles as studied by quantitative 19F-magnetic resonance imaging. *J Colloid Interface Sci*. 2017;488:1–9.
- [228] Lu N, Fan W, Yi X, Wang S, Wang Z, Tian R, et al. Biodegradable hollow mesoporous organosilica nanotheranostics for mild hyperthermia-induced bubble-enhanced oxygen-sensitized radiotherapy. *ACS Nano*. 2018;12:1580–91.
- [229] He K, Ran H, Su Z, Wang Z, Li M, Hao L. Perfluorohexane-encapsulated fullerene nanospheres for dual-modality US/CT imaging and synergistic high-intensity focused ultrasound ablation. *Int J Nanomedicine*. 2019;14:519–29.
- [230] Soto F, Martin A, Ibsen S, Vaidyanathan M, Garcia-Gradilla V, Levin Y, et al. Acoustic microcannons: toward advanced microballistics. *ACS Nano*. 2016;10:1522–8.
- [231] Soto F, Jeerapan I, Silva-López C, Lopez-Ramirez M, Chai I, Xiaolong L, et al. Noninvasive transdermal delivery system of lidocaine using an acoustic droplet-vaporization based wearable patch. *Small*. 2018;14:e1803266.
- [232] Ma T, Zhu L, Yang Y, Quan X, Huang L, Liu Z, et al. Enhanced in vivo survival of Schwann cells by a synthetic oxygen carrier promotes sciatic nerve regeneration and functional recovery. *J Tissue Eng Regen Med*. 2018;12:e177–89.
- [233] Epstein-Barash H, Orbey G, Polat BE, Ewoldt RH, Feshitan J, Langer R, et al. A microcomposite hydrogel for repeated on-demand ultrasound triggered drug delivery. *Biomaterials*. 2010;31:5208–17.

- [234] Khadjavi A, Magnetto C, Panariti A, Argenziano M, Gulino GR, Rivolta I, et al. Chitosan-shelled oxygen-loaded nanodroplets abrogate hypoxia dysregulation of human keratinocyte gelatinases and inhibitors: new insights for chronic wound healing. *Toxicol Appl Pharmacol*. 2015;286:198–206.
- [235] Prato M, Magnetto C, Jose J, Khadjavi A, Cavallo F, Quaglino E, et al. 2H,3H-Decafluoropentane-based nanodroplets: new perspectives for oxygen delivery to hypoxic cutaneous tissues. *PLoS One*. 2015;10:e0119769.
- [236] Moncion A, Lin M, Kripfgans OD, Franceschi RT, Putnam AJ, Fabiilli ML. Sequential payload release from acoustically responsive scaffolds using focused ultrasound. *Ultrasound Med Biol*. 2018;44:2323–35.
- [237] Lu X, Dong X, Natla S, Kripfgans OD, Fowlkes JB, Wang X, et al. Parametric study of acoustic droplet vaporization thresholds and payload release from acoustically-responsive scaffolds. *Ultrasound Med Biol*. 2019;45:2471–84.
- [238] Sontum P, Kvåle S, Healey AJ, Skurtveit R, Watanabe R, Matsumura M, et al. Acoustic cluster therapy (ACT) – a novel concept for ultrasound mediated, targeted drug delivery. *Int J Pharm*. 2015;495:1019–27.
- [239] van Wamel A, Sontum PC, Healey A, Kvåle S, Bush N, Bamber J, et al. Acoustic cluster therapy (ACT) enhances the therapeutic efficacy of paclitaxel and Abraxane® for treatment of human prostate adenocarcinoma in mice. *J Control Release*. 2016;236:15–21.
- [240] Hall RL, Juan-Sing ZD, Hoyt K, Sirsi SR. Formulation and characterization of chemically cross-linked microbubble clusters. *Langmuir*. 2019;35:10977–86.
- [241] Dewitte H, Van Lint S, Heirman C, Thielemans K, De Smedt SC, Breckpot K, et al. The potential of antigen and TriMix sonoporation using mRNA-loaded microbubbles for ultrasound-triggered cancer immunotherapy. *J Control Release*. 2014;194:28–36.
- [242] Yan F, Li L, Deng Z, Jin Q, Chen J, Yang W, et al. Paclitaxel-liposome-microbubble complexes as ultrasound-triggered therapeutic drug delivery carriers. *J Control Release*. 2013;166:246–55.
- [243] Zhang J, Wang S, Deng Z, Li L, Tan G, Liu X, et al. Ultrasound-triggered drug delivery for breast tumor therapy through IRGD-targeted paclitaxel-loaded liposome-microbubble complexes. *J Biomed Nanotechnol*. 2018;14:1384–95.
- [244] Prabhakar A, Banerjee R. Nanobubble liposome complexes for diagnostic imaging and ultrasound-triggered drug delivery in cancers: a theranostic approach. *ACS Omega*. 2019;4:15567–80.
- [245] Dwivedi P, Kiran S, Han S, Dwivedi M, Khatik R, Fan R, et al. Magnetic targeting and ultrasound activation of liposome-microbubble conjugate for enhanced delivery of anticancer therapies. *ACS Appl Mater Interfaces*. 2020;12:23737–51.
- [246] Batchelor DVB, Abou-Saleh RH, Coletta PL, McLaughlan JR, Peyman SA, Evans SD. Nested nanobubbles for ultrasound-triggered drug release. *ACS Appl Mater Interfaces*. 2020;12:29085–93.
- [247] Javadi M, Pitt WG, Belnap DM, Tsosie NH, Hartley JM. Encapsulating nanoemulsions inside eliposomes for ultrasonic drug delivery. *Langmuir*. 2012;28:14720–9.
- [248] de Matos MBC, Deckers R, van Elburg B, Lajoinie G, de Miranda BS, Versluis M, et al. Ultrasound-sensitive liposomes for triggered macromolecular drug delivery: formulation and in vitro characterization. *Front Pharmacol*. 2019;10:1463.
- [249] Ninomiya K, Yamashita T, Tanabe Y, Imai M, Takahashi K, Shimizu N. Targeted and ultrasound-triggered cancer cell injury using perfluorocarbon emulsion-loaded liposomes endowed with cancer cell-targeting and fusogenic capabilities. *Ultrason Sonochem*. 2016;28:54–61.
- [250] Shekhar H, Kleven RT, Peng T, Palaniappan A, Karani KB, Huang S, et al. In vitro characterization of sonothrombolysis and echocontrast agents to treat ischemic stroke. *Sci Rep*. 2019;9:9902.
- [251] Negishi Y, Ishii Y, Shiono H, Akiyama S, Sekine S, Kojima T, et al. Bubble liposomes and ultrasound exposure improve localized morpholino oligomer delivery into the skeletal muscles of dystrophic mdx mice. *Mol Pharm*. 2014;11:1053–61.
- [252] Wang Q, Li JM, Yu H, Deng K, Zhou W, Wang CX, et al. Fluorinated polymeric micelles to overcome hypoxia and enhance photodynamic cancer therapy. *Biomater Sci*. 2018;6:3096–107.
- [253] Chen J, Luo H, Liu Y, Zhang W, Li H, Luo T, et al. Oxygen-self-produced nanoplatform for relieving hypoxia and breaking resistance to sonodynamic treatment of pancreatic cancer. *ACS Nano*. 2017;11:12849–62.
- [254] Ping J, You F, Geng Z, Peng H. Facile synthesis of fluorinated nanophotosensitizers with self-supplied oxygen for efficient photodynamic therapy. *Nanotechnology*. 2019;30:345207.
- [255] Lim I, Vian A, van de Wouw HL, Day RA, Gomez C, Liu Y, et al. Fluorous soluble cyanine dyes for visualizing perfluorocarbons in living systems. *J Am Chem Soc*. 2020;142:16072–81.
- [256] Kislukhin AA, Xu H, Adams SR, Narsinh KH, Tsien RY, Ahrens ET. Paramagnetic fluorinated nanoemulsions for sensitive cellular fluorine-19 magnetic resonance imaging. *Nat Mater*. 2016;15:662–8.
- [257] Jahromi AH, Wang C, Adams SR, Zhu W, Narsinh K, Xu H, et al. Fluorous-soluble metal chelate for sensitive fluorine-19 magnetic resonance imaging nanoemulsion probes. *ACS Nano*. 2019;13:143–51.
- [258] Day RA, Estabrook DA, Logan JK, Sletten EM. Fluorous photosensitizers enhance photodynamic therapy with perfluorocarbon nanoemulsions. *ChemComm*. 2017;53:13043–6.
- [259] Zhang C, Moonshi SS, Wang W, Ta HT, Han Y, Han FY, et al. High F-content perfluoropolyether-based nanoparticles for targeted detection of breast cancer by <sup>19</sup>F magnetic resonance and optical imaging. *ACS Nano*. 2018;12:9162–76.
- [260] Klibanov AL. Preparation of targeted microbubbles: ultrasound contrast agents for molecular imaging. *Med Biol Eng Comput*. 2009;47:875–82.
- [261] Köse G, Darguzyte M, Kiessling F. Molecular ultrasound imaging. *Nanomaterials*. 2020;10:10101935.
- [262] Wang H, Gauthier M, Kelly JR, Miller RJ, Xu M, O'Brien WD, et al. Targeted ultrasound assisted cancer-selective chemical labeling and subsequent cancer imaging via click chemistry. *Angew Chem Int Ed Engl*. 2016;55:5452–6.
- [263] Slagle CJ, Thamm DH, Randall EK, Borden MA. Click conjugation of cloaked peptide ligands to microbubbles. *Bioconjug Chem*. 2018;29:1534–45.
- [264] Estabrook DA, Ennis AF, Day RA, Sletten EM. Controlling nanoemulsion surface chemistry with poly(2-oxazoline) amphiphiles. *Chem Sci*. 2019;10:3994–4003.
- [265] Ferrara KW, Borden MA, Zhang H. Lipid-shelled vehicles: engineering for ultrasound molecular imaging and drug delivery. *Acc Chem Res*. 2009;42:881–92.
- [266] Klibanov AL. Ultrasound molecular imaging of cancer: design and formulation strategies of targeted contrast agents. *Mol Imag Oncol*. 2020;216:319–36.
- [267] Rix A, Curaj A, Liehn E, Kiessling F. Ultrasound microbubbles for diagnosis and treatment of cardiovascular diseases. *Semin Thromb Hemost*. 2020;46:545–52.
- [268] Mulvana H, Eckersley RJ, Tang M-X, Pankhurst Q, Stride E. Theoretical and experimental characterisation of magnetic microbubbles. *Ultrasound Med Biol*. 2012;38:864–75.
- [269] Jamburidze A, Huerre A, Baresch D, Poulichet V, De Corato M, Garbin V. Nanoparticle-coated microbubbles for combined ultrasound imaging and drug delivery. *Langmuir*. 2019;35:10087–96.
- [270] Owen J, Stride E. Technique for the characterization of phospholipid microbubbles coatings by transmission electron microscopy. *Ultrasound Med Biol*. 2015;41:3253–8.
- [271] Beguin E, Bau L, Shrivastava S, Stride E. Comparing strategies for magnetic functionalization of microbubbles. *ACS Appl Mater Interfaces*. 2019;11:1829–40.
- [272] Lee S, Kim JH, Lee JH, Zen Y, Han JK. Imaging monitoring of Kupffer cell function and hepatic oxygen saturation in preneoplastic changes during cholangiocarcinogenesis. *Sci Rep*. 2017;7:14203.
- [273] Zhao R, Jiang J, Li H, Chen M, Liu R, Sun S, et al. Phosphatidylserine-microbubble targeting-activated microglia/macrophage in inflammation combined with ultrasound for breaking through the blood-brain barrier. *J Neuroinflammation*. 2018;15:334.
- [274] Sontum PC. Physicochemical characteristics of Sonazoid™, a new contrast agent for ultrasound imaging. *Ultrasound Med Biol*. 2008;34:824–33.
- [275] Wang H, Hyvelin J-M, Felt SA, Guracar I, Vilches-Moure JG, Cherkaoui S, et al. US molecular imaging of acute ileitis: anti-inflammatory treatment response monitored with targeted microbubbles in a preclinical model. *Radiology*. 2018;289:90–100.
- [276] Klibanov AL, McDannold NJ. Moving toward noninvasive, focused ultrasound therapeutic delivery of drugs in the brain: prolonged opening of blood-brain barrier may not be needed. *Radiology*. 2019;291:467–8.
- [277] Wischhusen J, Padilla F. Ultrasound molecular imaging with targeted microbubbles for cancer diagnostics: from bench to bedside. *IRBM*. 2019;40:3–9.
- [278] Kosareva A, Abou-Elkacem L, Chowdhury S, Lindner JR, Kaufmann BA. Seeing the invisible—ultrasound molecular imaging. *Ultrasound Med Biol*. 2020;46:479–97.
- [279] Lau C, Rivas M, Dinalo J, King K, Duddalwar V. Scoping review of targeted ultrasound contrast agents in the detection of angiogenesis. *J Ultrasound Med*. 2020;39:19–28.
- [280] Liu J, Xu F, Huang J, Xu J, Liu Y, Yao Y, et al. Low-intensity focused ultrasound (LIFU)-activated nanodroplets as a theranostic agent for noninvasive cancer molecular imaging and drug delivery. *Biomater Sci*. 2018;6:2838–49.
- [281] Hagimori M, Mendoza-Ortega EE, Krafft MP. Synthesis and physicochemical evaluation of fluorinated lipopeptide precursors of ligands for microbubble targeting. *Beilstein J Org Chem*. 2021;17:511–8.
- [282] Dayton T, Klibanov A, Brandenburger G, Ferrara K. Acoustic radiation force in vivo: a mechanism to assist targeting of microbubbles. *Ultrasound Med Biol*. 1999;25:1195–201.
- [283] Siemer S, Wünsch D, Khamis A, Lu Q, Scherberich A, Filippi M, et al. Nano meets micro-translational nanotechnology in medicine: nano-based applications for early tumor detection and therapy. *Nanomaterials*. 2020;10:383.
- [284] Faithfull NS. The concept of hemoglobin equivalency of perfluorochemical emulsions. *Adv Exp Med Biol*. 2003;530:271–85.
- [285] Cabrales P, Intaglietta M. Blood substitutes: evolution from non-carrying to oxygen and gas carrying fluids. *ASAIO J*. 2013;59:337–54.
- [286] Cabrales P, Tsai AG, Frangos JA, Briceno JC, Intaglietta M. Oxygen delivery and consumption in the microcirculation after extreme hemodilution with perfluorocarbons. *Am J Physiol Heart Circ Physiol*. 2004;287:H320–30.
- [287] Cheng Y, Cheng H, Jiang C, Qiu X, Wang K, Huan W, et al. Perfluorocarbon nanoparticles enhance reactive oxygen levels and tumour growth inhibition in photodynamic therapy. *Nat Commun*. 2015;6:8785.
- [288] Song X, Feng L, Liang C, Yang K, Liu Z. Ultrasound triggered tumor oxygenation with oxygen-shuttle nanoparticle-perfluorocarbon to overcome hypoxia-associated resistance in cancer therapies. *Nano Lett*. 2016:6145–53.
- [289] Vorob'ev SI. First- and second-generation perfluorocarbon emulsions. *Pharm Chem J (Russia)*. 2009;43:30–40.
- [290] Abutarboush R, Saha BK, Mullah SH, Arnaud FG, Haque A, Aligbe C, et al. Cerebral microvascular and systemic effects following intravenous administration of the perfluorocarbon emulsion Perforan. *J Funct Biomater*. 2016;7:29.
- [291] Latson G. Perforan (Vidaphor)-introduction to western medicine. *Shock*. 2019;52(15):65–9.
- [292] Shaw RF, Richard TJ. Rational development of Oxyfluor. In: Winslow RM, editor. *Blood Substitutes*. Amsterdam: Elsevier; 2006. p. 298–311 Chapter 27.
- [293] Weers JG, Arlauskas RA, Tarara TE, Pelura TJ. Characterization of fluorocarbon-in-water emulsions with added triglyceride. *Langmuir*. 2004;20:7430–5.
- [294] Maillard E, Juszcak MT, Langlois A, Kleiss C, Sancier MC, Bietler W, et al. Perfluorocarbon emulsions prevent hypoxia of pancreatic β cells. *Cell Transplant*. 2012;21:657–69.
- [295] Audonnet-Blaise S, Krafft MP, Smani Y, Mertes P-M, Marie P-Y, Labrude P, et al. Resuscitation of severe but brief haemorrhagic shock with PFC in rabbits restores



- skeletal muscle oxygen delivery and does not alter skeletal muscle metabolism. *Resuscitation*. 2006;70:124–32.
- [296] Haiss F, Jolivet R, Wyss MT, Reichold J, Brahm NB, Scheffold F, et al. Improved *in vivo* two-photon imaging after blood replacement by perfluorocarbon. *J Physiol*. 2009;587:3153–8.
- [297] Jacoby C, Temme S, Mayenfels F, Benoit N, Krafft MP, Schubert R, et al. Probing different perfluorocarbons for *in vivo* inflammation imaging by <sup>19</sup>F MRI: image reconstruction, biological half-lives and sensitivity. *NMR Biomed*. 2014;27:261–71.
- [298] Nienhaus F, Colley D, Jahn A, Pfeiler S, Flocke V, Temme S, et al. Phagocytosis of a PFOB-nanoemulsion for <sup>19</sup>F magnetic resonance imaging: first results in monocytes of patients with stable coronary artery disease and ST-elevation myocardial infarction. *Molecules*. 2019;24:2058.
- [299] Frumento RJ, Mongero L, Naka Y, Bennett-Guerrero E. Preserved gastric tonometric variables in cardiac surgical patients administered intravenous perflubron emulsion. *Anesth Analg*. 2002;94:809–14.
- [300] Verdin-Vasquez RC, Zepeda-Perez C, Ferra-Ferrer R, Chavez-Negrete A, Contreras F, Barroso-Aranda J. Use of Perforan emulsion to decrease allogeneic blood transfusion in cardiac surgery: clinical trial. *Artif Cells Blood Substit Biotechnol*. 2006;34:433–54.
- [301] Cabrales P, Briceno JC. Delaying blood transfusion in experimental acute anemia with a perfluorocarbon emulsion. *Anesthesiology*. 2011;114:901–11.
- [302] Kuzmiak-Glancy S, Covian R, Femnou AN, Glancy B, Jaimes R, Wengrowski AM, et al. Cardiac performance is limited by oxygen delivery to the mitochondria in the crystalloid-perfused working heart. *Am J Physiol Heart Circ Physiol*. 2018;314:H704–15.
- [303] Price CD, El-Badri NS, Haas DKA, Chaparro RE, Mangar D, Camporesi EM. The evaluation of the efficacy of Oxygent® as an oxygen-carrying substitute on cerebral blood flow. *Open Hematol J*. 2008;2:62–6.
- [304] Hou S, Ding H, Lv Q, Yin X, Song J, Landén NX, et al. Therapeutic effect of intravenous infusion of perfluorocarbon emulsion on LPS-induced acute lung injury in rats. *PLoS One*. 2014;9:e87826.
- [305] Seiffge DJ, Lapina NE, Tsagogiorgas C, Theisinger B, Henning RH, Schilling L. Improvement of oxygen supply by an artificial carrier in combination with normobaric oxygenation decreases the volume of tissue hypoxia and tissue damage from transient focal cerebral ischemia. *Exp Neurol*. 2012;237:18–25.
- [306] Zhou Z, Sun D, Lévassieur JE, Merenda A, Hamm RJ, Zhu J, et al. Perfluorocarbon emulsions improve cognitive recovery after lateral fluid percussion brain injury in rats. *Neurosurgery*. 2008;63:806–7.
- [307] Yacoub A, Hajec MC, Stanger R, Wan W, Young H, Mathern BE. Neuroprotective effects of perfluorocarbon (Oxycyte) after contusive spinal cord injury. *J Neurotrauma*. 2014;31:256–67.
- [308] Deuchar GA, van Kralingen JC, Work LM, Santosh C, Muir KW, McCabe C, et al. Pre-clinical validation of the therapeutic potential of Glasgow oxygen level dependent (GOLD) technology: a theranostic for acute stroke. *Transl Stroke Res*. 2019;10:583–95.
- [309] Votrin SV, Vorobyev SI, Bolevich S, Bolevich SS, Orlova A, Tachieva BI, et al. Use of perfluorocarbon based blood substitute Perforan in correction of hypoxia during acute anemia in animals. *Ser J Exp Clin Res*. 2019;20:245–50.
- [310] Torres Filho IP, Pedro JRP, Narayanan SV, Nguyen NM, Roseff SD, Spiess BD. Perfluorocarbon emulsion improves oxygen transport of normal and sickle cell human blood *in vitro*. *J Biomed Mater Res A*. 2014;102:2105–15.
- [311] Yao Y, Zhang M, Liu T, Zhou J, Gao Y, Wen Z, et al. Perfluorocarbon-encapsulated PLGA-PEG emulsions as enhancement agents for highly efficient reoxygenation to cell and organism. *ACS Appl Mater Interfaces*. 2015;7:18369–78.
- [312] Wang J, Wang R, Li N, Shen X, Huang G, Zhu J, et al. High-performance reoxygenation from PLGA-PEG/PFOB emulsions: a feedback relationship between ROS and HIF-1 $\alpha$ . *Int J Nanomedicine*. 2018;13:3027–38.
- [313] Zhou Z, Song J, Nie L, Chen X. Reactive oxygen species generating systems meeting challenges of photodynamic cancer therapy. *Chem Soc Rev*. 2016;45:6597–626.
- [314] Feng L, Betzer O, Tao D, Sadan T, Popovtzer R, Liu Z. Oxygen nanoshuttles for tumor oxygenation and enhanced cancer treatment. *CCS Chem*. 2019;1:239–50.
- [315] Krafft MP. Alleviating tumor hypoxia with perfluorocarbon-based oxygen carriers. *Curr Opin Pharmacol*. 2020;53:1–9.
- [316] Sahu A, Kwon I, Tae G. Improving cancer therapy through the nanomaterials-assisted alleviation of hypoxia. *Biomaterials*. 2020;228:119578.
- [317] Hatfield SM, Kjaergaard J, Lukashov D, Schreiber TH, Belikoff B, Abbott R, et al. Immunological mechanisms of the antitumor effects of supplemental oxygenation. *Sci Transl Med*. 2015;7:277ra30.
- [318] Hatfield SM, Sitkovsky M. A2A adenosine receptor antagonists to weaken the hypoxia-HIF-1 $\alpha$  driven immunosuppression and improve immunotherapies of cancer. *Curr Opin Pharmacol*. 2016;29:90–6.
- [319] Fuchs J, Thiele J. The role of oxygen in cutaneous photodynamic therapy. *Free Radic Biol Med*. 1998;26:835–47.
- [320] Feldman LA, Fabre M-S, Grasso C, Reid D, Broaddus WC, Lanza GM, et al. Perfluorocarbon emulsions radiosensitize brain tumors in carbogen breathing mice with orthotopic GL261 gliomas. *PLoS One*. 2017;12:e0184250.
- [321] Xiang Y, Bernards N, Hoang B, Zheng J, Matsuura N. Perfluorocarbon nanodroplets can reoxygenate hypoxic tumors *in vivo* without carbogen breathing. *Nanotherapeutics*. 2019;3:135–44.
- [322] Song G, Ji C, Liang C, Song X, Yi X, Dong Z, et al. TaOx decorated perfluorocarbon nanodroplets as oxygen reservoirs to overcome tumor hypoxia and enhance cancer radiotherapy. *Biomaterials*. 2017;112:257–63.
- [323] Zhou Z, Zhang B, Wang H, Yuan A, Hu Y, Wu J. Two-stage oxygen delivery for enhanced radiotherapy by perfluorocarbon nanoparticles. *Theranostics*. 2018;8:4898–911.
- [324] Hong AC, Young CJ, Hurlley MD, Wallington TJ, Mabury SA. Perfluorotributylamine: a novel long-lived greenhouse gas. *Geophys Res Lett*. 2013;40:6010–5.
- [325] Li J, Shang W, Li Y, Fu S, Tian J, Lu L. Advanced nanomaterials targeting hypoxia to enhance radiotherapy. *Int J Nanomedicine*. 2018;13:5925–36.
- [326] Scheer A, Kirsch M, Ferenz KB. Perfluorocarbons in photodynamic and photothermal therapy. *J Nanosci Nanomed*. 2017;1:21–7.
- [327] Tang X, Cheng Y, Huang S, Zhi F, Yuan A, Hu Y, et al. Overcome the limitation of hypoxia against photodynamic therapy to treat cancer cells by using perfluorocarbon nanodroplet for photosensitizer delivery. *Biochem Biophys Res Commun*. 2017;487:483–7.
- [328] Li X, Kwon N, Guo T, Liu Z, Yoon J. Innovative strategies for hypoxic-tumor photodynamic therapy. *Angew Chem Int Ed Engl*. 2018;57:11522–31.
- [329] Tang W, Yang Z, Wang S, Wang Z, Song J, Yu G, et al. Organic semiconducting photoacoustic nanodroplets for laser-activatable ultrasound imaging and combinational cancer therapy. *ACS Nano*. 2018;12:2610–22.
- [330] Yu M, Xu X, Cai Y, Zou L, Shuai X. Perfluorohexane-cored nanodroplets for stimulations-responsive ultrasonography and O<sub>2</sub>-potentiated photodynamic therapy. *Biomaterials*. 2018;175:61–71.
- [331] Zhao C, Tong Y, Li X, Shao L, Chen L, Lu J, et al. Photosensitive nanoparticles combining vascular-independent intratumor distribution and on-demand oxygen-depot delivery for enhanced cancer photodynamic therapy. *Small*. 2018;14:201703045.
- [332] Hu D, Zhong L, Wang M, Li H, Qu Y, Liu Q, et al. Perfluorocarbon-loaded and redox-activatable photosensitizing agent with oxygen supply for enhancement of fluorescence/photoacoustic imaging guided tumor photodynamic therapy. *Adv Funct Mater*. 2019;29:1806199.
- [333] Larue L, Myrzakhmetov B, Ben-Mihoub A, Moussaron A, Thomas N, Arnoux P, et al. Fighting hypoxia to improve PDT. *Pharmaceutics*. 2019;12:163.
- [334] Liu C, Dong H, Wu N, Cao Y, Zhang X. Plasmonic resonance energy transfer enhanced photodynamic therapy with Au@SiO<sub>2</sub>@Cu<sub>2</sub>O/perfluorohexane nanocomposites. *ACS Appl Mater Interfaces*. 2018;10:6991–7002.
- [335] Hong L, Wang J-L, Geng J-X, Zhao Y-H, Zhou G-X, Zhang J, et al. Rational design of an oxygen-enriching nanoemulsion for enhanced near-infrared laser activatable photodynamic therapy against hypoxic tumors. *Colloids Surf B Biointerfaces*. 2021;198:111500.
- [336] Sheng D, Liu T, Deng L, Zhang L, Li X, Xu J, et al. Perfluorooctyl bromide & indocyanine green coloaded nanoliposomes for enhanced multimodal imaging-guided phototherapy. *Biomaterials*. 2018;165:1–13.
- [337] Wood AKW, Sehgal CM. A review of low-intensity ultrasound for cancer therapy. *Ultrasound Med Biol*. 2015;41:905–28.
- [338] McHale AP, Callan JF, Nomikou N, Fowley C, Callan B. Sonodynamic therapy: concept, mechanism and application to cancer treatment. *Adv Exp Med Biol*. 2016;880:429–50.
- [339] Qian X, Zheng Y, Chen Y. Micro/nanoparticle-augmented sonodynamic therapy (SDT): breaking the depth shallow of photoactivation. *Adv Mater*. 2016;28:8097–129.
- [340] Yang Y, Tu J, Yang D, Raymond JL, Roy RA, Zhang D. Photo- and sono-dynamic therapy: a review of mechanisms and considerations for pharmacological agents used in therapy incorporating light and sound. *Curr Pharm Des*. 2019;25:401–12.
- [341] Huang B, Chen S, Pei W, Xu Y, Jiang Z, Niu C, et al. Oxygen-sufficient nanoplatform for chemo-sonodynamic therapy of hypoxic tumors. *Front Chem*. 2020;8:358.
- [342] Song D, O'Reilly Berings A, Zhuang Z, Joshi G, Tran TH, Claffey KP, et al. Overcoming hypoxia-induced chemoresistance to cisplatin through tumor oxygenation monitored by optical imaging. *Nanotheranostics*. 2019;3:223–35.
- [343] Ma X, Yao M, Shi J, Li X, Gao Y, Luo Q, et al. High intensity focused ultrasound-responsive and ultrastable cerasomal perfluorocarbon nanodroplets for alleviating tumor multidrug resistance and epithelial–mesenchymal transition. *ACS Nano*. 2020;14:15904–18.
- [344] Zhou Z, Zhang B, Wang S, Zai W, Yuan A, Hu Y, et al. Perfluorocarbon nanoparticles mediated platelet blocking disrupt vascular barriers to improve the efficacy of oxygen-sensitive antitumor drugs. *Small*. 2018;14:1801694.
- [345] Zhou Z, Zhang B, Zai W, Kang L, Yuan A, Hu Y, et al. Perfluorocarbon nanoparticle-mediated platelet inhibition promotes intratumoral infiltration of T cells and boosts immunotherapy. *Proc Natl Acad Sci U S A*. 2019;116:11972–7.
- [346] Huang W, Chiang W, Cheng Y, Lin W, Yu C, Yen C, et al. Tumor-tropic monocyte-mediated delivery of echogenic polymer bubbles and therapeutic vesicles for chemotherapy of tumor hypoxia. *Biomaterials*. 2015;71:71–83.
- [347] Hwang SC, Hwang DS, Kim H, Kim M, Kang Y, Byun S, et al. Development of bone regeneration strategies using human periosteum-derived osteoblasts and oxygen-releasing microparticles in mandibular osteomyelitis model of miniature pig. *J Biomed Mater Res A*. 2019;107:2183–94.
- [348] Kim HY, Kim SY, Lee HY, Lee JH, Rho GJ, Lee HJ, et al. Oxygen-releasing microparticles for cell survival and differentiation ability under hypoxia for effective bone regeneration. *Biomacromolecules*. 2019;20:1087–97.
- [349] Pilarek M. Liquid perfluorochemicals as flexible and efficient gas carriers applied in bioprocess engineering: An updated overview and future prospects. *Chem Process Engineer*. 2014;35:463–87.
- [350] White JC, Godsey ME, Bhatia SR. Perfluorocarbons enhance oxygen transport in alginate-based hydrogels. *Polymers Adv Technol*. 2014;25:1242–6.
- [351] Okumura S, Uemura T, Zhao X, Masano Y, Tsuruyama T, Fujimoto Y, et al. Liver graft preservation using perfluorocarbon improves the outcomes of simulated donation after cardiac death liver transplantation in rats. *Liver Transpl*. 2017;23:1171–85.
- [352] Sanchez-Dominguez M, Krafft MP, Maillard E, Siegrist S, Belcourt A. Prevention of adhesion and promotion of pseudoislets formation from a beta cell line by fluorocarbon emulsions. *ChemBioChem*. 2006;7:1160–3.

- [353] Maillard E, Sanchez-Dominguez M, Kleiss C, Langlois A, Sancier MC, Vohouhe C, et al. Perfluorocarbons: new tools for islets preservation in vitro. *Transplant Proc.* 2008;40:372–4.
- [354] Lambert E, Gorantla VS, Janjic JM. Pharmaceutical design and development of perfluorocarbon nanocolloids for oxygen delivery in regenerative medicine. *Nanomedicine.* 2019;14:2697–712.
- [355] Logan K, Foglietta F, Nesbitt H, Sheng Y, McKaig T, Kamila S, et al. Targeted chemodynamic therapy treatment of breast tumours using ultrasound responsive microbubbles loaded with paclitaxel, doxorubicin and Rose Bengal. *Eur J Pharm Biopharm.* 2019;139:224–31.
- [356] Nesbitt H, Sheng Y, Kamila S, Logan K, Thomas K, Callan B, et al. Gemcitabine loaded microbubbles for targeted chemodynamic therapy of pancreatic cancer. *J Control Release.* 2018;279:8–16.
- [357] Sheng Y, Beguin E, Nesbitt H, Kamila S, Owen J, Barnsley LC, et al. Magnetically responsive microbubbles as delivery vehicles for targeted sonodynamic and antimetabolite therapy of pancreatic cancer. *J Control Release.* 2017;262:192–200.
- [358] Yang C, Xia H, Sun Y, Zhu L, Gao Y, Kwok S, et al. Lipid microbubbles as ultrasound-stimulated oxygen carriers for controllable oxygen release for tumor reoxygenation. *Ultrasound Med Biol.* 2018;44:416–25.
- [359] Eisenbrey JR, Shraim R, Liu J-B, Li J, Stanczak M, Oeffinger B, et al. Sensitization of hypoxic tumours to radiation therapy using ultrasound-sensitive oxygen microbubbles. *Int J Radiat Oncol Biol Phys.* 2018;101:88–96.
- [360] Delaney LJ, Ciraku L, Oeffinger BE, Wessner CE, Liu JB, Li J, et al. Breast cancer brain metastasis response to radiation after microbubble oxygen delivery in a murine model. *J Ultrasound Med.* 2019;38:3221–8.
- [361] Ho Y-J, Chu S-W, Liao E-C, Fan C-H, Chan H-L, Wei K-C, et al. Normalization of tumor vasculature by oxygen microbubbles with ultrasound. *Theranostics.* 2019;9:7370–83.
- [362] Wang H, Wang P, Li L, Zhang K, Wang X, Liu Q. Microbubbles enhance the antitumor effects of sinoporphyrin sodium mediated sonodynamic therapy both in vitro and in vivo. *Int J Biol Sci.* 2015;11:1401–9.
- [363] Sun J, Yin M, Zhu S, Liu L, Zhu Y, Wang Z, et al. Ultrasound-mediated destruction of oxygen and paclitaxel loaded lipid microbubbles for combination therapy in hypoxic ovarian cancer cells. *Ultrasound Sonochem.* 2016;28:319–26.
- [364] Luo T, Sun J, Zhu S, He J, Hao L, Xiao L, et al. Ultrasound-mediated destruction of oxygen and paclitaxel loaded dual-targeting microbubbles for intraperitoneal treatment of ovarian cancer xenografts. *Cancer Lett.* 2017;391:1–11.
- [365] Lundgren CE, Bergoe GW, Tyssebotn IM. Intravascular fluorocarbon-stabilized microbubbles protect against fatal anemia in rats. *Artif Cells Blood Substit Immobil Biotechnol.* 2006;34:473–86.
- [366] Tyssebotn IM, Lundgren CE, Olszowka AJ, Bergoe GW. Hypoxia due to shunts in pig lung treated with O<sub>2</sub> and fluorocarbon-derived intravascular microbubbles. *Artif Cells Blood Substit Immobil Biotechnol.* 2010;38:79–89.
- [367] Arthur MC, Brown A, Carlson K, Lowery J, Skinner RD, Culp WC. Dodecafluoropentane improves neurological function following anterior ischemic stroke. *Mol Neurobiol.* 2017;54:4764–70.
- [368] Culp WC, Brown AT, Lowery JD, Arthur MC, Roberson PK, Skinner RD. Dodecafluoropentane emulsion extends window for tPA therapy in a rabbit stroke model. *Mol Neurobiol.* 2015;52:979–84.
- [369] Fitzgerald RT, Ou X, Nix JS, Arthur MC, Brown AT, Skinner RD, et al. Dodecafluoropentane emulsion delays and reduces MRI markers of infarction in a rat stroke model: a preliminary report. *Magn Reson Imaging.* 2015;33:236–9.
- [370] Liu Z, Barber C, Gupta A, Wan L, Won YW, Furenli L, et al. Imaging assessment of cardioprotection mediated by a dodecafluoropentane oxygen-carrier administered during myocardial infarction. *Nucl Med Biol.* 2019;70:67–77.
- [371] Mullah SH, Saha BK, Abutarboush R, Walker PB, Haque A, Arnaud FG, et al. Perfluorocarbon NVX-108 increased cerebral oxygen tension after traumatic brain injury in rats. *Brain Res.* 2016;1634:132–9.
- [372] Swyer TW, Strom J, Larson DF. Nanoparticle oxygen delivery to the ischemic heart. *Perfusion.* 2014;29:539–43.
- [373] Graham K, Moon-Massatt PF, Unger EC. Dodecafluoropentane emulsion (DDFPe) as a resuscitation fluid for treatment of hemorrhagic shock and traumatic brain injury: a review. *Shock.* 2019;52(Suppl. 1):50–4.
- [374] Jayaraman MS, Graham K, Unger EC. In vitro model to compare the oxygen offloading behaviour of dodecafluoropentane emulsion (DDFPe). *Artif Cells Nanomed Biotechnol.* 2019;47:783–9.
- [375] Woods SD, Skinner RD, Ricca AM, Brown AT, Lowery JD, Borrelli MJ, et al. Progress in dodecafluoropentane emulsion as a neuroprotective agent in a rabbit stroke model. *Mol Neurobiol.* 2013;48:363–7.
- [376] Johnson JLH, Leos RA, Baker AF, Unger EC. Radiosensitization of Hs-766T pancreatic tumor xenografts in mice dosed with dodecafluoropentane nano-emulsion—preliminary findings. *J Biomed Nanotechnol.* 2015;11:274–81.
- [377] Culp WC, Onteddu SS, Brown A, Nalleballe K, Sharma R, Skinner RD, et al. Dodecafluoropentane emulsion in acute ischemic stroke: A phase Ib/II randomized and controlled dose-escalation trial. *J Vasc Interv Radiol.* 2019;30:1244–50 el.
- [378] Chen S, Liu Y, Zhu S, Chen C, Xie W, Xiao L, et al. Dual-mode imaging and therapeutic effects of drug-loaded phase-transition nanoparticles combined with near-infrared laser and low-intensity ultrasound on ovarian cancer. *Drug Deliv.* 2018;25:1683–93.
- [379] Xie W, Zhu S, Yang B, Chen C, Chen S, Liu Y, et al. The destruction of laser-induced phase-transition nanoparticles triggered by low-intensity ultrasound: An innovative modality to enhance the immunological treatment of ovarian cancer cells. *Int J Nanomedicine.* 2019;14:9377–93.
- [380] Que Y, Liu Y, Tan W, Feng C, Shi P, Li Y, et al. Enhancing photodynamic therapy efficacy by using fluorinated nanoplatfom. *ACS Macro Lett.* 2016;5:168–73.
- [381] Yang G, Tian J, Chen C, Jiang D, Xue Y, Wang C, et al. An oxygen self-sufficient NIR-responsive nanosystem for enhanced PDT and chemotherapy against hypoxic tumors. *Chem Sci.* 2019;10:5766–72.
- [382] Xing L, Gong J-H, Wang Y, Zhu Y, Huang Z-J, Zhao J, et al. Hypoxia alleviation-triggered enhanced photodynamic therapy in combination with IDO inhibitor for preferable cancer therapy. *Biomaterials.* 2019;206:170–82.
- [383] Tao D, Feng L, Chao Y, Liang C, Song X, Wang H, et al. Covalent organic polymers based on fluorinated porphyrin as oxygen nanoshuttles for tumor hypoxia relief and enhanced photodynamic therapy. *Adv Funct Mater.* 2018;28:1804901.
- [384] Choi M, Park S, Park K, Jeong H, Hong J. Nitric oxide delivery using biocompatible perfluorocarbon microemulsion for antibacterial effect. *ACS Biomater Sci Eng.* 2019:1378–83.
- [385] Lafond M, Shekhar H, Panmanee W, Collins SD, Palaniappan A, McDaniel CT, et al. Bactericidal activity of lipid-shelled nitric oxide-loaded microbubbles. *Front Pharmacol.* 2020;10:1540.
- [386] Sutton JT, Raymond JL, Verleye M, Pyne-Geithman GJ, Holland CK. Pulsed ultrasound enhances the delivery of nitric oxide from bubble liposomes to ex vivo porcine carotid tissue. *Int J Nanomedicine.* 2014;9:4671–83.
- [387] Workie YA, Sabrina, Imae T, Krafft MP. Nitric oxide gas delivery by fluorinated poly(ethylene glycol)@graphene oxide carrier toward pharmacotherapeutics. *ACS Biomater Sci Eng.* 2019;5:2926–34.
- [388] Krathumkhet N, Sabrina, Imae T, Krafft MP. Nitric oxide gas in carbon nanohorn/fluorinated dendrimer/fluorinated poly(ethylene glycol)-based hierarchical nanocomposites as therapeutic nanocarriers. *ACS Appl Biomater.* 2021. <https://doi.org/10.1021/acsbm.0c01577>.
- [389] He Y, Zhang B, Chen Y, Jin Q, Wu J, Yan F, et al. Image-guided hydrogen gas delivery for protection from myocardial ischemia–reperfusion injury via microbubbles. *ACS Appl Mater Interfaces.* 2017;9:21190–9.
- [390] Shekhar H, Palaniappan A, Peng T, Lafond M, Moody MR, Haworth KJ, et al. Characterization and imaging of lipid-shelled microbubbles for ultrasound-triggered release of xenon. *Neurotherapeutics.* 2019;16:878–90.
- [391] Lundgren C, Bergoe G, Olszowka A, Tyssebotn I. Tissue nitrogen elimination in oxygen-breathing pigs is enhanced by fluorocarbon-derived intravascular microbubbles. *Undersea Hyperb Med.* 2005;32:215–26.
- [392] Sheppard RL, Regis DP, Mahon RT. Dodecafluoropentane (DDFPe) and decompression sickness-related mortality in rats. *Aerosol Med Hum Perform.* 2015;86:21–6.
- [393] Mahon RT, Cronin WA, Bodo M, Tirumala S, Regis DP, Auker CR. Cardiovascular parameters in a mixed-sex swine study of severe decompression sickness treated with the emulsified perfluorocarbon Oxyocyte. *J Appl Physiol.* 2015;118:71–9.
- [394] Mayer D, Ferenz KB. Perfluorocarbons for the treatment of decompression illness: how to bridge the gap between theory and practice. *Eur J Appl Physiol.* 2019;119:2421–33.
- [395] Torres LN, Spiess BD, Torres Filho IP. Effects of perfluorocarbon emulsions on microvascular blood flow and oxygen transport in a model of severe arterial gas embolism. *J Surg Res.* 2014;187:324–33.
- [396] Lee Y-H, Yeh Y-L. Reduction of oxygen inhibition effect for microalgal growth using fluoroalkylated methoxy polyethylene glycol-stabilized perfluorocarbon nano-oxygen carriers. *Process Biochem.* 2015;50:1119–27.
- [397] Radhakrishnan K, Holland CK, Haworth KJ. Scavenging dissolved oxygen via acoustic droplet vaporization. *Ultrasound Sonochem.* 2016;31:394–403.
- [398] Haworth KJ, Goldstein BH, Mercado-Shekhar KP, Srivastava R, Arunkumar P, Su H, et al. Dissolved oxygen scavenging by acoustic droplet vaporization using intravascular ultrasound. *IEEE Int Ultrason Symp.* 2017. <https://doi.org/10.1109/ULTSYM.2017.8091704>.
- [399] Ahrens ET, Helfer BM, O'Hanlon CF, Schirda C. Clinical cell therapy imaging using a perfluorocarbon tracer and fluorine-19 MRI. *Magn Reson Med.* 2014;72:1696–701.
- [400] Zhang C, Moonshi SS, Han Y, Puttick S, Peng H, Magoling BJA, et al. PFPE-based polymeric <sup>19</sup>F MRI agents: a new class of contrast agents with outstanding sensitivity. *Macromolecules.* 2017;50:5953–63.
- [401] Hequet E, Henoumont C, Muller RN, Laurent S. Fluorinated MRI contrast agents and their versatile applications in the biomedical field. *Future Med Chem.* 2019;11:1157–75.
- [402] Jirak D, Galisova A, Kolouchova K, Babuka D, Hruby M. Fluorine polymer probes for magnetic resonance imaging: quo vadis? *MAGMA.* 2019;32:173–85.
- [403] Wu L, Liu F, Liu S, Xu X, Liu Z, Sun X. Perfluorocarbons-based <sup>19</sup>F magnetic resonance imaging in biomedicine. *Int J Nanomedicine.* 2020;15:7377–95.
- [404] Schmieder AH, Caruthers SD, Keupp J, Wickline SA, Lanza GM. Recent advances in <sup>19</sup>fluorine magnetic resonance imaging with perfluorocarbon emulsions. *Engineering (Beijing).* 2015;1:475–89.
- [405] Peterson KL, Srivastava K, Pierre VC. Fluorinated paramagnetic complexes: sensitive and responsive probes for magnetic resonance spectroscopy and imaging. *Front Chem.* 2018;6:160.
- [406] Simkins JW, Stewart PS, Codd SL, Seymour JD. Non-invasive imaging of oxygen concentration in a complex in vitro biofilm infection model using <sup>19</sup>F MRI: persistence of an oxygen sink despite prolonged antibiotic therapy. *Magn Reson Med.* 2019;82:2248–56.
- [407] Yu J-X, Hallac RR, Chiguru S, Mason RP. New frontiers and developing applications in <sup>19</sup>F NMR. *Prog Nucl Magn Reson Spectrosc.* 2013;70:25–49.
- [408] Moore JK, Chen J, Pan H, Gaut JP, Jain S, Wickline SA. Quantification of vascular damage in acute kidney injury with fluorine magnetic resonance imaging and spectroscopy. *Magn Reson Med.* 2018;79:3144–53.
- [409] Chapelin F, Capitini CM, Ahrens ET. Fluorine-19 MRI for detection and quantification of immune cell therapy for cancer. *J Immunother.* 2018;6:105.
- [410] Hingorani DV, Chapelin F, Stares E, Adams SR, Okada H, Ahrens ET. Cell penetrating peptide functionalized perfluorocarbon nanoemulsions for targeted cell labeling and enhanced fluorine-19 MRI detection. *Magn Reson Med.* 2020;83:974–87.



- [411] Amiri H, Srinivas M, Veltien A, van Uden MJ, de Vries IJ, Heerschap A. Cell tracking using (19)F magnetic resonance imaging: technical aspects and challenges towards clinical applications. *Eur Radiol*. 2015;25:726–35.
- [412] Fink C, Smith M, Sehl OC, Gaudet JM, Meagher TC, Sheikh NA, et al. Quantification and characterization of granulocyte macrophage colony-stimulating factor activated human peripheral blood mononuclear cells by fluorine-19 cellular MRI in an immunocompromised mouse model. *Diagn Intervent Imag*. 2020;101:577–88.
- [413] Bouchlaka MN, Ludwig KD, Gordon JW, Kutz MP, Bednarz BP, Fain SB, et al. <sup>19</sup>F-MRI for monitoring human NK cells in vivo. *Oncol Immunology*. 2016;5:e1143996.
- [414] Kennis BA, Michel KA, Brugmann WB, Laureano A, Tao R-H, Somanchi SS, et al. Monitoring of intracerebellarly-administered natural killer cells with fluorine-19 MRI. *J Neurooncol*. 2019;142:395–407.
- [415] Makela AV, Foster FS. Preclinical <sup>19</sup>F MRI cell tracking at 3 tesla. *MAGMA*. 2019;32:123–32.
- [416] Richard J-P, Hussain U, Gross S, Taga A, Kouser M, Almad A, et al. Perfluorocarbon labeling of human glial-restricted progenitors for <sup>19</sup>F magnetic resonance imaging. *Stem Cells Transl Med*. 2019;8:355–65.
- [417] Rothe M, Jahn A, Weiss K, Hwang J, Szendroedi J, Kelm M, et al. In vivo <sup>19</sup>F MR inflammation imaging after myocardial infarction in a large animal model at 3 T. *MAGMA*. 2019;32:5–13.
- [418] O'Hanlon CF, Fedczyna T, Eaker S, Shingleton WD, Helfer BM. Integrating a <sup>19</sup>F MRI tracer agent into the clinical scale manufacturing of a T-cell immunotherapy. *Contrast Media Mol Imaging*. 2017;2017:9548478.
- [419] Constantinides C, McNeill E, Carnicer R, Al Haj Zen A, Sainz-Urruela R, Shaw A, et al. Improved cellular uptake of perfluorocarbon nanoparticles for in vivo murine cardiac <sup>19</sup>F MRS/MRI and temporal tracking of progenitor cells. *Nanomedicine NBM*. 2019;18:391–401.
- [420] Darçot E, Colotti R, Brennan D, Deuchar GA, Santosh C, van Heeswijk RB. A characterization of ABL-101 as a potential tracer for clinical fluorine-19 MRI. *NMR Biomed*. 2020;33:e4212.
- [421] de Vries A, Moonen R, Yildirim M, Langereis S, Lamerichs R, Pikkemaat JA, et al. Relaxometric studies of gadolinium-functionalized perfluorocarbon nanoparticles for MR imaging. *Contrast Media Mol Imaging*. 2014;9:83–91.
- [422] Owen J, Crake C, Lee JY, Carugo D, Beguin E, Khrapitchev AA, et al. A versatile method for the preparation of particle-loaded microbubbles for multimodality imaging and targeted drug delivery. *Drug Deliv Transl Res*. 2018;8:342–56.
- [423] Schmieder AH, Wang K, Zhang H, Senpan A, Pan D, Keupp J, et al. Characterization of early neovascular response to acute lung ischemia using simultaneous <sup>19</sup>F/<sup>1</sup>H MR molecular imaging. *Angiogenesis*. 2014;17:51–60.
- [424] Temme S, Grapentin C, Quast C, Jacoby C, Grandoch M, Ding Z, et al. Noninvasive imaging of early venous thrombosis by <sup>19</sup>F magnetic resonance imaging with targeted perfluorocarbon nanoemulsions. *Circulation*. 2015;131:1405–14.
- [425] Guden-Silber T, Temme S, Jacoby C, Flögel U. Biomedical <sup>19</sup>F MRI using perfluorocarbons. *Methods Mol Biol*. 2018;1718:235–57.
- [426] Chong WK, Papadopolou V, Dayton PA. Imaging with ultrasound contrast agents: current status and future. *Abdom Radiol*. 2018;43:762–72.
- [427] Chowdhury SM, Abou-Elkacem L, Lee T, Dahl J, Lutz AM. Ultrasound and microbubble mediated therapeutic delivery: underlying mechanisms and future outlook. *J Control Release*. 2020;326:75–90.
- [428] Wang S, Hossack JA, Klibanov AL. From anatomy to functional and molecular biomarker imaging and therapy: ultrasound is safe, ultrafast, portable, and inexpensive. *Invest Radiol*. 2020;55:559–72.
- [429] Burgess MT, Apostolakis I, Konofagou EE. Power cavitation-guided blood-brain barrier opening with focused ultrasound and microbubbles. *Phys Med Biol*. 2018;15:065009.
- [430] Yang Y, Zhang X, Ye D, Laforest R, Williamson J, Liu Y, et al. Cavitation dose painting for focused ultrasound-induced blood-brain barrier disruption. *Sci Rep*. 2019;9:2840.
- [431] Averkiou MA, Bruce MF, Powers JE, Sheeran PS, Burns PN. Imaging methods for ultrasound contrast agents. *Ultrasound Med Biol*. 2020;46:498–517.
- [432] Qin S, Caskey CF, Ferrara KW. Ultrasound contrast microbubbles in imaging and therapy: physical principles and engineering. *Phys Med Biol*. 2009;54:R27.
- [433] Azmin M, Mohamedi G, Edirisinghe M, Stride EP. Dissolution of coated microbubbles: the effect of nanoparticles and surfactant concentration. *Mat Sci Engineer C*. 2012;32:2654–8.
- [434] Frinking P, Segers T, Luan Y, Tranquart F. Three decades of ultrasound contrast agents: a review of the past, present and future improvements. *Ultrasound Med Biol*. 2020;46:892–908.
- [435] Piscaglia F, Nolsøe C, Dietrich CF, Cosgrove DO, Gilja OH, Bachmann Nielsen M, et al. The EFSUMB guidelines and recommendations on the clinical practice of contrast enhanced ultrasound (CEUS): update 2011 on non-hepatic applications. *Ultraschall Med*. 2012;33:33–59.
- [436] Barr RG. Off-label use of ultrasound contrast agents for abdominal imaging in the United States. *J Ultrasound Med*. 2013;32:7–12.
- [437] Appis AW, Tracy MJ, Feinstein SB. Update on the safety and efficacy of commercial ultrasound contrast agents in cardiac applications. *Echo Res Pract*. 2015;2:R55–62.
- [438] El Kaffas A, Sigris RMS, Fisher G, Bachawal S, Liu J, Wang H, et al. Quantitative three-dimensional dynamic contrast-enhanced ultrasound imaging: first-in-human pilot study in patients with liver metastases. *Theranostics*. 2017;7:3745–58.
- [439] Forsberg F, Sridharan A, Piccoli CW, Sevrukov A, Wilkes A, Ojeda-Fournier H, et al. Combining quantitative 3D subharmonic imaging and clinical assessments for accurate characterization of breast masses. *IEEE Int Ultrason Symp Glasgow (UK)*. 2019;1:177–80.
- [440] Pesapane F, Leenknegt B, Ammar T, Panella S, Garzillo G, Huang DY. Intraoperative microvascular assessment with contrast-enhanced ultrasound (CEUS) during uterine artery embolisation (UAE): A case report and literature review. *J Ultrasound*. 2020. <https://doi.org/10.1007/s40477-020-00441-2>.
- [441] Schwarze V, Marschner C, Negrão de Figueiredo G, Rübenthaler J, Clevert DA. Single-center study: Evaluating the diagnostic performance and safety of contrast-enhanced ultrasound (CEUS) in pregnant women to assess hepatic lesions. *Ultraschall Med*. 2020;41:29–35.
- [442] Marsico M, Gabbani T, Lunardi S, Lei B, Lucarini M, Cuffari B, et al. Computed tomography or contrast-enhanced ultrasonography for follow-up of liver metastases after Cyberknife therapy? A prospective pilot study. *J Ultrasound Med*. 2019;38:649–55.
- [443] Patil HR, Main ML. Revisiting the safety profile of echocardiography contrast agents. *Am Coll Cardiol*. 2016. <https://www.acc.org/latest-in-cardiology/articles/2016/06/23/08/23/revisiting-the-safety-profile-of-echocardiography-contrast-agents>.
- [444] Kummer T, Oh L, Phelan MB, Huang RD, Nomura JT, Adhikari S. Emergency and critical care applications for contrast-enhanced ultrasound. *Am J Emerg Med*. 2018;36:1287–94.
- [445] Porter TR, Mulvagh SL, Abdelmoneim SS, Becher H, Belcik JT, Bierig M, et al. Clinical applications of ultrasonic enhancing agents in echocardiography: 2018 American society of echocardiography guidelines update. *J Am Soc Echocardiogr*. 2018;31:241–74.
- [446] Dietrich CF, Nolsøe CP, Barr RG, Berzigotti A, Burns PN, Cantisani V, et al. Guidelines and good clinical practice recommendations for contrast-enhanced ultrasound (CEUS) in the liver—update 2020 WFUMB in cooperation with EFSUMB, AFSUMB, AIUM, and FLAUS. *Ultrasound Med Biol*. 2020;46:2579–604.
- [447] Zhao C, Zhang R, Luo Y, Liu S, Tang T, Yang F, et al. Multimodal VEGF-targeted contrast-enhanced ultrasound and photoacoustic imaging of rats with inflammatory arthritis: using dye-VEGF-antibody-loaded microbubbles. *Ultrasound Med Biol*. 2020;46:2400–11.
- [448] Meng Z, Zhou X, She J, Zhang Y, Feng L, Liu Z. Ultrasound-responsive conversion of microbubbles to nanoparticles to enable background-free in vivo photoacoustic imaging. *Nano Lett*. 2019;19:8109–17.
- [449] Hartman RK, Hallam KA, Donnelly EM, Emelianov SY. Photoacoustic imaging of gold nanorods in the brain delivered via microbubble-assisted focused ultrasound: a tool for in vivo molecular neuroimaging. *Laser Phys Lett*. 2019;16:025603.
- [450] Hernandez-Gil J, Braga M, Harriss BI, Carroll LS, Leow CH, Tang M-X, et al. Development of <sup>68</sup>Ga-labelled ultrasound microbubbles for whole-body PET imaging. *Chem Sci*. 2019;10:5603–15.
- [451] Arif WM, Elsinga PH, Gasca-Salas C, Versluis M, Martínez-Fernández R, Dierckx RAJO, et al. Focused ultrasound for opening blood-brain barrier and drug delivery monitored with positron emission tomography. *J Control Release*. 2020;324:303–16.
- [452] Lazarova N, Causey PW, Lemon JA, Czorny SK, Forbes JR, Zlitni A, et al. The synthesis, magnetic purification and evaluation of <sup>99m</sup>Tc-labeled microbubbles. *Nucl Med Biol*. 2011;38:1111–8.
- [453] Warram JM, Sorace AG, Mahoney M, Samuel S, Harbin B, Joshi M, et al. Biodistribution of P-selectin targeted microbubbles. *J Drug Target*. 2014;22:387–94.
- [454] Huang HY, Liu HL, Hsu PH, Chiang CS, Tsai CH, Chi HS, et al. A multitheragnostic nanobubble system to induce blood-brain barrier disruption with magnetically guided focused ultrasound. *Adv Mater*. 2015;27:655–61.
- [455] Huang Y, Alkins R, Schwartz ML, Hynynen K. Opening the blood-brain barrier with MR imaging-guided focused ultrasound: preclinical testing on a trans-human skull porcine model. *Radiology*. 2017;282:123–30.
- [456] Abou-Elkacem L, Bachawal SV, Willmann JK. Ultrasound molecular imaging: moving towards clinical translation. *Eur J Radiol*. 2015;84:1685–93.
- [457] Yeh JS-M, Sennoga CA, McConnell E, Eckersley R, Tang M-X, Nourshargh S, et al. A targeting microbubble for ultrasound molecular imaging. *PLoS One*. 2015;10:e0129681.
- [458] Güvener N, Appold L, de Lorenzi F, Golombek SK, Rizzo LY, Lammers T, et al. Recent advances in ultrasound-based diagnosis and therapy with micro and nanometer-sized formulations. *Methods*. 2017;130:4–13.
- [459] Rix A, Lederle W, Theek B, Lammers T, Moonen C, Schmitz G, et al. Advanced ultrasound technologies for diagnosis and therapy. *J Nucl Med*. 2018;59:740–6.
- [460] Zlitni A, Gambhir SS. Molecular imaging agents for ultrasound. *Curr Opin Chem Biol*. 2018;45C:113–20.
- [461] Baier J, Rix A, Kiessling F. Molecular ultrasound imaging. *Recent Results Cancer Res*. 2020;216:509–31.
- [462] Sun R, Tian J, Zhang J, Wang L, Guo J, Liu Y. Monitoring inflammation injuries in the progression of atherosclerosis with contrast enhanced ultrasound molecular imaging. *PLoS One*. 2017;12:e0186155.
- [463] Wang S, Unnikrishnan S, Herbst EB, Klibanov AL, Mauldin W, Hossack JA. Ultrasound molecular imaging of inflammation in mouse abdominal aorta. *Invest Radiol*. 2017;52:499–506.
- [464] Atkinson T, Packwood W, Xie A, Liang S, Qi Y, Ruggeri Z, et al. Assessment of novel antioxidant therapy in atherosclerosis by contrast ultrasound molecular imaging. *J Am Soc Echocardiogr*. 2018;31:1252–9.
- [465] Moccetti F, Weinkauff CC, Davidson BP, Belcik JT, Marinelli ER, Unger E, et al. Ultrasound molecular imaging of atherosclerosis using small-peptide targeting ligands against endothelial markers of inflammation and oxidative stress. *Ultrasound Med Biol*. 2018;44:1155–63.
- [466] Yan F, Sun Y, Mao Y, Wu M, Deng Z, Li S, et al. Ultrasound molecular imaging of atherosclerosis for early diagnosis and therapeutic evaluation through leucocyte-like multiple targeted microbubbles. *Theranostics*. 2018;8:1879–91.

- [467] Luong A, Smith D, Tai C-H, Cotter B, Luo C, Strachan M, et al. Development of a translatable ultrasound molecular imaging agent for inflammation. *Ultrasound Med Biol.* 2020;46:690–702.
- [468] Ozawa K, Lindner JR. Ultrasound molecular imaging: insights into cardiovascular pathology. *J Echocardiogr.* 2020;18:86–93.
- [469] Liu J, Chen Y, Wang G, Lv Q, Yang Y, Wang J, et al. Ultrasound molecular imaging of acute cardiac transplantation rejection using nanobubbles targeted to T lymphocytes. *Biomaterials.* 2018;162:200–7.
- [470] Helbert A, Von Wrónski M, Colevret D, Botteron C, Padilla F, Bettinger T, et al. Ultrasound molecular imaging with BR55, a predictive tool of antiangiogenic treatment efficacy in a chemo-induced mammary tumor model. *Invest Radiol.* 2020;55:657–65.
- [471] Yuan H-X, Wang W-P, Wen J-X, Lin L-W, Exner AA, Guan P-S, et al. Dual-targeted microbubbles specific to integrin  $\alpha V\beta 3$  and vascular endothelial growth factor receptor 2 for ultrasonography evaluation of tumor angiogenesis. *Ultrasound Med Biol.* 2018;44:1460–7.
- [472] Du J, Li X-Y, Hu H, Xu L, Yang S-P, Li F-H. Preparation and imaging investigation of dual-targeted  $C_3F_8$ -filled PLGA nanobubbles as a novel ultrasound contrast agent for breast cancer. *Sci Rep.* 2018;8:3887.
- [473] Shimazu K, Miyake T, Tanei T, Naoi Y, Shimoda M, Kagara N, et al. Real-time visualization of lymphatic flow to sentinel lymph nodes by contrast-enhanced ultrasonography with SonoZoid in patients with breast cancer. *Ultrasound Med Biol.* 2019;45:2634–40.
- [474] Shi G, Cui W, Benchimol M, Liu Y-T, Mattrey RF, Mukthavaram R, et al. Isolation of rare tumor cells from blood cells with buoyant immuno-microbubbles. *PLoS One.* 2013;8:e58017.
- [475] Liou Y-R, Wang Y-H, Lee C-Y, Li P-C. Buoyancy-activated cell sorting using targeted biotinylated albumin microbubbles. *PLoS One.* 2015;10:e0125036.
- [476] Wang G, Benasutti H, Jones JF, Shi G, Benchimol M, Pingle S, et al. Isolation of breast cancer CTCs with multitargeted buoyant immunomicrobubbles. *Colloids Surf B Biointerfaces.* 2018;161:200–9.
- [477] Zhu L, Cheng G, Ye D, Nazeri A, Yue Y, Liu W, et al. Focused ultrasound-enabled brain tumor liquid biopsy. *Sci Rep.* 2018;8:6553.
- [478] Lahtinen O, Eloranta M, Anttila M, Kärkkäinen H, Sironen R, Vanninen R, et al. Pre-operative sentinel lymph node localization in vulvar cancer: preliminary experience with inguinal intradermal contrast-enhanced ultrasound. *Eur Radiol.* 2018;28:2089–95.
- [479] Bertelsen C, King KG, Swanson M, Duddalwar V, Pepper JP. Contrast-enhanced ultrasound with perflubutane for sentinel lymph node mapping in cutaneous melanoma: a pilot study. *Laryngoscope.* 2019;129:1117–22.
- [480] Cox K, Taylor-Phillips S, Sharma N, Weeks J, Mills P, Sever A, et al. Enhanced pre-operative axillary staging using intradermal microbubbles and contrast-enhanced ultrasound to detect and biopsy sentinel lymph nodes in breast cancer: a potential replacement for axillary surgery. *Br J Radiol.* 2018;91:20170626.
- [481] Ou D-L, Lin Y-Y, Hsu C-L, Lin Y-Y, Chen C-W, Yu J-S, et al. Development of a PD-L1-expressing orthotopic liver cancer model: implications for immunotherapy for hepatocellular carcinoma. *Liver Cancer.* 2019;8:155–71.
- [482] Kripfgans OD, Zhang M, Fabiilli ML, Carson PL, Padilla F, Swanson SD, et al. Acceleration of ultrasound thermal therapy by patterned acoustic droplet vaporization. *J Acoust Soc Am.* 2014;135:537–44.
- [483] Chang N, Lu S, Qin D, Xu T, Han M, Wang S, et al. Efficient and controllable thermal ablation induced by short-pulsed HIFU sequence assisted with perfluorohexane nanodroplets. *Ultrason Sonochem.* 2018;45:57–64.
- [484] Kopechek JA, Park E-J, Zhang Y-Z, Vykhotseva NI, McDannold NJ, Porter TM. Cavitation-enhanced MR-guided focused ultrasound ablation of rabbit tumors in vivo using phase shift nanoemulsions. *Phys Med Biol.* 2014;59:3465–81.
- [485] Moyer LC, Timbie KF, Sheeran PS, Price RJ, Miller GW, Dayton PA. High-intensity focused ultrasound ablation enhancement in vivo via phase-shift nanodroplets compared to microbubbles. *J Ther Ultrasound.* 2015;3:7.
- [486] Shin SH, Park E-J, Min C, Choi SI, Jeon S, Kim Y-H, et al. Tracking perfluorocarbon nanoemulsion delivery by  $^{19}F$  MRI for precise high intensity focused ultrasound tumor ablation. *Theranostics.* 2017;7:562–72.
- [487] Perera RH, Solorio L, Wu H, Gangolli M, Silverman E, Hernandez C, et al. Nanobubble ultrasound contrast agents for enhanced delivery of thermal sensitizer to tumors undergoing radiofrequency ablation. *Pharm Res.* 2014;31:1407–17.
- [488] Zhao Y, Song W, Wang D, Ran H, Wang R, Yao Y, et al. Phase-shifted PFH@PLGA/Fe $_3$ O $_4$  nanocapsules for MRI/US imaging and photothermal therapy with near-infrared irradiation. *ACS Appl Mater Interfaces.* 2015;7:14231–42.
- [489] Xu Y, Niu C, An S, Tang S, Xiao P, Peng Q, et al. Thermal-sensitive magnetic nanoparticles for dual-modal tumor imaging and therapy. *RSC Adv.* 2017;7:40791–802.
- [490] Liu W-W, Liu S-W, Liou Y-R, Wu Y-H, Yang Y-C, Wang C-RC, et al. Nanodroplet-vaporization-assisted sonoporation for highly effective delivery of photothermal treatment. *Sci Rep.* 2016;6:24753.
- [491] Cheng C, Xiao Z, Huang G, Zhang L, Bai J. Enhancing ablation effects of a microbubble contrast agent on high-intensity focused ultrasound: An experimental and clinical study. *Brit J Obstetr Gynaecol.* 2017;124:78–86.
- [492] Bader KB, Vlasisvljevic E, Maxwell AD. For whom the bubble grows: physical principles of bubble nucleation and dynamics in histotripsy ultrasound therapy. *Ultrasound Med Biol.* 2019;45:1056–80.
- [493] Aydin O, Vlasisvljevic E, Yuksel Durmaz Y, Xu Z, ElSayed MEH. Noninvasive ablation of prostate cancer spheroids using acoustically-activated nanodroplets. *Mol Pharm.* 2016;5:4054–65.
- [494] McDannold N, Zhang Y, Vykhotseva N. Nonthermal ablation in the rat brain using focused ultrasound and an ultrasound contrast agent: long-term effects. *J Neurosurg.* 2016;125:1539–48.
- [495] Miller DL, Lu X, Dou C, Zhu YI, Fuller R, Fields K, et al. Ultrasonic cavitation-enabled treatment for therapy of hypertrophic cardiomyopathy: proof of principle. *Ultrasound Med Biol.* 2018;44:1439–50.
- [496] Bader KB, Bouchoux G, Holland CK. Sonothrombolysis. *Adv Exp Med Biol.* 2016;880:339–62.
- [497] Chen Z, Xue T, Huang H, Xu J, Shankar S, Yu H, et al. Efficacy and safety of sonothrombolysis versus non-sonothrombolysis in patients with acute ischemic stroke: a meta-analysis of randomized controlled trials. *PLoS One.* 2019;14:e0210516.
- [498] Zenyach A, Fournier L, Chauvierre C. Nanomedicine progress in thrombolytic therapy. *Biomaterials.* 2020;120297.
- [499] Petit B, Bohren Y, Gaud E, Bussat P, Arditi M, Yan F, et al. Sonothrombolysis: the contribution of stable and inertial cavitation to clot lysis. *Ultrasound Med Biol.* 2015;41:1402–10.
- [500] Schleicher N, Tomkins AJ, Kampschulte M, Hyvelin J-M, Botteron C, Juenemann M, et al. Sonothrombolysis with BR38 microbubbles improves microvascular patency in a rat model of stroke. *PLoS One.* 2016;11:e0152898.
- [501] Pajek D, Burgess A, Huang Y, Hynynen K. High intensity focused ultrasound sonothrombolysis: the use of perfluorocarbon droplets to achieve clot lysis at reduced acoustic powers. *Ultrasound Med Biol.* 2014;40:2151–61.
- [502] Kim J, Deruiter RM, Goel L, Xu Z, Jiang X, Dayton PA. A comparison of sonothrombolysis in aged clots between low-boiling-point phase-change nanodroplets and microbubbles of the same composition. *Ultrasound Med Biol.* 2020;46:3059–68.
- [503] Slikkerveer J, Juffermans LJM, van Royen N, Appelman Y, Porter TR, Kamp O. Therapeutic application of contrast ultrasound in ST elevation myocardial infarction: role in coronary thrombolysis and microvascular obstruction. *Eur Heart J Acute Cardiovasc Care.* 2019;8:45–53.
- [504] Nacu A, Kvistad CE, Naess H, Øygarden H, Logallo N, Assmus J, et al. NOR-SASS (Norwegian Sonothrombolysis in Acute Stroke Study) randomized controlled contrast-enhanced sonothrombolysis in an unselected acute ischemic stroke population. *Stroke.* 2017;48:335–41.
- [505] Mathias W, Tsutsui JM, Tavares BG, Fava AM, Aguiar MOD, Borges BC, et al. Sonothrombolysis in ST-segment elevation myocardial infarction treated with primary percutaneous coronary intervention. *J Am Coll Cardiol.* 2019;73:2832–42.
- [506] Matsuura N, Koonar E, Zhu S, Leung B, Seo M, Sivapalan N, et al. Inducing antivasculature effects in tumors with ultrasound stimulated micron-sized bubbles. *IEEE Int Ultrasonics Symp Proceed.* 2015:1–4.
- [507] Hunt SJ, Gade T, Soulen MC, Pickup S, Sehgal CM. Antivasculature ultrasound therapy. Magnetic resonance imaging validation and activation of the immune response in murine melanoma. *J Ultrasound Med.* 2015;34:275–87.
- [508] Harmon JS, Kabinejadian F, Seda R, Fabiilli ML, Kuruvilla S, Kuo CC, et al. Minimally invasive gas embolization using acoustic droplet vaporization in a rodent model of hepatocellular carcinoma. *Sci Rep.* 2019;9:11040.
- [509] Lai P, Tarapacki C, Tran WT, El Kaffas A, Lee J, Hupple C, et al. Breast tumor response to ultrasound mediated excitation of microbubbles and radiation therapy in vivo. *Oncoscience.* 2016;3:98–108.
- [510] Hou R, Xu Y, Lu Q, Zhang Y, Hu B. Effect of low-frequency low-intensity ultrasound with microbubbles on prostate cancer hypoxia. *Tumor Biol.* 2017;39:1010428317719275.
- [511] Jordão JF, Thévenot E, Markham-Coultes K, Scarcelli T, Weng Y-Q, Xhima K, et al. Amyloid- $\beta$  plaque reduction, endogenous antibody delivery and glial activation by brain-targeted, transcranial focused ultrasound. *Exp Neurol.* 2013;248:16–29.
- [512] Burgess A, Dubej S, Yeung S, Hough O, Eterman N, Aubert I, et al. Alzheimer disease in a mouse model: MR imaging-guided focused ultrasound targeted to the hippocampus opens the blood-brain barrier and improves pathologic abnormalities and behavior. *Radiology.* 2014;273:736–45.
- [513] Poon CT, Shah K, Lin C, Tse R, Kim KK, Mooney S, et al. Time course of focused ultrasound effects on  $\beta$ -amyloid plaque pathology in the TgCRND8 mouse model of Alzheimer's disease. *Sci Rep.* 2018;8:14061.
- [514] Mooney SJ, Nobrega JN, Levitt AJ, Hynynen K. Antidepressant effects of focused ultrasound induced blood-brain barrier opening. *Behav Brain Res.* 2018;342:57–61.
- [515] Lipsman N, Meng Y, Bethune AJ, Huang Y, Lam B, Masellis M, et al. Blood-brain barrier opening in Alzheimer's disease using MR-guided focused ultrasound. *Nat Commun.* 2018;9:2336.
- [516] Abrahamo A, Meng Y, Llinas M, Huang Y, Hamani C, Mainprize T, et al. First-in-human trial of blood-brain barrier opening in amyotrophic lateral sclerosis using MR-guided focused ultrasound. *Nat Commun.* 2019;10:4373.
- [517] Payne AH, Hawryluk GW, Anza Y, Odéon H, Ostlie MA, Reichert EC, et al. Magnetic resonance imaging-guided focused ultrasound to increase localized blood-spinal cord barrier permeability. *Neural Regen Res.* 2017;12:2045–9.
- [518] Montero A-S, Bielle F, Goldwirt L, Lalot A, Bouchoux G, Canney M, et al. Ultrasound-induced blood-spinal cord barrier opening in rabbits. *Ultrasound Med Biol.* 2019;45:2417–26.
- [519] Yu FTH, Chen X, Straub AC, Pacella JJ. The role of nitric oxide during sonoperfusion of microvascular obstruction. *Theranostics.* 2017;7:3527–38.
- [520] Belcik JT, Mott BH, Xie A, Zhao Y, Kim S, Lindner NJ, et al. Augmentation of limb perfusion and reversal of tissue ischemia produced by ultrasound-mediated microbubble cavitation. *Circul Cardiovasc Imag.* 2015;8:e002979.
- [521] Winkler H, Jacoby K, Kalota S, Snyder J, Cline K, Robertson K, et al. Twelve-month efficacy and safety data for the "stress incontinence control, efficacy and safety study": a phase III, multicenter, prospective, randomized, controlled study treating female stress urinary incontinence using the Vesair intravesical balloon. *Female Pelvic Med Reconstr Surg.* 2017;24:222–31.
- [522] McCammon K, Jacoby K, Kalota S, Snyder J, Cline K, Robertson K, et al. Three-month primary efficacy data for the SUCCESS trial: a phase III, multi-center, prospective,



- randomized, controlled study treating female stress urinary incontinence with the Vesair intravesical balloon. *Neurourol Urodyn.* 2018;37:440–8.
- [523] Mullin LB, Phillips LC, Dayton PA. Nanoparticle delivery enhancement with acoustically activated microbubbles. *IEEE Trans Ultrason Ferroelectr Freq Control.* 2013;60:65–77.
- [524] Kooiman K, Vos HJ, Versluis M, de Jong N. Acoustic behavior of microbubbles and implications for drug delivery. *Adv Drug Deliv Rev.* 2014;72:28–48.
- [525] Unger E, Porter T, Lindner J, Grayburn P. Cardiovascular drug delivery with ultrasound and microbubbles. *Adv Drug Deliv Rev.* 2014;72:110–26.
- [526] Timbie KF, Mead BP, Price RJ. Drug and gene delivery across the blood-brain barrier with focused ultrasound. *J Control Release.* 2015;219:61–75.
- [527] Cai X, Jiang Y, Lin M, Zhang J, Guo H, Yang F, et al. Ultrasound-responsive materials for drug/gene delivery. *Front Pharmacol.* 2020;10:1650.
- [528] Justeau C, Vela-Gonzalez AV, Jourdan A, Riess JG, Krafft MP. Adsorption of cerium salts and cerium oxide nanoparticles on microbubbles can be induced by a fluorocarbon gas. *ACS Sustain Chem Eng.* 2018;6:11450–6.
- [529] Mendoza-Ortega EE, Dubois M, Krafft MP. Fluorocarbon gas exposure induces disaggregation of nanodiamond clusters and enhanced adsorption, enabling medical microbubble formation. *ACS Appl Nano Mater.* 2020;3:8897–905.
- [530] Aryal M, Arvanitis CD, Alexander PM, McDannold N. Ultrasound-mediated blood barrier disruption for targeted drug delivery in the central nervous system. *Adv Drug Deliv Rev.* 2014;72:94–109.
- [531] Wu S-K, Chu P-C, Chai W-Y, Kang S-T, Tsai C-H, Fan C-H, et al. Characterization of different microbubbles in assisting focused ultrasound-induced blood-brain barrier opening. *Sci Rep.* 2017;7:46689.
- [532] Snipstad S, Sulheim E, de Lange Davies C, Moonen C, Storm G, Kiessling F, et al. Sonopermeation to improve drug delivery to tumors: from fundamental understanding to clinical translation. *Expert Opin Drug Deliv.* 2018;15:1249–61.
- [533] Ho Y-J, Wang T-C, Fan C-H, Yeh C-K. Spatially uniform tumor treatment and drug penetration by regulating ultrasound with microbubbles. *ACS Appl Mater Interfaces.* 2018;10:17784–91.
- [534] Qin P, Han T, Yu ACH, Xu L. Mechanistic understanding the bioeffects of ultrasound-driven microbubbles to enhance macromolecule delivery. *J Control Release.* 2018;272:169–81.
- [535] De Cock I, Zagato E, Braeckmans K, Luan Y, de Jong N, De Smedt SC, et al. Ultrasound and microbubble mediated drug delivery: acoustic pressure as determinant for uptake via membrane pores or endocytosis. *J Control Release.* 2015;197:20–8.
- [536] Song K-H, Fan AC, Brlansky JT, Trudeau T, Gutierrez-Hartmann A, Calvisi ML, et al. High efficiency molecular delivery with sequential low-energy sonoporation bursts. *Theranostics.* 2015;5:1419–27.
- [537] Bouakaz A, Zeghimi A, Doinikov AA. Sonoporation: concept and mechanisms. *Adv Exp Med Biol.* 2016;880:175–89.
- [538] Kotopoulos S, Stigen E, Popa M, Safont MM, Healey A, Kvåle S, et al. Sonoporation with acoustic cluster therapy (ACT®) induces transient tumour volume reduction in a subcutaneous xenograft model of precreatic ductal adenocarcinoma. *J Control Release.* 2017;245:70–80.
- [539] Theek B, Baues M, Ojha T, Möckel D, Veettil SK, Steitz J, et al. Sonoporation enhances liposome accumulation and penetration in tumors with low EPR. *J Control Release.* 2016;231:77–85.
- [540] Wang Y, Li Y, Yan K, Shen L, Yang W, Gong J, et al. Clinical study of ultrasound and microbubbles for enhancing chemotherapeutic sensitivity of malignant tumors in digestive system. *Chin J Cancer Res.* 2018;30:553–63.
- [541] Downs ME, Buch A, Sierra C, Karakatsani ME, Chen S, Konofagos EE, et al. Long-term safety of repeated blood-brain barrier opening via focused ultrasound with microbubbles in non-human primates performing a cognitive task. *PLoS One.* 2015;10:e0125911.
- [542] Burgess A, Hynynen K. Microbubble-assisted ultrasound for drug delivery in the brain and central nervous system. In: Escoffier J-M, Bouakaz A, editors. *Therapeutic ultrasound, advances in experimental medicine and biology.* Springer; 2016. p. 293–308.
- [543] Dasgupta A, Liu M, Ojha T, Storm G, Kiessling F, Lammers T. Ultrasound-mediated drug delivery to the brain: principles, progress and prospects. *Drug Discov Today Technol.* 2016;20:41–8.
- [544] Song K-H, Harvey BK, Borden MA. State-of-the-art of microbubble-assisted blood-brain barrier disruption. *Theranostics.* 2018;8:4393–408.
- [545] McMahon D, Poon C, Hynynen K. Evaluating the safety profile of focused ultrasound and microbubble-mediated treatments to increase blood-brain barrier permeability. *Expert Opin Drug Deliv.* 2019;16:129–42.
- [546] Wu S-Y, Fix SM, Arena C, Chen CC, Zheng W, Olumolade OO, et al. Focused ultrasound-facilitated brain drug delivery using optimized nanodroplets: Vaporization efficiency dictates large molecular delivery. *Phys Med Biol.* 2019;63:035002.
- [547] Lin C-Y, Lin Y-C, Huang C-Y, Wud S-R, Chene C-M, Liu H-L. Ultrasound-responsive neurotrophic factor-loaded microbubble-liposome complex: preclinical investigation for Parkinson's disease treatment. *J Control Release.* 2020;321:519–28.
- [548] Karakatsani ME, Blesa J, Konofagos EE. Blood brain barrier opening with focused ultrasound in experimental models of Parkinson's disease. *Mov Disord.* 2019;34:1252–61.
- [549] Yuan H, Hu H, Sun J, Shi M, Yu H, Li C, et al. Ultrasound microbubble delivery targeting intraplaque neovascularization inhibits atherosclerotic plaque in an APOE-deficient mouse model. *In Vivo.* 2018;32:1025–32.
- [550] Shen J, Zhuo N, Xu S, Song Z, Hu Z, Hao J, et al. Resveratrol delivery by ultrasound-mediated nanobubbles targeting nucleus pulposus cells. *Nanomedicine.* 2018;13:1433–46.
- [551] Chowdhury SM, Lee T, Willmann JK. Ultrasound-guided drug delivery in cancer. *Ultrasonography.* 2017;36:171–84.
- [552] Luo MH, Yeh CK, Situ B, Yu JS, Li BC, Chen ZY. Microbubbles: a novel strategy for chemotherapy. *Curr Pharm Des.* 2017;23:3383–90.
- [553] Jain A, Tiwari A, Verma A, Jain SK. Ultrasound-based triggered drug delivery to tumors. *Drug Deliv Transl Res.* 2018;8:150–64.
- [554] Fu J-W, Lin Y-S, Gan S-L, Li Y-R, Wang Y, Feng S-T, et al. Multifunctionalized micro-scale ultrasound contrast agents for precise theranostics of malignant tumors. *Contrast Media Mol Imaging.* 2019;2019:3145647.
- [555] Kuo T-T, Wang C-H, Wang J-Y, Chiou H-J, Fan C-H, Yeh C-K. Concurrent osteosarcoma theranostic strategy using contrast-enhanced ultrasound and drug-loaded bubbles. *Pharmaceutics.* 2019;11:223.
- [556] Jing Y, Xiu-Juan Z, Hong-Jiao C, Zhi-Kui C, Qing-Fu Q, En-Sheng X, et al. Ultrasound-targeted microbubble destruction improved the antiangiogenic effect of Endostar in triple-negative breast carcinoma xenografts. *J Cancer Res Clin Oncol.* 2019;145:1191–200.
- [557] Marano F, Rinella L, Argenziano M, Cavalli R, Sassi F, D'Amelio P, et al. Targeting taxanes to castration-resistant prostate cancer cells by nanobubbles and extracorporeal shock waves. *PLoS One.* 2016;11:e0168553.
- [558] Marano F, Argenziano M, Frairia R, Adami A, Bosco O, Rinella L, et al. Doxorubicin-loaded nanobubbles combined with extracorporeal shock waves: basis for a new drug delivery tool in anaplastic thyroid cancer. *Thyroid.* 2016;26:705–16.
- [559] Yoon YI, Kwon Y-S, Cho H-S, Heo S-H, Park KS, Park SG, et al. Ultrasound-mediated gene and drug delivery using a microbubble-liposome particle system. *Theranostics.* 2014;4:1133–44.
- [560] Bae YJ, Yoon YI, Yoon T-J, Lee HJ. Ultrasound-guided delivery of siRNA and a chemotherapeutic drug by using microbubble complexes: in vitro and in vivo evaluations in a prostate cancer model. *Korean J Radiol.* 2016;17:497–508.
- [561] Fan X, Wang L, Guo Y, Xiong X, Zhu L, Fang K. Inhibition of prostate cancer growth using doxorubicin assisted by ultrasound-targeted nanobubble destruction. *Int J Nanomedicine.* 2016;11:3585–96.
- [562] Meng X, Xu Y, Lu Q, Sun L, An X, Zhang J, et al. Ultrasound-responsive alkaline nanorobots for the treatment of lactic acidosis-mediated doxorubicin resistance. *Nanoscale.* 2020;12:13801–10.
- [563] Luo Z, Jin K, Pang Q, Shen S, Yan Z, Jiang T, et al. On-demand drug release from dual-targeting small nanoparticles triggered by high-intensity focused ultrasound enhanced glioblastoma-targeting therapy. *ACS Appl Mater Interfaces.* 2017;9:31612–25.
- [564] Zhang N, Song J, Liu Y, Liu M, Zhang L, Sheng D, et al. Photothermal therapy mediated by phase-transformation nanoparticles facilitates delivery of anti-PD1 antibody and synergizes with antitumor immunotherapy for melanoma. *J Control Release.* 2019;306:15–28.
- [565] Tang H, Guo Y, Peng L, Fang H, Wang Z, Zheng Y, et al. In vivo targeted, responsive, and synergistic cancer nanotheranostics by magnetic resonance imaging-guided synergistic high-intensity focused ultrasound ablation and chemotherapy. *ACS Appl Mater Interfaces.* 2018;10:15428–41.
- [566] Dimcevski G, Kotopoulos S, Bjånes T, Hoem D, Schjøtt J, Gjertsen BT, et al. A human clinical trial using ultrasound and microbubbles to enhance gemcitabine treatment of inoperable pancreatic cancer. *J Control Release.* 2016;243:172–81.
- [567] Carpentier A, Canney M, Vignot A, Reina V, Beccaria K, Horodyckid C, et al. Clinical trial of blood-brain barrier disruption by pulsed ultrasound. *Sci Transl Med.* 2016;8:343re2.
- [568] Idbaih A, Canney M, Belin L, Desseaux C, Vignot A, Bouchoux G, et al. Safety and feasibility of repeated and transient blood-brain barrier disruption by pulsed ultrasound in patients with recurrent glioblastoma. *Clin Cancer Res.* 2019;25:3793–801.
- [569] Mainprize T, Lipsman N, Huang Y, Meng Y, Bethune A, Ironside S, et al. Blood-brain barrier opening in primary brain tumors with noninvasive MR-guided focused ultrasound: a clinical safety and feasibility study. *Sci Rep.* 2019;9:321.
- [570] Rychak JJ, Klibanov AL. Nucleic acid delivery with microbubbles and ultrasound. *Adv Drug Deliv Rev.* 2014;72:82–93.
- [571] Dewitte H, Roovers S, De Smedt SC, Lentacker I. Enhancing nucleic acid delivery with ultrasound and microbubbles. *Methods Mol Biol.* 1943;2019:241–51.
- [572] Shapiro G, Wong A, Bez M, Yang F, Tam S, Even L, et al. Multiparameter evaluation of in vivo gene delivery using ultrasound-guided, microbubble-enhanced sonoporation. *J Control Release.* 2016;223:157–64.
- [573] Kopeček JA, Carson AR, McTiernan CF, Chen X, Klein EC, Villanueva FS. Cardiac gene expression knockdown using small inhibitory RNA-loaded microbubbles and ultrasound. *PLoS One.* 2016;11:e0159751.
- [574] Xhima K, Nabbouh F, Hynynen K, Aubert I, Tandon A. Non-invasive delivery of an  $\alpha$ -synuclein gene silencing vector with MR-guided focused ultrasound. *Mov Disord.* 2018;33:1567–79.
- [575] Wu M, Zhao H, Guo L, Wang Y, Song J, Zhao X, et al. Ultrasound-mediated nanobubble destruction (UMND) facilitates the delivery of A10-3.2 aptamer targeted and siRNA-loaded cationic nanobubbles for therapy of prostate cancer. *Drug Deliv.* 2018;25:226–40.
- [576] Cai W, Lv W, Feng Y, Yang H, Zhang Y, Yang G, et al. The therapeutic effect in gliomas of nanobubbles carrying siRNA combined with ultrasound-targeted destruction. *Int J Nanomedicine.* 2018;13:6791–87.
- [577] Lee WY, Li N, Lin S, Wang B, Lan HY, Li G. miRNA-29b improves bone healing in mouse fracture model. *Mol Cell Endocrinol.* 2016;430:97–107.
- [578] Song ZJ, Ye YJ, Zhang Z, Shen JL, Hu ZM, Wang ZG, et al. Noninvasive, targeted gene therapy for acute spinal cord injury using LIFU-mediated BDNF-loaded cationic nanobubble destruction. *Biochem Biophys Res Commun.* 2018;496:911–20.
- [579] Alkins R, Burgess A, Kerbel R, Wels WS, Hynynen K. Early treatment of HER2-amplified brain tumors with targeted NK-92 cells and focused ultrasound improves survival. *Neuro Oncol.* 2016;18:974–81.
- [580] Yang C, Du M, Yan F, Chen Z. Focused ultrasound improves NK-92MI cells infiltration into tumors. *Front Pharmacol.* 2019;10:326.

- [581] Bulner S, Prodeus A, Garipey J, Hynynen K, Goertz DE. Enhancing checkpoint inhibitor therapy with ultrasound stimulated microbubbles. *Ultrasound Med Biol*. 2019; 45:500–12.
- [582] Guo H, Wang Z, Du Q, Li P, Wang Z, Wang A. Stimulated phase-shift acoustic nanodroplets enhance vancomycin efficacy against methicillin-resistant *Staphylococcus aureus* biofilms. *Int J Nanomedicine*. 2017;12:4679–90.
- [583] Horsley H, Owen J, Browning R, Carugo D, Malone-Lee J, Stride E, et al. Ultrasound-activated microbubbles as a novel intracellular drug delivery system for urinary tract infection. *J Control Release*. 2019;301:166–75.
- [584] Lattwein KR, Shekhar H, Kouijzer JJP, van Wamel WJB, Holland CK, Kooiman K. Sonobactericide: an emerging treatment strategy for bacterial infections. *Ultrasound Med Biol*. 2020;46:193–215.
- [585] Alovici C, Panico C, de Sanctis U, Eandi CM. Vitreous substitutes: old and new materials in vitreoretinal surgery. *J Ophthalmol*. 2017;2017:3172138.
- [586] Lafond M, Aptel F, Mestas J-L, Lafon C. Ultrasound-mediated ocular delivery of therapeutic agents: a review. *Expert Opin Drug Deliv*. 2017;14:539–50.
- [587] Bleyl JU, Ragaller M, Tschöh U, Regner M, Hübler M, Kanzow M, et al. Changes in pulmonary function and oxygenation during application of perfluorocarbon vapor in healthy and oleic acid-injured animals. *Crit Care Med*. 2002;30:1340–7.
- [588] Lehmler HJ. Anti-inflammatory effects of perfluorocarbon compounds. *Expert Rev Respir Med*. 2008;2:273–89.
- [589] Kohlhauer M, Boissady E, Lidouren F, de Rochefort L, Nadeau M, Rambaud J, et al. A new paradigm for lung-conservative total liquid ventilation. *EBioMedicine*. 2020; 52:102365.
- [590] Ding H, Lv Q, Wu S, Hou S, Liu Z, Landén NX, et al. Intratracheal instillation of perfluorohexane modulates the pulmonary immune microenvironment by attenuating early inflammatory factors in patients with smoke inhalation injury: a randomized controlled clinical trial. *J Burn Care Res*. 2017;38:251–9.
- [591] Li Z, Chen G, Ding L, Wang Y, Zhu C, Wang K, et al. Increased survival by pulmonary treatment of established lung metastases with dual STAT3 CXCR4 inhibition by siRNA nanoemulsions. *Molec Ther*. 2019;27:2100–10.
- [592] Swystun V, Green FHY, Dennis JH, Rampakakis E, Lalli G, Fadayomi M, et al. A phase IIa proof-of-concept, placebo-controlled, randomized, double-blind, crossover, single-dose clinical trial of a new class of bronchodilator for acute asthma. *Trials*. 2018;19:321.
- [593] Weers JG, Miller DP, Tarara TE. Spray-dried Pulmosphere™ formulations for inhalation comprising crystalline drug particles. *AAPS PharmSciTech*. 2019;20:103.
- [594] Weers J, Tarara T. The PulmoSphere™ platform for pulmonary drug delivery. *Ther Deliv*. 2014;5:277–95.
- [595] Weers J. Comparison of phospholipid-based particles for sustained release of ciprofloxacin following pulmonary administration to bronchiectasis patients. *Pulm Ther*. 2019;5:127–50.
- [596] Cui X, Han X, Yu L, Zhang B, Chen Y. Intrinsic chemistry and design principle of ultrasound-responsive nanomedicine. *Nano Today*. 2019;28:100773.
- [597] Zhou L-Q, Li P, Cui X-W, Dietrich CF. Ultrasound nanotheranostics in fighting cancer: advances and prospects. *Cancer Lett*. 2020;470:204–19.
- [598] Liu Y, Bhattarai P, Dai Z, Chen X. Photothermal therapy and photoacoustic imaging via nanotheranostics in fighting cancer. *Chem Soc Rev*. 2019;48:2053–108.
- [599] Wang L-S, Zheng S-S. Advances in low-frequency ultrasound combined with microbubbles in targeted tumor therapy. *J Zhejiang Univ Sci*. 2019;20:291–9.
- [600] Cho MH, Shin SH, Park SH, Kadayakkara DK, Kim D, Choi Y. Targeted, stimulative, and theranostic <sup>19</sup>F magnetic resonance imaging probes. *Bioconjug Chem*. 2019;30:2502–18.